Durham E-Theses

Data processing and computer techniques for marine seismic interpretation

Birch, Roger W. J.

How to cite:

Use policy

DATA   PROCESSING   AND   COMPUTER   TECHNIQUES

FOR   MARINE   SEISMIC   INTERPRETATION

by

Roger W. J. Birch

A thesis submitted for the degree of
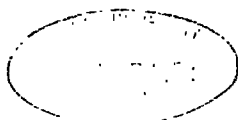

Doctor of Philosophy

in the

University of Durham

Graduate Society   December 1973

ADDENDUM

Page 12. Due to numerous difficulties and failures with the
compressor, which supplied the air for the air-guns, the
number of air-gun profiles performed was greatly reduced.

Page 29. The first sentence should read:-

The structure causing the gravity 'low' north-west of the
Faeroe Islands is apparently due to an infilled valley of
fairly limited aerial extent.

Page 88. The third sentence in section 3.7 should read:-

The two assumptions that are made throughout this theory are
that the acoustic interfaces should ideally have a finite dip,
and the aperture over which the reflections (primary and
multiples) have been produced for each layer is assumed
horizontal for each shot.

ACKNOWLEDGEMENTS

Abstract

This work is divided into two sections, the first containing results and interpretations from marine seismic reflection profiling performed by Durham University (1972) in a region to the north of the Faeroe Islands, and the second containing theories for the removal of multiple reflection effects from marine seismic records by means of digital data processing techniques.

The seismic profiling investigations were carried out to ascertain the geological structure causing the gravity 'low' north of the Faeroes which had previously been proposed by Bott, Browitt and Stacey (1971) to be caused by an infilled valley. Results from the 1972 survey shows that this infilled valley has a limited aerial extent containing relatively large basement undulations. Further work was carried out to obtain information about the sedimentary sequencies and to try and correlate these with sediments in surrounding regions where data had been obtained by previous workers. The profiling work (1972) indicated three major sequencies within the sedimentary column with an overall thickening of sediments away from the uplifted areas of the Iceland – Faeroe Ridge and Faeroe Islands.

The data processing section deals principally with the removal of multiple reflections from marine seismic records. An introduction is given to the basic concepts involved throughout this work, and includes a description of noise theory and types of multiple reflections encountered in marine seismic profiling. Some previous methods for multiple elimination are improved upon and then two new techniques are developed, applied to seismic sections, and finally a comparison made between the techniques used.

All programs are written in FORTRAN IV for use on the IBM 360 computer, and for displaying purposes, facilities available with the Durham IBM 1130 plotting system were used.

CONTENTS

Contents for the data processing section

CHAPTER 1

1.1 <u>Introduction</u>

Seismic reflection profiling data was obtained by the Durham cruise of 1972 (M.V. Miranda) in a region north of the Faeroe Islands defined by the lines of latitude 62° 15'N and 63° 23'N and lines of longitude 9° 15'W and 4° 10'W. One of the aims of this profiling work was to investigate the areas where previous Durham gravity surveys had shown a gravity 'high' (immediately north of the Faeroe Islands), and a gravity 'low' running north-east from the Iceland – Faeroe Ridge to the Norwegian Sea. This latter anomaly had been interpreted by Bott, Browitt and Stacey (1971) as being caused by a sediment filled valley that had been formed by possible subaerial processes. Investigations of the sedimentary sequencies of this survey area were carried out to gain an insight into their nature and structure, and also to correlate them to sedimentary data obtained by previous workers in surrounding regions (Ewing and Ewing, 1959; Jones, Ewing, Ewing and Eittreim, 1970; Talwani and Eldholm, 1972).

A brief resumé of the geological, geophysical and hydrographical data, obtained by previous workers in this and surrounding areas, is given in chapter 1 whilst in chapter 2 and chapter 3 results and interpretations of the Durham profiling data are produced.

Finally it must be stated that the application of the digital data processing techniques, developed in the second part of this work, was not possible due to computational difficulties at the time, and overall lack of time at the end.
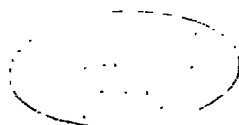
Fig.1.1   General bathymetry of the north-east Atlantic

Contours are in metres, major areas of shallow bathymetry
are named.
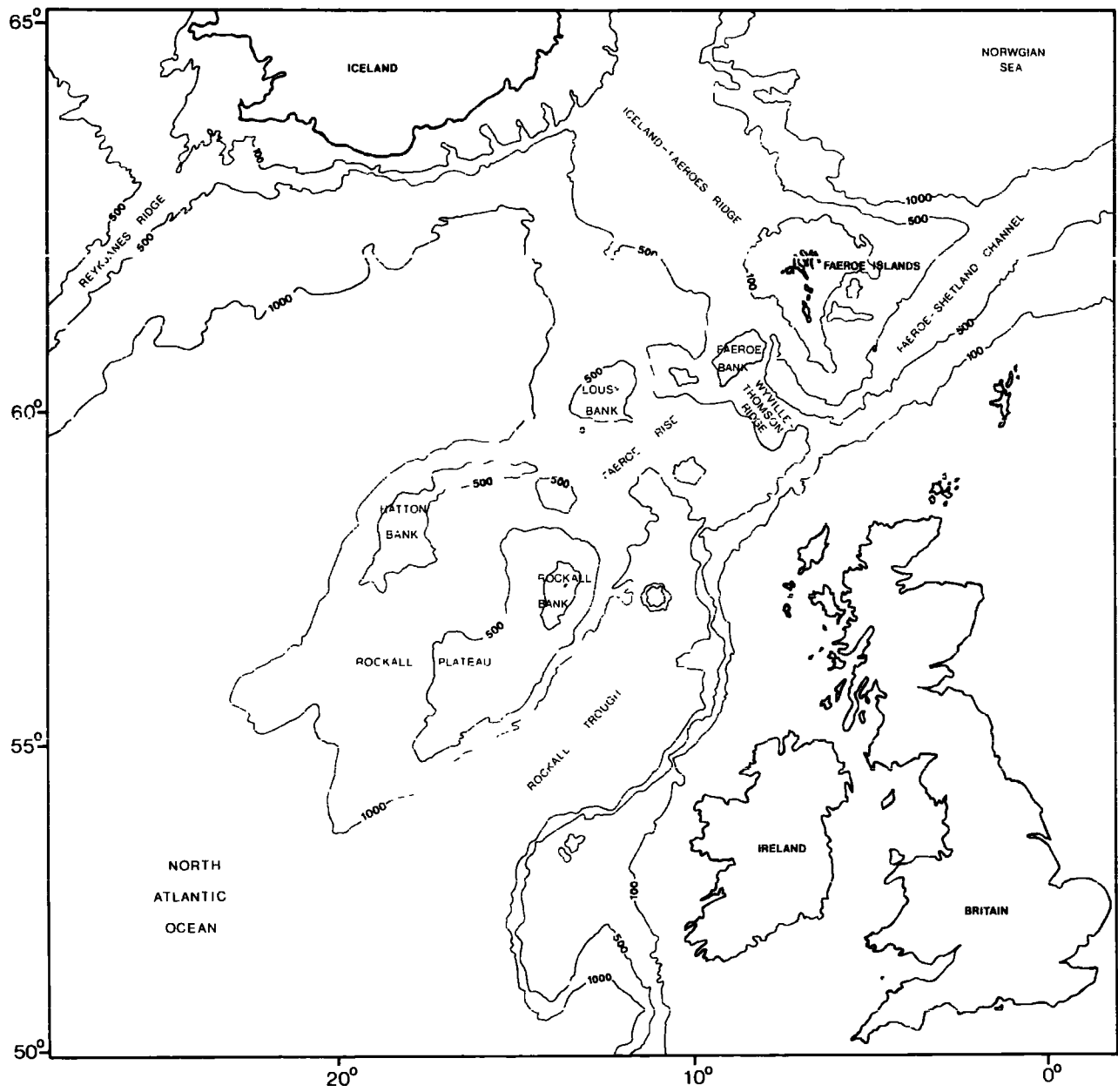
1.2   General geology and topography

A bathymetric rise which extends from East Greenland through Iceland to north-west Scotland separates the Norwegian and Greenland Seas from the rest of the North Atlantic Ocean.   Most prominent within this bathymetric rise is the Iceland - Faeroe Ridge which extends from eastern Iceland south - east to the Faeroes shelf, a distance of some 350 kms.   Transverse to this feature are a number of other rises including the Reykjanes Ridge, Iceland - Jan Mayen Ridge and the Faeroes Rise.   The latter incorporates the Faeroes Bank, Rockall Bank, Wyville-Thompson Rise and several other minor banks (Fig.1.1).

Geologically this area of the North Atlantic may be included in the Thulean Igneous Province, which extends from the Bristol Channel, north-east Ireland, west Scotland and to Greenland (Dobinson, 1970).   Support for the igneous origin of the Greenland to Scotland ridges, excluding the Rockall Bank, may be implied by the lack of space for them in palaeographical reconstructions of the land masses as they could have been before continental drift took place (Bullard, Everett and Smith, 1965).

During the Tertiary period this region, particularly the Faeroe Islands and the Hebridean - Irish Sea, was the site of intense igneous activity resulting in vast plateaus of basaltic lavas.   Alternating periods of explosive and intrusive activity followed culminating in widespread injection of dykes and sills, several hundred of which have been found in the Faeroe Islands (Noe-Nygaard, 1962).

1.2.1 The Faeroe Islands

This group of islands lie at the north-east end of a series of shallow

banks which incorporate the Rockall Plateau and the Faeroes Bank. The
Faeroe Islands are built up almost entirely of Tertiary basalt lavas with
a total visible thickness of about 3000 metres (Noe-Nygaard, 1962), the
age of which has been confirmed by radioactive dating techniques, Tarling
and Gale (1968), as being lower Tertiary (55-60 m.y. B.P.). Thus these
lavas appear to pre-date those of Iceland whose age was fixed at 12.5-16 m.y.
B.P. (Miocene) by Moorbath et.al. (1968), although no information was
obtained from the true base of the Iceland lava pile below sea level.

Three major subdivisions of these Faeroe lavas have been made by
Noe-Nygaard, (1962): 1) a lower lava series of about 900 metres thickness
containing columnar jointing and erosional surfaces; 2) a middle lava
series of 1350 metres which is made up of very thin zeolitic lava flows,
but shows a lack of the columnar jointing associated with the lower series;
and 3) an upper lava series of 625 metres depth consisting of individual lava
flows with minor columnar jointing within the thickest flows. Between the
lower and middle series of lavas is found a series of sedimentary strata
consisting of a coal bearing bed overlain with agglomerates (hardened clays
with local intercalations of sands and pebble beds).

Density measurements have been carried out by Saxov and Abrahmsen (1964)
on these lavas with the following results:

Upper series mean density   — 2.86 ± 0.06 gms/cm^3

Middle series mean density   — 2.82 ± 0.09 gms/cm^3

Lower series mean density   — 2.90 ± 0.04 gms/cm^3

giving a mean density for all the lava series of 2.86 ± 0.08 gms/cm^3.

1.3 Previous geophysical work in the Faeroes region

Seismic investigations of the basalt lavas of the Faeroe Islands have

been carried out from two refraction profiles by Pálmason (1965) on the islands of Streymoy and Suduroy. Arrivals from three seismic horizons were received indicating velocities of 3.9, 4.9, and 6.4 kms/sec for P-wave phases. A correlation between these arrivals and the three major basaltic lava sequencies may be made with the result that the 3.9 kms/sec arrival may be associated with the upper basalt series, whilst the 4.9 kms/sec arrival may be a combination of the middle and lower basalt series. The 6.4 kms/sec horizon shows a dip of 7° southward, its depth ranging from 2.5 kms to 5.0 kms over the area of study. This lower layer ties in with the substratum below Iceland which has an average P-wave velocity of 6.3 kms/sec. However this may be due to underlying continental crust with a higher than average crustal velocity. Indirect evidence from the fit of the continents by Bott and Watts (1971) shows that the incorporation of the Faeroe Rise and Faeroe Islands considerably improves the fit and also gives a continuity to the Caledonian front.

Saxov and Abrahmsen (1964) performed a gravity survey of the Faeroe Islands which revealed a gravimetric syncline of -7m.gals. in the north-western region and a less defined gravimetric anticline in the south. A possible interpretation of the gravimetric syncline/anticline is that there is a localized depression in the crust which increases in thickness from east to west. The general trend for the anomaly values to increase towards the east is probably related to the general tilting of the islands. This tilting has been verified by seismic reflection profiling performed by Watts (1970), who observed that the seismic basement dips gently south-east away from the Faeroe Islands.

A gravity 'high' of large aerial extent runs from north-west of the Faeroe Islands eastwards towards the Faeroes – Shetland channel (indicated by H in fig. 2.2). This has been interpreted (Stacey, 1968; Bott and Watts,

1970) as being partially due to lateral variations in the crustal density beneath the Iceland – Faeroe Ridge and the lower density continental crust beneath the Faeroe Islands. Explanation of the northward extension of the gravity 'high' may be in the crustal changes between the Faeroes shelf and the thinner oceanic crust underlying the Norwegian Basin. Associated with the gradual decrease of the gravity 'high' H eastwards are long wavelength magnetic anomalies which suggests that the basement dips gently south-eastward towards the Faeroe – Shetland Channel and is overlain by sedimentary sequencies (Watts, 1970).

1.3.1 The Iceland – Faeroe Ridge

This submarine topographic feature forms a shallow platform between the Faeroe Islands and south-east Iceland having an average depth of 150 fathoms along its crest, and separating the Norwegian Sea from the eastern North Atlantic (Fig. 1.1.).

Formation of the Iceland – Faeroe Ridge appears to have been initiated during the Tertiary opening of the North Atlantic causing the separation of Greenland from Northern Europe and the Rockall Plateau. During its formation the ridge was probably underlain by an anomalous low density upper mantle, and assuming isostatic equilibrium the Ridge would have been about 2 kms. above its present position at its point of formation. Movement of the spreading centre then resulted in the mantle returning to stable conditions, causing subsidence of the Ridge (Bott et.al. 1971).

Previous geophysical work on this feature and its relationship with Iceland and neighbouring regions have been performed and will be briefly described here.

A study of several seismic refraction profiles across Iceland (Pálmason, 1967, 1970; Báth, 1960) indicate that there is a substantial mass deficiency in the underlying mantle in relation to the normal mantle. This anomalous upper mantle is in common with other oceanic ridge systems forming a possible 'hot spot' (Bott et.al., 1971). Iceland is also characterized by a thicker crust than normal oceanic ridges, but thinner than normal continental crust, and consisting of mostly Tertiary basaltic lavas.

Marked similarities in the crustal thickness and layering of Iceland and the ridge have been observed, a simple model being shown:-

	ICELAND (after Pálmason)	ICELAND-FAEROE RIDGE (after Browitt)
	(velocity kms/sec)	(velocity kms/sec)
LAYER 1	4.2	3.2 - 4.6
LAYER 2	5.1	5.8
LAYER 3	6.5	6.8
LAYER 4	7.2	7.8

An asymmetric pattern in the sediments of the ridge has been revealed by seismic reflection profiling (Jones et.al., 1970). Sedimentary cover is absent on the crest and south-west slopes of the ridge, with the exception of localized basins, whilst on the north-east flank the sediments thicken towards the Norwegian Sea. This thickening of the sediments on the north-east flank has been attributed to the overflow water crossing the ridge from the Norwegian Sea and entering the Rockall Trough (Jones et.al., 1970).

Gravity surveys have shown a 145 m.gal. change in the Bouger anomaly across the region between Iceland and the ridge. Interpretation of the Bouger anomaly (Bott et.al., 1971) has shown it to be partially due to crustal

variations and more significantly by lateral variations in the density of the upper mantle. This is analogous to the transition between normal oceanic ridges and oceanic basins, in this case both Iceland and the ridge have an anomalously thick crust. A steep gradient of the Bouger anomaly between the ridge and the Faeroe Islands (2 m.gals/km) may again be attributed to the lateral variation of the mean crustal density, and variations in the crustal thickness. This transition has been interpreted as being due to the change from dense, anomalous, Icelandic type crust to continental crust beneath the Faeroes (Bott and Watts, 1970). The general pattern of gravity anomalies along the ridge indicate approximate isostatic equilibrium which may be related to a crustal thickness of 20 kms, in agreement with the seismic structure obtained from refraction lines (Bott et.al., 1971).

Finally magnetic surveys have shown a complicated pattern of large amplitude and short wavelength anomalies over the ridge in contrast to the Raff-Mason type magnetic lineations of the Reykjanes Ridge and Norwegian Sea. These show that the basement rocks are highly magnetic, of igneous origin, and must occur at shallow depth over much of the crest of the ridge. Also apparent from these anomalies is the fact that there is a fundamental difference in the crust of the ridge compared to that of normal oceanic crust (Stacey, 1968; Bott et.al., 1971).

1.4 Introduction to the marine sedimentary sequencies

Important to the nature of deposition of marine sediments in this area and the remainder of the North-east Atlantic is the circulation pattern of the waters which in turn must be related to the tectonic movements of the Atlantic Ocean. Late Cretaceous and Tertiary periods appear to bear most influence on these circulation patterns. By the end of the Cretaceous the rifting in the North Atlantic had switched from the west side of Greenland

to the east side, the Rockall Trough and the Faeroe Channel having formed even earlier during the Triassic (Bott and Watts, 1971). Initiation of the split between the Faeroe Rise and Greenland occurred some 60 m.y. B.P. during the early Tertiary period and may be contemporaneous with the extensive Eocene volcanism of the Brito-Arctic shelf areas.

During the late Cretaceous the North Atlantic was a region of shallow shelf seas, the remainder of the Atlantic occupying a much smaller area than in the Tertiary. It is therefore likely that the circulation pattern in the Cretaceous showed a marked difference from that during the Cenozoic period. A characteristic of the circulation pattern in the Upper Cretaceous was the flow of the Gulf Stream eastwards to Tethys and little towards the higher latitudes. Further the warmer climates of this period and the limited size of the Norwegian and Labrador Seas probably inhibited large volumes of cold water flowing into the Atlantic from the north (Jones et.al., 1970).

Climatic changes during the Tertiary period to more colder conditions, and the newly opened basins, would cause the entering into the Atlantic Ocean of cold water from the Norwegian Sea, which appears to have continued up to the present time. A possible effect of this overflow water is the control of sedimentation on the Iceland - Faeroe Ridge. Further evidence for the over-flow comes from Jones et.al. (1970) working in the Rockall Trough where sedimentary sequences indicate an initial deposition over the older sediments during the Eocene/Oligocene eras.

1.4.1 <u>Previous geophysical and hydrographical data on the sedimentary</u>

<u>sequencies</u>

Much of the previous work performed in the area around the Faeroe Islands has been concerned with the overflow of North-east Atlantic water from the Norwegian Sea across the Iceland - Faeroe Ridge and the Faeroe - Shetland

Channel and subsequently into the Rockall Trough. Evidence supporting this current flow has come mainly from hydrographic and reflection profiling in the relevant areas.

Estimates of the volume transport shows influxes through the Faeroe Bank Channel and across the Iceland – Faeroes Ridge are comparable, however the flow over the ridge is found to be intermittent, whilst in the Faeroe Bank Channel it is continuous (Crease, 1965). The pattern of sediments across the ridge show marked differences. On the crest of the ridge there is relatively little sedimentation, and similarly on the south facing slopes of the ridge, although here sedimentary deposits of up to 500 metres have been found. These sediments appear thicker near the base of the slope and are overlapped by highly stratified, horizontally bedded sediments. As a consequence of this sedimentation any irregularities of the basement have been smoothed out, although localized erosional unconformaties may still be seen (Jones et.al., 1970). The flow of water on these south facing slopes is at an appreciable angle, the current flowing along the foot of the slope south of Iceland. Velocities of 20 to 30 cms/sec. on the crest and southern slopes of the ridge for these currents have been recorded by Jones et.al. (1970). The current may be divided into two parts, a mixed, fast flowing current, and a slower moving layer at depth. A possible explanation of these two types of current may come from their two possible origins, the upper from the more turbulant overflow across the ridge, and the lower from a quieter influx from the Faeroe Bank Channel (Steele et.al., 1962).

On the north facing slopes of the ridge the sediments become thicker and more continuous as they extend eastwards to the Norwegian Sea, depths of 800 metres having been recorded. An important feature found within these sedimentary sequencies is the horizon R (after Jones et.al. 1970), below which the sediments show very little stratification and attain recorded

depths of up to 2 kms. This horizon R was first recognised in the Rockall Trough and has been dated as middle to upper Eocene in age. It does not appear to follow the underlying basement contours, and its apparent smoothness may indicate a process of levelling before its formation (Jones et.al., 1970).

It is worthwhile stating that in fixing the age of horizon R it has been assumed that this is the same horizon drilled by the Deep Sea Drilling Project, i.e. horizon A. This horizon A was penetrated in two instances during the project. The first in the North American Basin where it was found to contain beds of mid-Eocene chert formed by silification of turbidites and radiolarian muds, and secondly on a run between New Jersey and Senegal where it consisted of interbedded cherts and clays. Both were dated as mid-Eocene age. Unfortunately not all corings of horizon A have showed this age. Seven of twenty-five cores drilled in the south western corner of the Hatteras abyssal plain, where horizon A outcrops, showed no presence of fossils younger than Cretaceous in the turbidite sections of the cores (Ewing, Worzel, Ewing and Windisch, 1966; Saito, Burckle and Ewing, 1966). Peterson et.al. (1970) suggested three possible explanations of this age dating of horizon A: 1) the mid-Eocene cherts may not be horizon A (unlikely since reflection profiling performed at sites); 2) horizon A may be of varying age away from the region where it has been drilled; and 3) the coring in the Hatteras abyssal plain area may have sampled beds older than horizon A.

Explanation of the varied thickness and pattern of sediments may be explained by several factors. Firstly strong bottom currents associated with the flow of water toward the Atlantic and rapid sinking of dense Norwegian Sea water must tend to create a nondepositional and/or erosional environment on the crest and southern flanks of the ridge. Curves showing

the relationships between current velocity and erosion, transportation and deposition, indicate that the observed bottom currents would tend to inhibit deposition of all but coarse gravel-sized material whilst at the same time being capable of eroding the finer grained materials. The over-flow across the ridge is intermittent and absent in some places and would thus explain the locally thick deposits of sediment. These should be particularly thick close to the Faeroes which supply large amounts of terrigneous material to the surrounding areas. On the north facing slopes conditions change to a more tranquil state, the inflowing waters from the Atlantic remaining at shallow depth because of its associated low density. Deposition within this region has probably been fairly continuous since Tertiary time resulting in the observed thickness of sediments (Jones et.al., 1970, Steele et.al., 1962).

Seismic investigation of the sedimentary sequencies within the survey area (Durham, 1972) is described in chapter 2 where correlation to the surrounding areas of the work mentioned above is made. A major concern of this correlation is the possible continuation of horizon R to the region north of the Faeroe Islands that was surveyed.

CHAPTER 2

2.1 Profiling Lines

A total of 17 vertical incidence reflection profiles were obtained from the survey consisting of 5 air-gun profiles (lines 3, 6, 10, 11 and an incomplete line 5), and 12 sparker profiles (remaining lines, fig. 2.1). The aim of this profiling was to obtain information into the structure causing the gravity low north-west of the Faeroe Islands (indicated by L in fig. 2.3), and its possible extension eastward to the Norwegian Sea. At the same time the pattern of sedimentary sequencies of this area was also observed and related to data interpreted by other workers in this and surrounding areas.

Profiles were performed along the southern limits of the Iceland – Faeroes Ridge and then extended eastwards across the gravity anomaly in north-south directions into the Norwegian Sea. Lines transverse to these were then profiled through the major axis of the anomaly, notably lines 11, 12 and 15. Finally the southern ends of lines 5, 6, 7 and 8 were used to find any possible shallow crustal structure causing the gravity 'high' immediately north of the Faeroe Islands (indicated by H in fig. 2.3).

2.2 Instrumentation

Two methods of seismic reflection shooting were employed on the surveying vessel: 1) two air-guns at an operating pressure of 3000 p.s.i. (a simplified explanation of the air-gun design is given by Ewing and Zaunere, 1964); and 2) a sparker system with an output of 7 kJ. A track showing which system was used on each profiling line is given in Fig. 2.1.

Fig.2.1   Track chart

Lettering on the lines indicate the positions of reflection profiles shown in other diagrams.

Air-gun profile lines – 3, 5, 6, 10, 11

Sparker profile lines – 1, 2, 4, 7 – 9, 12 – 17

FAEROE ISLANDS
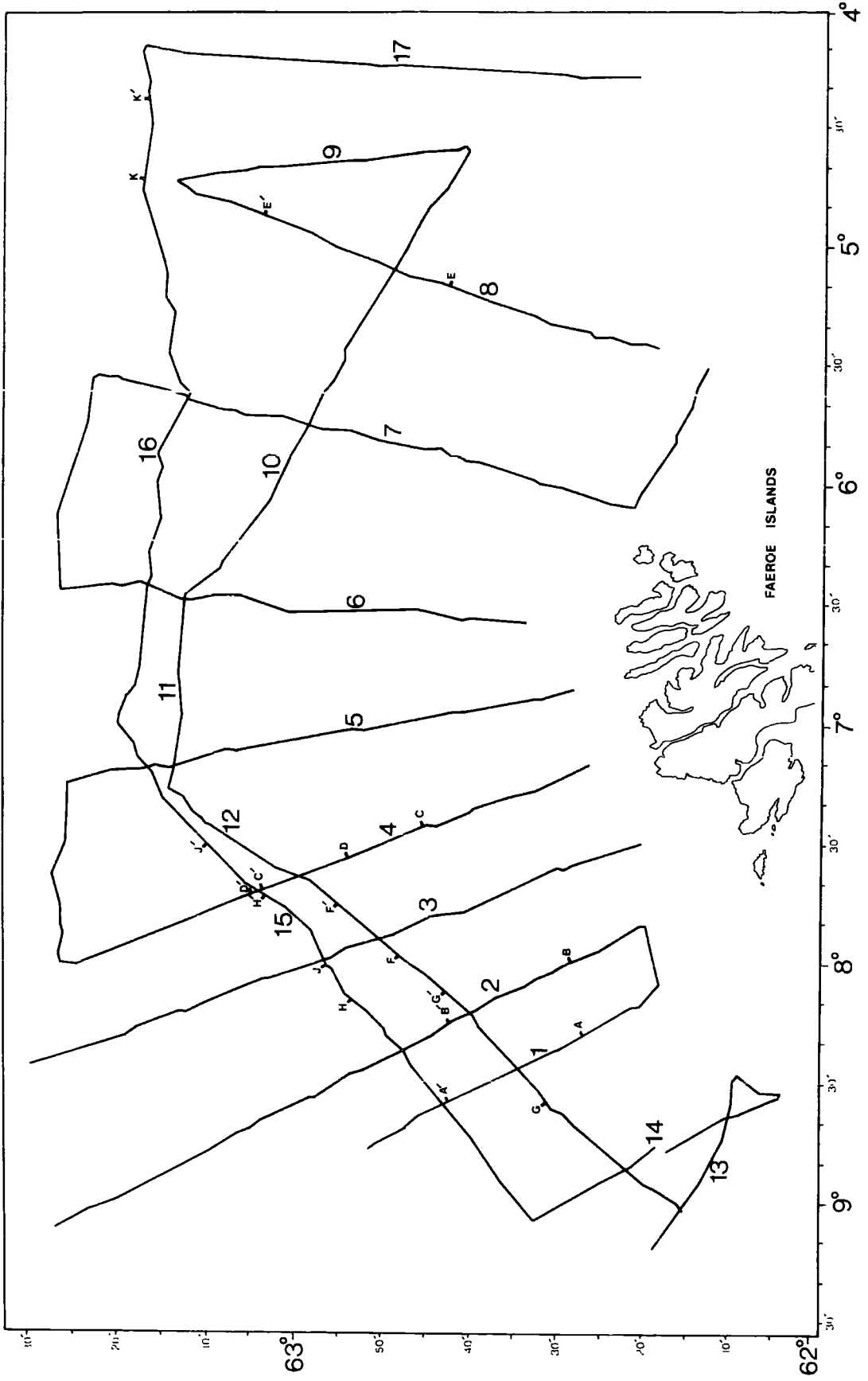
For receiving purposes a four section Geoméchanique array was towed behind
the vessel. This array consisted of active sections of 60 metres length
separated from one another by passive sections of 80 metres length.

The periodicity of air-gun shots was every 18 seconds, each signal
from the four active sections of the seismic array being recorded wide band
on F.M. magnetic tape enabling the records to be processed at a later date.
The air-gun records were displayed on a variable area recorder whilst the
sparker records were displayed directly on a Gifft variable density recorder
and not stored on magnetic tape. When replaying the air-gun records from
magnetic tape, with automatic gain control, several filter settings were
used but that found to be most satisfactory was a band-pass filter of
16-84 c/s.

During the profiling work, wide angle data was obtained using a
disposable sono-buoy system, the signal received being transmitted to the
ship and stored in the same manner on magnetic tape. The purpose of these
wide angle experiments was to obtain a velocity/depth profile using tech-
niques developed by Le Pichon et.al. (1968). Since this method requires
a knowledge of the dip of each horizon, vertical incidence reflection
profiles were recorded close to the wide-angle profile enabling any dip to
be measured. The full theory and method of picking the reflected and
direct arrivals is given in the paper by Le Pichon et.al. (1968).

Bathymetry was recorded continuously throughout the profiling work
using an O.R.E. precision depth recorder (P.D.R.). Loran C and Decca
navigational systems were used during the survey to track the ships position.
The accuracy was limited by the fact that the navigational lanes for each
system intersected at small angles, thus causing some errors particularly

Fig. 2.2 Bathymetry of the survey area

Contour lines are in 100 metre intervals.

Two dominant features shown are 1) the steep rise from the

Norwegian Sea onto the Faeroe block in the north-west, and 2) the

shallow area in the north-east delineating the southern extremity

of the Iceland – Faeroe Ridge.

FAERCIE ISLANDS
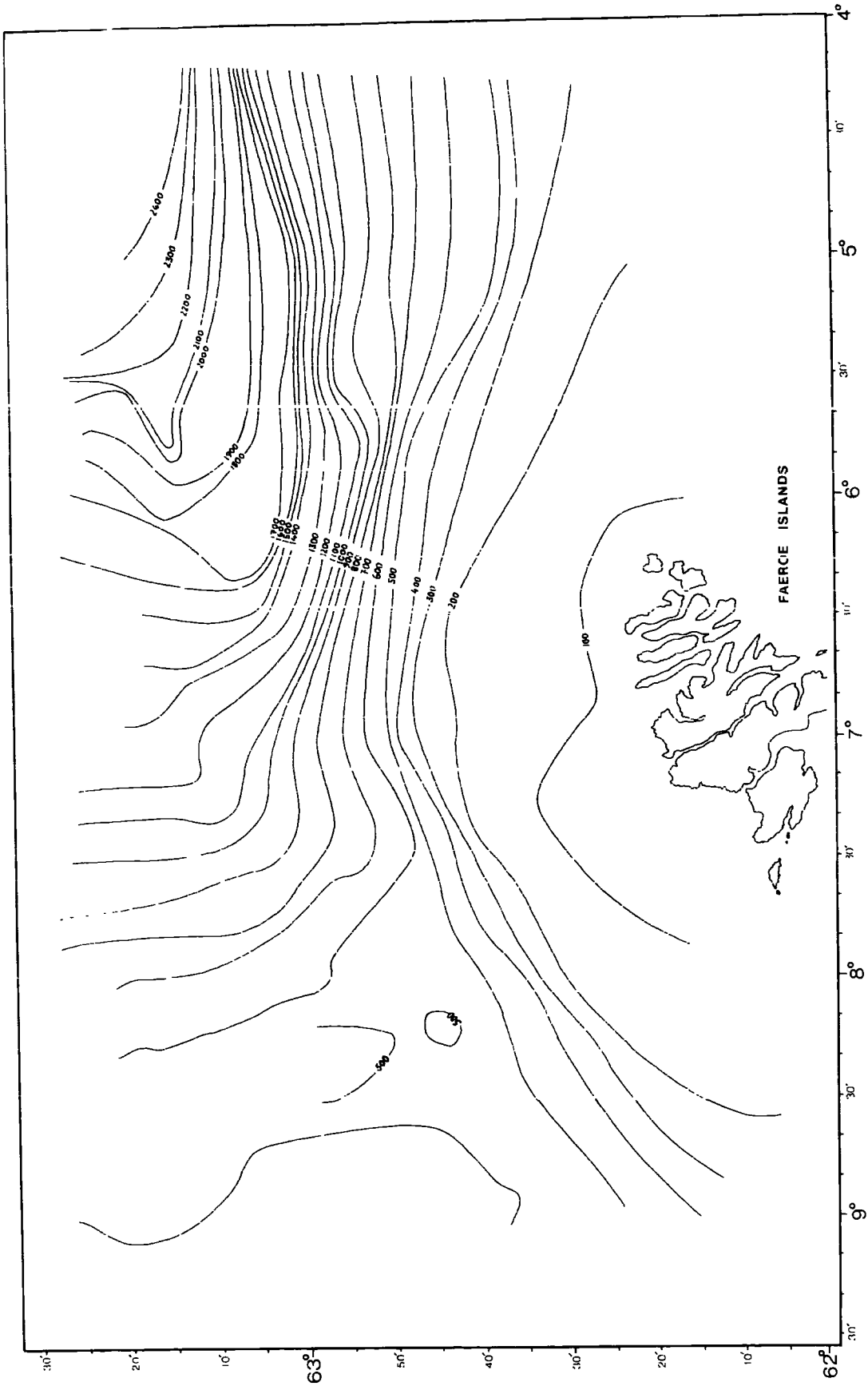
when there was a 'jump' of lanes.

2.3 Bathymetry of the survey region

Bathymetry was logged continuously throughout the survey by means of a precision depth recorder (P.D.R.). A plot of the bathymetry is shown in fig. 2.2. Important features relating to the bathymetry are, 1) the Iceland – Faeroes Ridge, delineated in the north-west section of the profiling by the 600 metre contour; 2) the shelf region of the Faeroe Islands, indicated approximately by the 200 metre contour; and 3) the steep bathymetric rise from the Norwegian Sea onto the Faeroes block. Further more detailed description of the sea bottom and sedimentary cover is given in section. 2.5.

2.4 General description of the basement topography

Generally the contours of the two-way travel time to the seismic basement follow those of the bathymetry with few exceptions (Fig. 2.4). There is a steep gradient from the Faeroes block northwards to the Norwegian Sea, the basement appearing smooth with very few undulations. As the Norwegian Sea is approached depths of up to 3.8 kms. for the seismic basement were observed (with an assumed velocity/depth function obtained from wide angle data), although greater depths must occur further north as the contours indicate an increasing trend of basement depth north-eastwards. No large scale erosional features associated with current flow, or undulations from folding processes are apparent on the profiles east of the Iceland – Faeroe Ridge or north of the Faeroes. The exceptions to this lie in a well defined region just off the ridge in a position associated with the gravity 'low' (F in fig. 2.4, and enlarged in fig. 2.6). Profiles across this structure

Fig. 2.3 Free air gravity of the survey area

Contours are in m.gals.

L and H refer to areas of gravity 'low' and 'high' respectively.

FAEROE ISLANDS
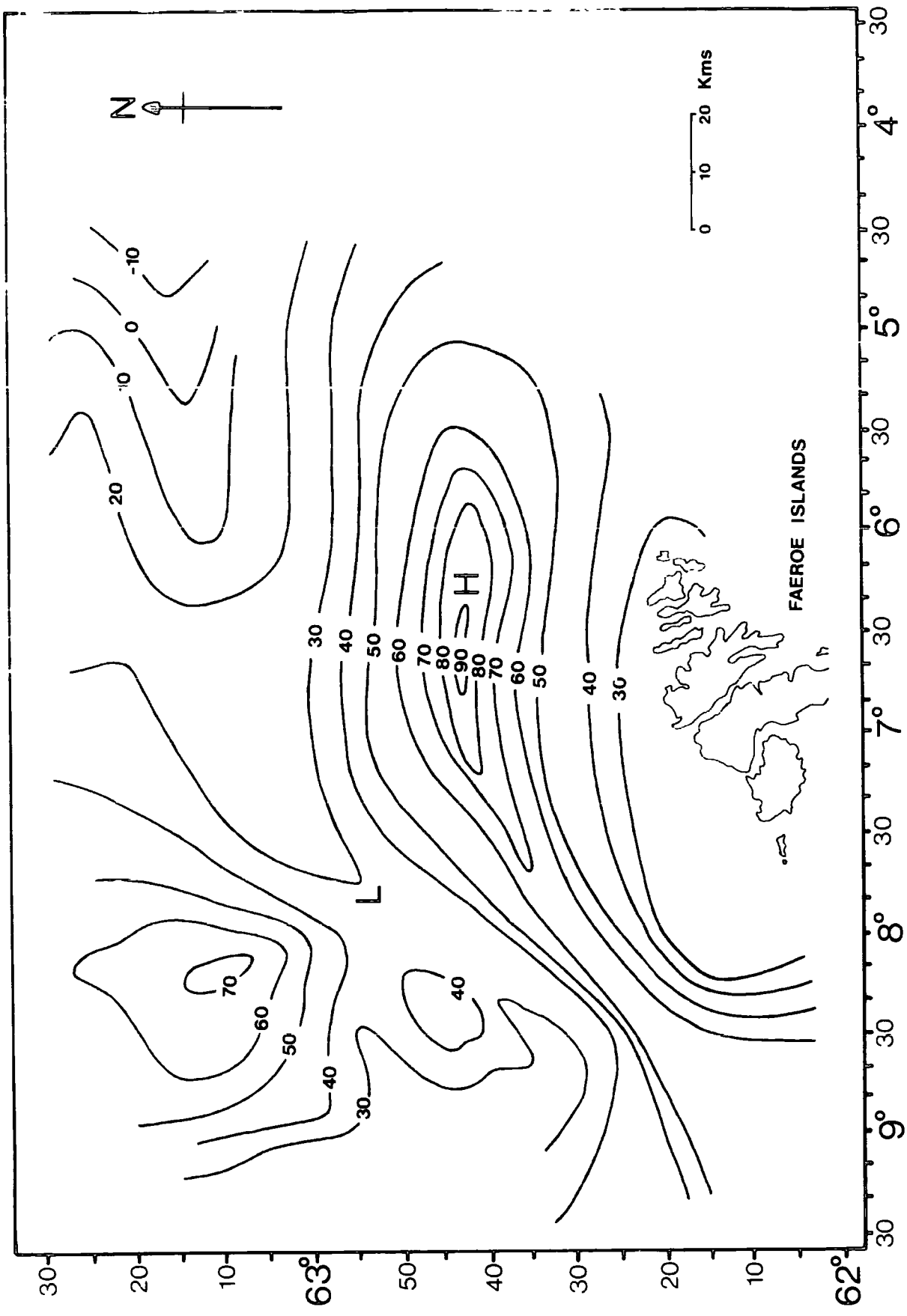
Fig. 2.4 Basement contours of the survey area

These contours indicate the 2-way travel time to the basement
in seconds in regions where there is a cover of sediments.

E and F indicate the positions of the sediment filled basin
and basement undulations respectively.

FAEROE ISLANDS

N

20 KMS
0   10   20

30'
63°
30'
62°

4° 5° 6° 7° 8° 9°
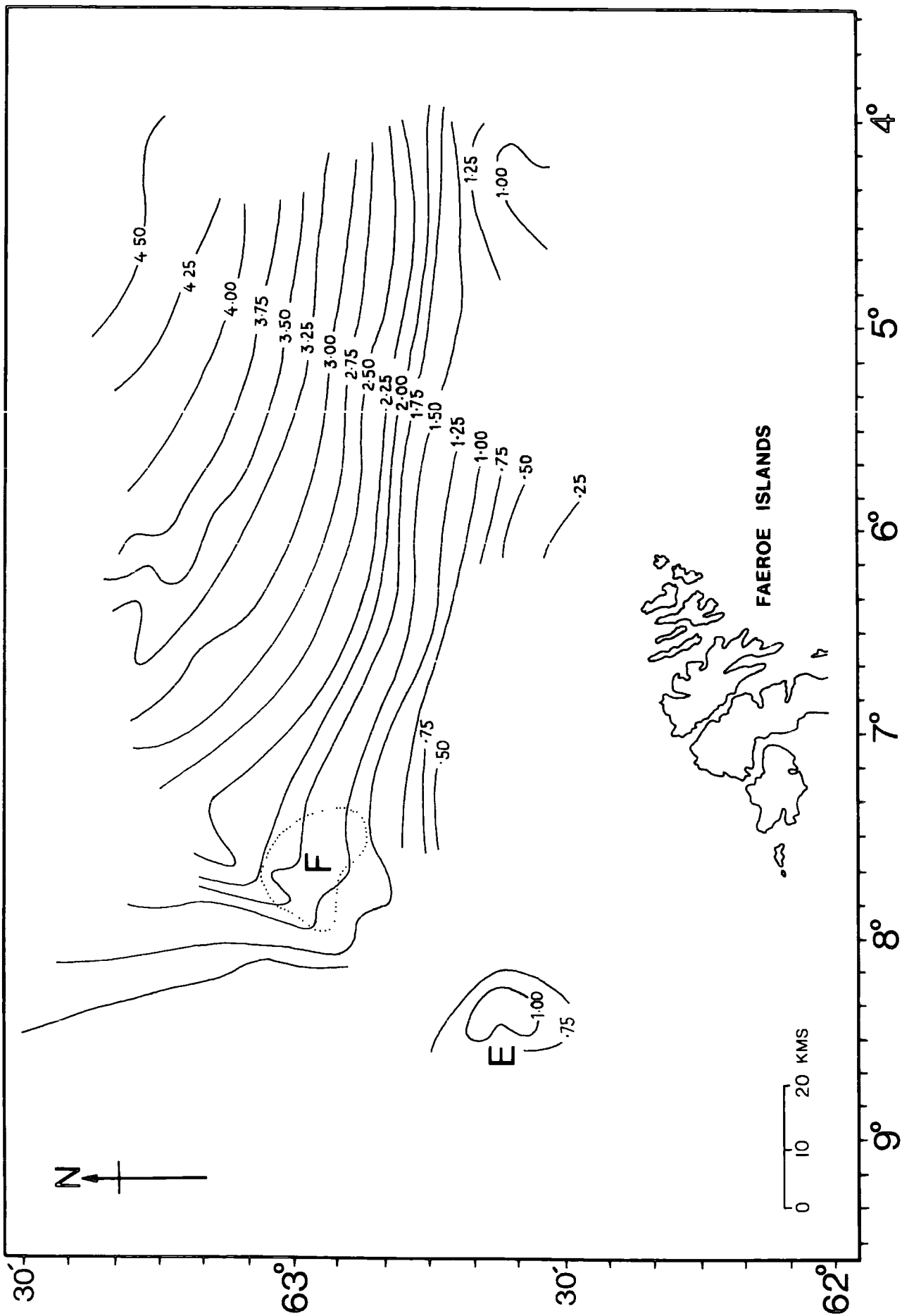
show large undulations in the basement topography whilst still following the general trend of increasing depth towards the Norwegian Sea. South-west/north-east profiles show these basement undulations to be of greater amplitude than those running north/south. The sedimentary sequencies above the basement having the same overall thickness in both directions. A more detailed discussion into this basement feature is given in section 2.7. Other smaller localised basement irregularities occur within the confines of the Norwegian Sea, although none with the same amplitude of those mentioned above.

Running south onto the Faeroes block the basement warps up steeply showing minor irregularities in some places as the sediments thin. On the shelf the sediment cover cannot be observed and can only at the most be tens of metres thick. Similarly the basement rises up onto the Iceland – Faeroe Ridge with subsequent thinning of the sediments, which is in agreement with the work carried out by Jones et.al. (1970) and Browitt (1971). Within the confines of the rise the basement shows a small, well developed, sediment filled basin-like structure which is closed on all sides. This appears to be one of a number of sediment filled basins interpreted by Bott, Browitt and Stacey (1971) which run along the crest of the Iceland – Faeroe Ridge (Fig.2.10).

Below the basement no large continuous structures are observed, only minor layering of limited length and shallow depth with respect to the basement. Generally the basement is seen as a good reflector with strong multiples over the whole region indicating that it is of a fairly consolidated nature. This may also be inferred from an unreversed refraction line performed by Talwani and Eldholm (1972) at 65° $50'$N 0° $45'$W, where the apparent seismic basement has a velocity greater than

Fig. 2.5 Basement undulations

The upper diagram shows a section of profile line 4, the lower
diagram a section of profile line 15.
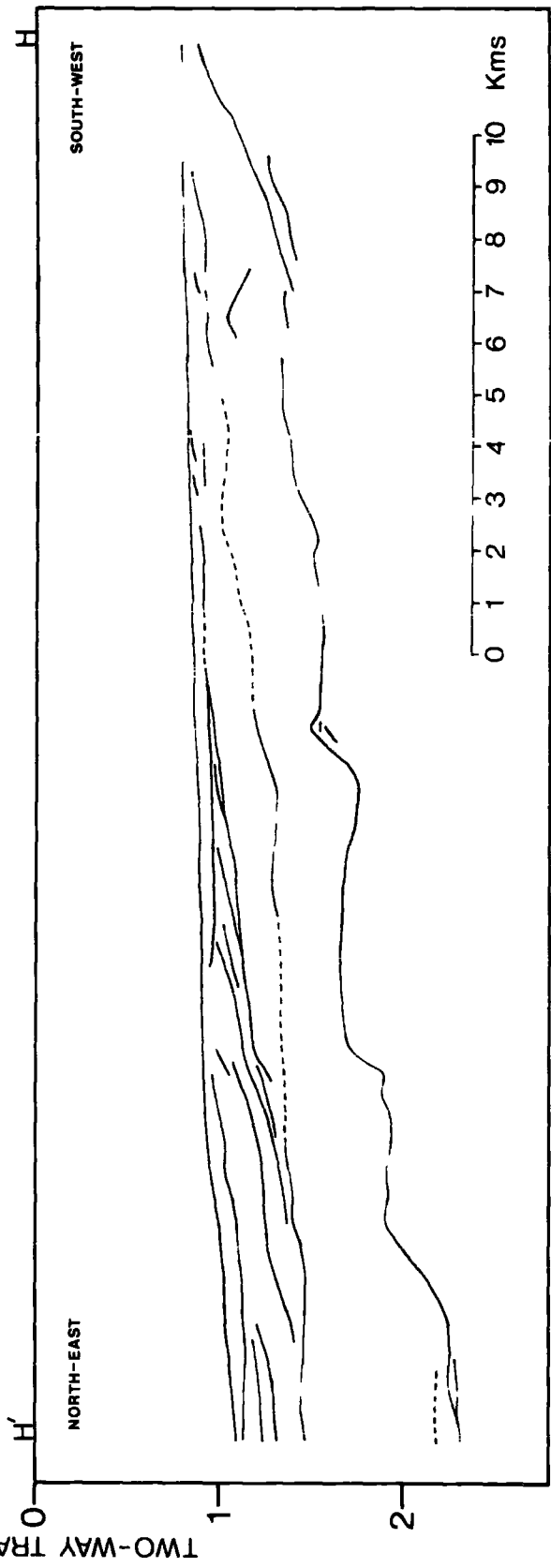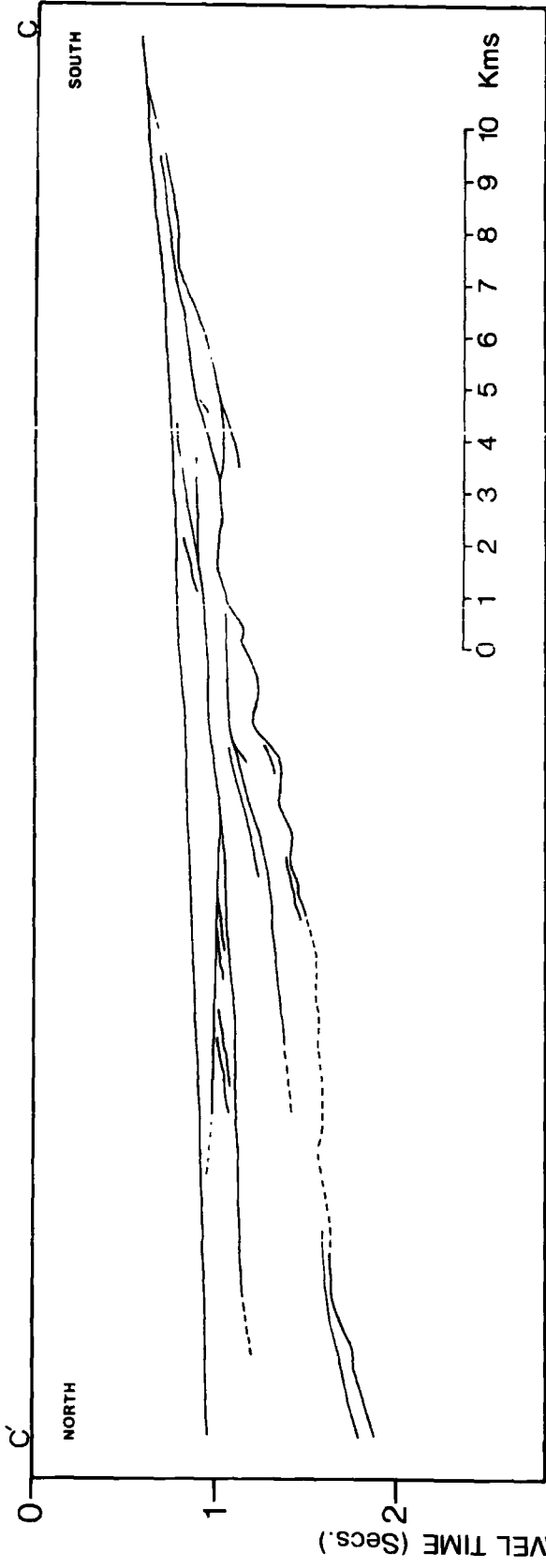
Fig. 2.6 Enlargement of the area of basement undulations

This shows in greater detail the basement contours of the region F indicated in Fig.2.4.

X and Y indicate the positions of possible river channels, which appear to have a south to north direction, i.e. from the Faeroe Islands toward the Norwegian Sea.

TWO-WAY TRAVEL TIME (Secs.)

2·2
2·1
2·0
1·9
1·8
1·7
1·6
1·5
1·4
1·3
1·2
1·1
1·0

·········· Delineates region of basement undulations

—·—·— Possible river channels

X

Y

15′
10′
5′
63°
55′
50′
45′

20′
7°30′
40′
50′
8°
10′
20′
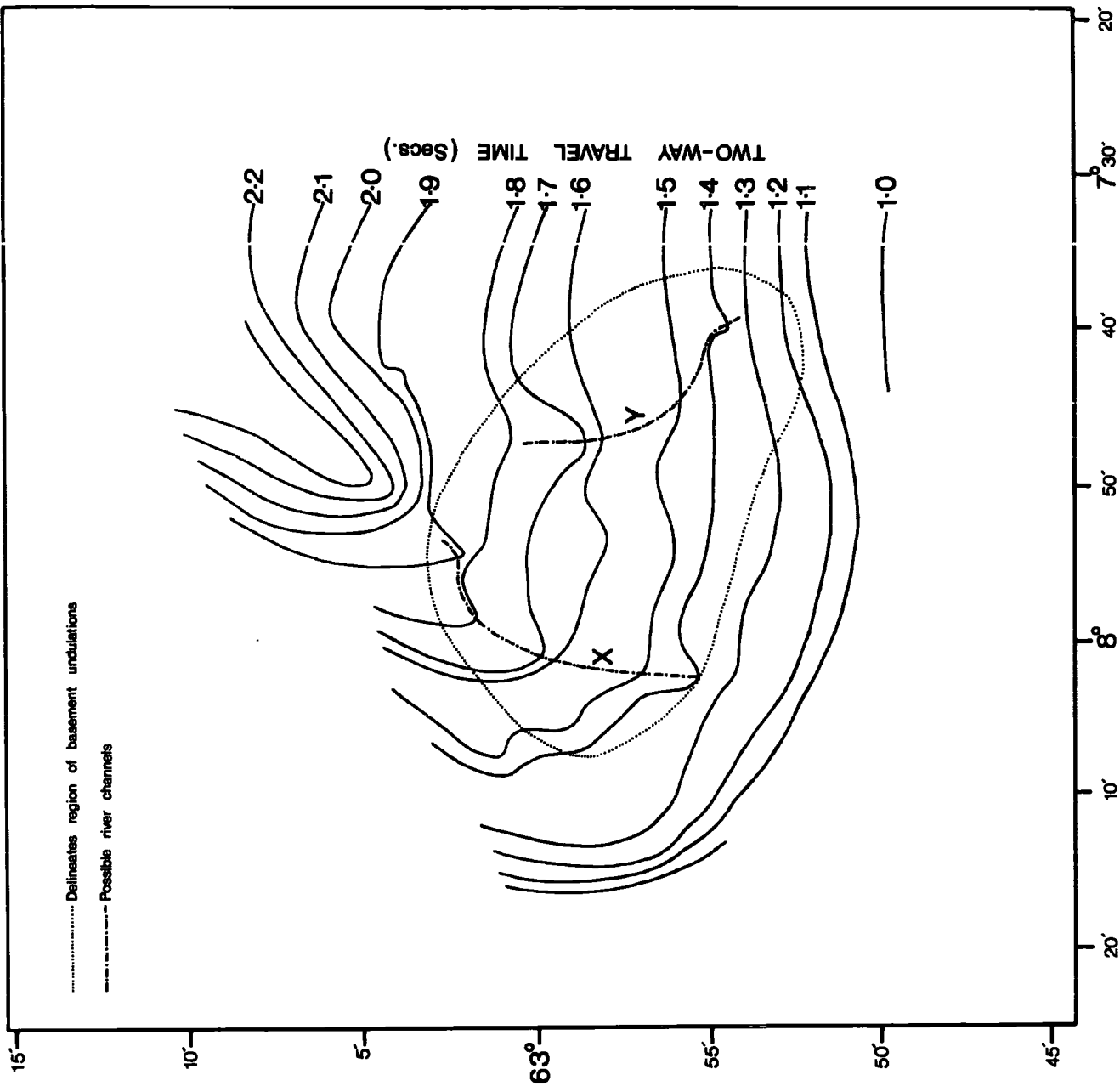
4.9 kms/sec. The relative smoothness of the basement (i.e. no large scale undulations or deeper large scale basement layering), particularly on the Iceland – Faeroe Ridge, Faeroes shelf and in that part of the Norwegian Sea profiled, suggests that the plateau basalts of the Faeroes might be widespread throughout this region of survey. However the magnetic anomalies produced by Avery et.al. (1968) show a distinct change to the area just north of the region profiled in this work. The magnetic anomalies change to a more linear pattern paralleling the mid-oceanic ridge in the Norwegian Sea, which have been interpreted in support of sea floor spreading in this area (Avery, 1968; Talwani and Eldholm, 1972). This change of magnetic anomalies may also indicate the boundary between the oceanic basalts and the basalt lavas associated with the Faeroes.

2.5 Results from the profiling work on the sedimentary sequencies

The general pattern for sediments in this area is for a thickening away from the Iceland – Faeroe Ridge and the Faeroes shelf. Depths for the total sediment column is of the order of 1.4 kms. in the north-east section of the survey region (assuming a velocity/depth function) which decreases to tens of metres and apparent absence on the above mentioned uplifted areas. This observed lack of sedimentary cover on the ridge is in accordance with the theory of current flow across its crest, and in agreement with previous data obtained in this area. Minor localized pockets of sedimentation are found in a few places along the ridge but no fine stratification is observed within these pockets. The exception to this is a small closed basin-like structure showing larger amounts of sediment deposition and finer layering within (section 2.8, and fig.2.10). Overall the sea bottom sediment cover shows no irregularities which may be associated with large scale current channels, although in two places

Fig. 2.7   Sedimentary sequencies

All the major sedimentary horizons are shown, being layers A,
B and C. The lowest continuous horizon is that of the seismic base-
ment.

R' indicates the reflecting horizon between Layers B and C.
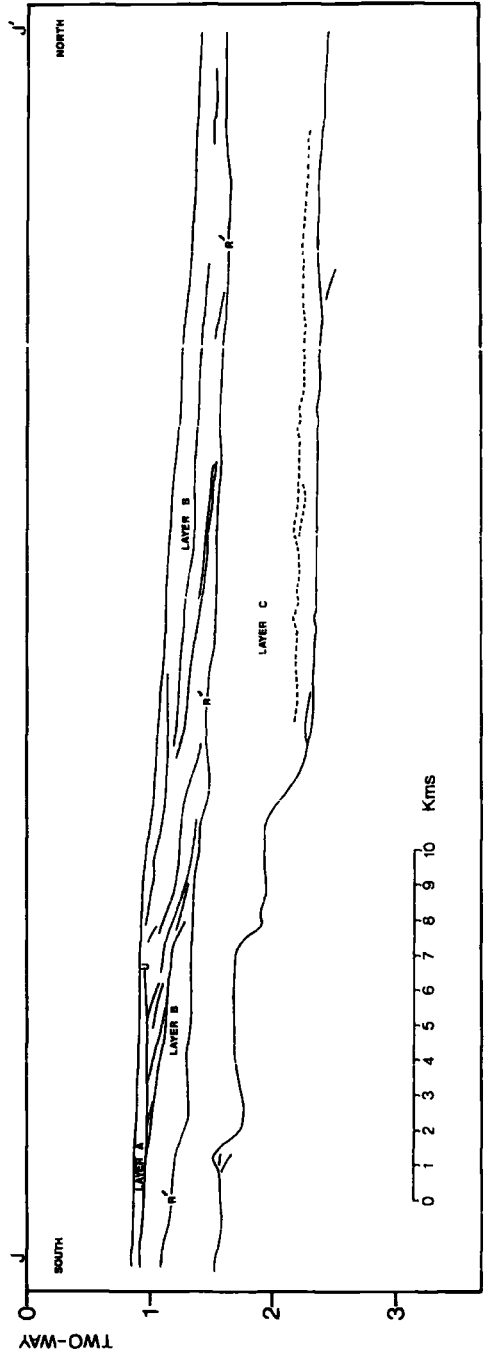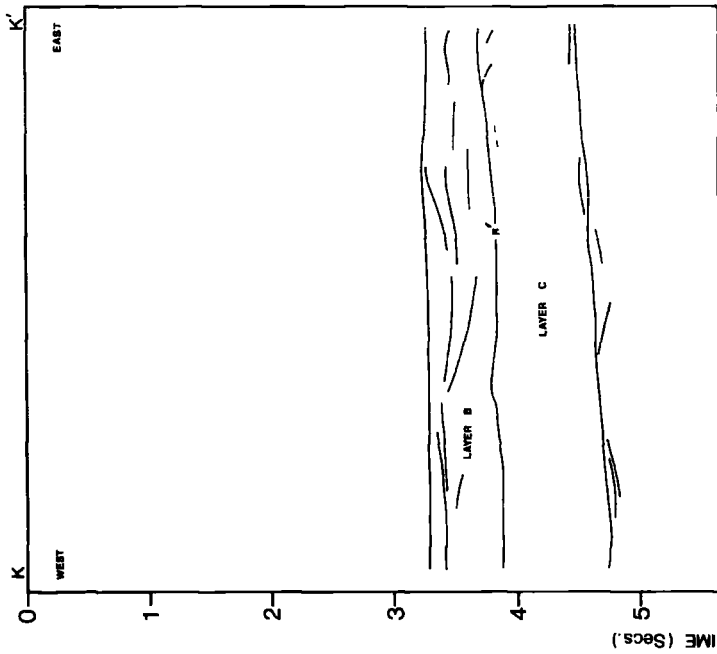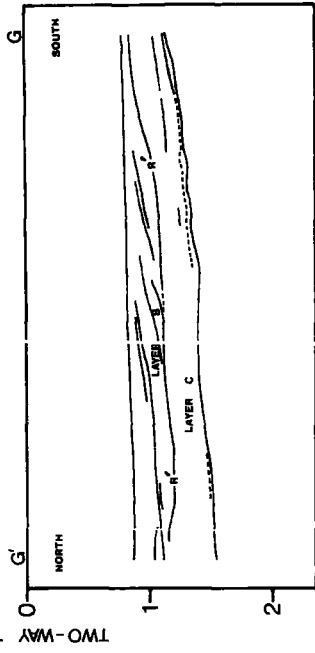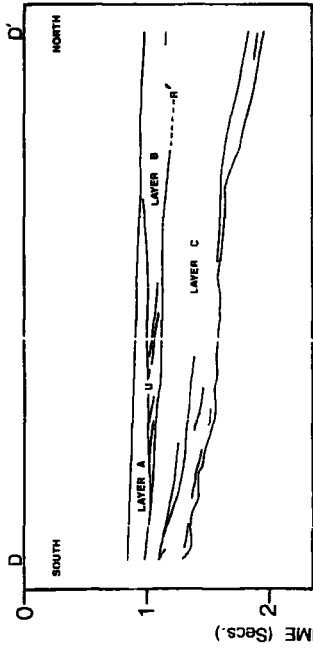
in the deeper regions of the Norwegian Sea, low amplitude long wavelength undulations of the sea bottom are observed. Since these appear to be only on a confined scale they may infer localized irregularities within the sea bottom currents.

Off the ridge and the Faeroes shelf the sedimentary sequencies may be divided into three major groups (Fig.2.7): 1) Layer C, an acoustically transparent layer resting on the seismic basement; 2) Layer B, a highly stratified layer; and 3) Layer A, a relatively thin layer overlying Layer B in a few areas close to the Faeroe Islands. These arc now dealt with in greater detail.

1)   Layer C

This is characterized by its acoustic transparence throughout, the lower limit being defined by the seismic basement and its upper limit by the abrupt change with Layer B. However close into the Faeroe Islands, where the sediments thin appreciably, some minor stratification is observed within Layer C which may be partially due to the presence of turbidite currents at the time of formation. It may be possible to correlate this interface with Layer B across to regions south of the Faeroes (e.g. Rockall Trough), where this interface has been given the notation R by Jones et.al. (1970). A reflection line shot by Durham University (1968) close to the Faeroe Bank and the Wyville-Thompson Ridge also shows the presence of this horizon R. Evidence for the possible extension of horizon R into the Faeroe-Shetland Channel may be forthcoming from the Durham University survey of 1973. However the reflection lines S4 and S6 reproduced by Talwani and Eldholm (1972) in the Faeroe-Shetland Channel indicate the presence of a strong reflecting horizon within the sedimentary sequence which may be the continuation of horizon

R from south of the Faeroes described by Jones et.al., 1970. Throughout

this work this interface between layers B and C found north of the

Faeroes will be given the notation R′.

In the profiling area north of the Faeroes horizon R′ appears as a

strong reflector (with respect to other sedimentary layering above),

becoming rather diffuse in the regions where it upwarps with the under-

lying basement as the latter approaches the ridge and shelf areas. The

strong reflective nature of R′ points towards a sharp change of sedimentary

deposition throughout this region, further evidence coming from the change

in nature of layering above and below R′. R′ may be Eocene in age making

it contemporaneous with the widespread lower-middle Eocene reflectors

rich in chert found by JOIDES cores in basins of the North Atlantic.

Horizon R′, although following the general trend of basement depth

increase towards the Norwegian Sea, does not reflect the large undulations

associated with the basin like structure mentioned previously (F in fig.

2.4), or any other basement irregularities. Because of the smoothness in

topography of R′ the process of sedimentation prior to it being formed

must have been largely one of levelling and not pelagic deposition since

the depth of sediments below R′ appear too thick for such a process to

have occurred.

In its deeper limits Layer C has an apparent thickness of 800 metres

decreasing to 100 metres as the basement rises up, becoming absent on the

shelf and ridge areas.

2)   Layer B

Above Layer C is the highly stratified Layer B (Fig.2.7 and Fig.2.8),

Fig. 2.8 Fine sedimentary sequencies of Layer B

R' indicates the interface between the more stratified Layer B
and Layer C. All layering shows the general trend of the seismic
basement, i.e. to dip away from the Faeroe block.
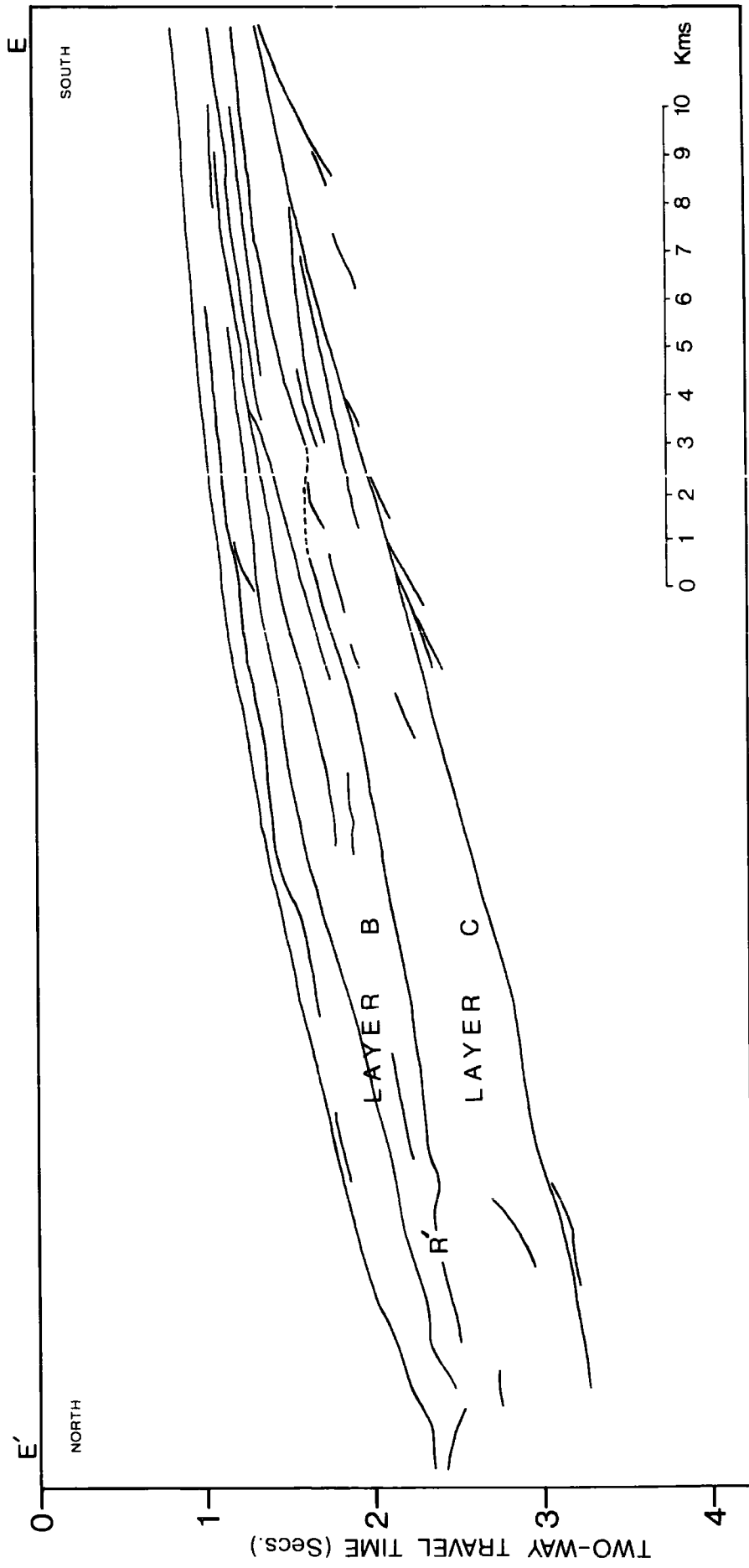
which in regions close to the Iceland–Faeroe Ridge, appears to lie unconformably on Layer C. This layering of B is always observed to dip down towards the Norwegian Sea away from the uplifted areas, but as the basement levels out in the deeper sections of the Norwegian Sea there is a general trend for the layering to become more horizontal (Fig.2.7). Dips of between 6° and 7° are observed near the Ridge. In regions close to the Faeroes this layering becomes very prominent, the individual horizons showing up as fairly strong reflectors. Further north–east however the layering becomes far less marked and those horizons that can be observed are of a relatively weak reflective intensity.

The possible explanation of this stratification of Layer B comes from current flow, the source for this current deposition originating from the nearby land masses. During the Pleistocene epoch much of northern Europe was heavily glaciated and associated with this glaciation was a drop in sea level of some 200 metres. As a consequence large areas of erodable material were exposed which were subsequently deposited by subaerial and marine processes in the surrounding areas. This erosion/ deposition would be a fairly rapid process causing slumping within the sediments as they built up, thus giving the observed pattern of sedimenta- tion within Layer B.

3) **Layer A**

This is only observed in small localized pockets close to the Faeroes and the Ridge. It lies unconformably on Layer B and has a maximum observed thickness of about 500 metres. Within this Layer A no major horizons can be observed and as it moves away from the influence of the higher basement areas its thickness decreases and may well be absent over

the part of the Norwegian Sea profiled. These sediments possibly originate from land derived material of the Faeroe Islands, and are probably still being deposited by the Atlantic currents flowing across the Ridge and near the Faeroes.

2.6 Wide angle data

Unfortunately only velocities from one wide angle run were obtained, allowing the sedimentary velocities to be determined but no basement velocity, as deeper structures were not penetrated. The position for this data was on line 10 at latitude $62^{\circ}15'N$ and longitude $5^{\circ}14'W$.

This data shows two well defined velocities for the sedimentary layers, one of 1.65 kms/sec. and the other of 1.95 kms/sec., which may be associated with Layers B and C respectively. Neither of these velocities indicate that the two layers are consolidated, particularly the 1.65 kms/sec. layer.

In Fig.2.9 is shown the results of the wide angle data obtained by Durham surveys and also from Ewing and Ewing (1959). The position of R´ and R within the sedimentary column are marked. The overall thickness and velocities of sediments from the wide angle data north of the Faeroes are compatible with those obtained by Ewing and Ewing (1959) in the Norwegian Sea (Results by Ewing and Ewing were from refraction surveys – F7 and F9). Thus the pattern of sedimentary layering within the Norwegian Sea appears to have been of similar nature throughout its entirety .

2.7 Profiling across the gravity 'low'

Basement contours show a general increase of depth away from the

Fig. 2.9 Wide angle measurements

Shows the velocity depth relationships obtained from the areas

in the north-east Atlantic by workers at Durham and by Ewing and

Ewing (1959).

The positioning of R within the sedimentary column has been

found by extrapolation from the nearest reflection profiles of Jones

et.al., 1970 (E10 and E11).

R′ indicates the interface between layers B and C found in

regions north of the Faeroe Islands.

Depth in Kms

ROCKALL TROUGH E 10 — EWING & EWING. 1959: 1·50, 1·71, 2·65, 3·22, R

ROCKALL TROUGH F 11 — EWING & EWING 1959: 1·50, 1·71, 2·08, 4·97, R

SHELF OF BRITAIN E 12 — EWING & EWING. 1959: 1·50, 1·73, 2·24, 4·91

SOUTH FAEROES 60°N 9°W — DURHAM. 1968: 1·48, 1·71, 2·0, 2·36, R

NORWEGIAN SEA F9 — EWING & EWING. 1959: 1·50, 1·70, 1·87, 5·36, 8·04

NORWEGIAN SEA F7 — EWING & EWING. 1959: 1·50, 1·80, 2·0, 5·37, 6·94

NORTH FAEROES 62°15'N 5°14'W — DURHAM. 1972: 1·48, 1·65, 1·95, R'

Depth axis: 0 1 2 3 4 5 6 7

Iceland-Faeroe Ridge, becoming more horizontal in the Norwegian Sea.
Signals received from the seismic basement in the area of the gravity
'low' show it to be a good reflector with few deeper structures, those
which were observed were of very short extent dipping gently away from
the basement.

The most notable feature of the basement associated with the gravity
'low' is the marked undulations confined to an area on the slope of the
Iceland-Faeroe Ridge (Figs. 2.5 and 2.6). The apparent amplitude of
these undulations appears greater in the east/west direction, whilst
their wavelength becomes smaller in the north/south direction. Maximum
dips recorded in the east/west direction were of the order of 17° dipping
down in an easterly direction towards the Norwegian Sea. Overall the
contours of the basement in this region show a structure similar to that
of a valley, closed in the west as the basement rises up onto the Ridge
crest, and open in the east towards the Norwegian Sea. Undulations of
the basement appear to be fairly well confined to the central part of
the valley (Fig. 2.5) and cannot be observed over any other of the
profiling lines across the gravity 'low'.

The sedimentary sequencies above the basement do not follow these
undulations, but do follow the general trend of basement dip towards the
Norwegian Sea. These sediments increase in overall thickness as they
get further away from the Iceland-Faeroe Ridge.

2.7.1 Formation of the basement topography

Since the sediments above the basement do not follow its topography
then it seems highly probable that these sediments were laid down after

the formation of the basement undulations. If Layer C can be correlated to the layer below horizon R, mentioned by Jones et.al. (1970), and since work by the JOIDES drilling experiment has put a possible age to the layer B/layer C interface in the Eocene epoch (Geotimes, 1965), it is reasonable to assume that the basement is late Mesozoic, early Cenozoic in age, thus making it contemporaneous with the Tertiary basalt lavas of the Faeroe Islands which were widespread throughout the Brito-Arctic area.

The actual origin of the basement topography is a little less obvious, and four major possibilities are mentioned here.

1) Folding

The age of the folding may be related either to the sinking of the Iceland-Faeroe Ridge, or to the pre-Cambrian folding mechanisms similar to those found in north-west Scotland. If this is pre-Cambrian it must be a small block of material left from the split between Greenland and Scotland, although why such a small block should still remain is uncertain and improbable. Observation of the basement throughout this region shows no contact horizon with the Tertiary basalts of the ridge which may rule out this hypothesis.

2) Faulting

Block faulting appears to be the most satisfactory type of faulting mechanism which might explain the basement features. The possible cause of this faulting may be due to the subsidence of the Iceland-Faeroe Ridge as the mantle 'hot spot' beneath Iceland moved away relative to the Faeroe Islands. As the seas invaded this area there was quick sediment deposition thus preserving the topographic features of the basement.

Unfortunately for this theory no apparent extension of the fault boundaries into the basement have been observed, which again may rule out this hypothesis.

3)   Marine Erosion

The undulations may have occurred as a process of erosion subsequent to the faulting mentioned above, or as an independent effect of the sea. Some submarine canyons, such as the Hudson and Congo, appear to be seaward extensions of land rivers; others are not obviously connected with land rivers. Unless they have been eroded no features attributable to river passage are observed in the section of the Iceland-Faeroe Ridge profiled, and how strong current flow which may have eroded this feature can fit into the idea of quiet seas in this region is difficult to explain. These last two points create difficulties for this theory and make it appear unlikely.

4)   Subaerial erosion

This idea fits the observed data more conclusively than those mentioned above. The order of events in this hypothesis is as follows:-

(i)   The Iceland-Faeroe Ridge is uplifted above the sea-level then present.

(ii)   Erosion by river flow into the observed basement topography, possibly two or three major rivers being fed by smaller ones.

(iii)   Subsequent subsidence of this area in conjunction with the subsidence of the Iceland-Faeroe Ridge. Rapid inflow of water and sedimentation then followed, thus perserving the erosional features of (ii) above.

(iv)   Glaciation over Europe causes the sea level to drop some 200

metres with resulting rapid deposition by turbidite currents

of the newly exposed land areas.

(v)   Retreat of the glaciation causes the sea level to rise again

covering this area and allowing Faeroes derived sediments to

be deposited.

Support for these stages of development of the basement topography

and overlying sedimentary sequencies comes from the following (numbering

is in accordance with the numbering above):-

(i)   Previous hypotheses concerning the structure and formation of the

Iceland-Faeroe Ridge indicate that it was originally uplifted

above sea level (Bott et.al., 1971). This allows the possibility

of subaerial erosion to take place.

(ii)   Erosion by river flow in other parts of the world show this type

of topography. In this case possible river channels can be

observed through the undulations, and are marked X and Y in

Fig.2.5. With this type of erosion coarser grained material

might be expected to be slowly transported along the river bed

and deposited not too far away on the seaward side of the mouth

of the river. Profile lines 4 and 15 clearly show this phenomenon

(Fig.2.6), and in some places it appears as a strong reflector

indicating larger grain size material.

(iii) Again previous theories have shown that the ridge has subsided,

being associated with the relative movement of the mantle 'hot spot'

beneath Iceland as it moved away from this region (Bott et.al.,

1971).

(iv) & (v)   Pleistocene glaciation over much of northern Europe

provided the mechanism for the sea level to drop over many areas,

causing previously submerged material to be exposed. Sediments associated with the type of sedimentary erosion and deposition which followed can be seen in Layer B. Faeroes derived sediments may be indicated by Layer A which lies unconformably on Layer B.

In summary the hypothesis of subaerial erosion followed by submerence fits the observed features more satisfactorily than the other ideas, although why this structure has only been observed on one part of the ridge is not evident. One possibility is the influence of the Faeroe Islands which might have been a large source of water for the formation of rivers in this area. This source would presumably not have been available to other parts of the Iceland-Faeroe Ridge. Evidence for this Faeroes source is shown in Fig.2.5. In this diagram X and Y indicate possible river channels, both appear to be in a north/south direction. Thus a source from the south would cause this observed flow direction.

2.8 Sediment filled basin on the Ridge

Lying some 20 kms. south-west of the basement undulations mentioned in section 2.7, and with no apparent connection with it, is a sediment filled basin closed on all sides. Later erosion however may have removed the connection between the two areas. This basin has some structures similar in appearance to the other region notably some basement irregularities (Profile line 1, fig. 2.10) and similar sedimentary sequencies above. The lower of these sediments has little stratification, compared with

Layer C, whilst the upper, although having a marked boundary with the layer below, also has a lack of stratification which may indicate the absence of Layer B and the presence of Layer A, the possibly Faeroes

Fig. 2.10 Infilled basin on the Iceland - Faeroe Ridge

These profile sections show the sediment filled basin indicated by E in Fig.2.3.

The upper diagram (profile line 1) clearly shows a major horizon in the middle of the sedimentary column with several other minor structures near the edge of the basin.

In the middle diagram the seismic basement is not so clearly defined and has a number of minor undulations which are also apparent in some of the sedimentary horizons above it.
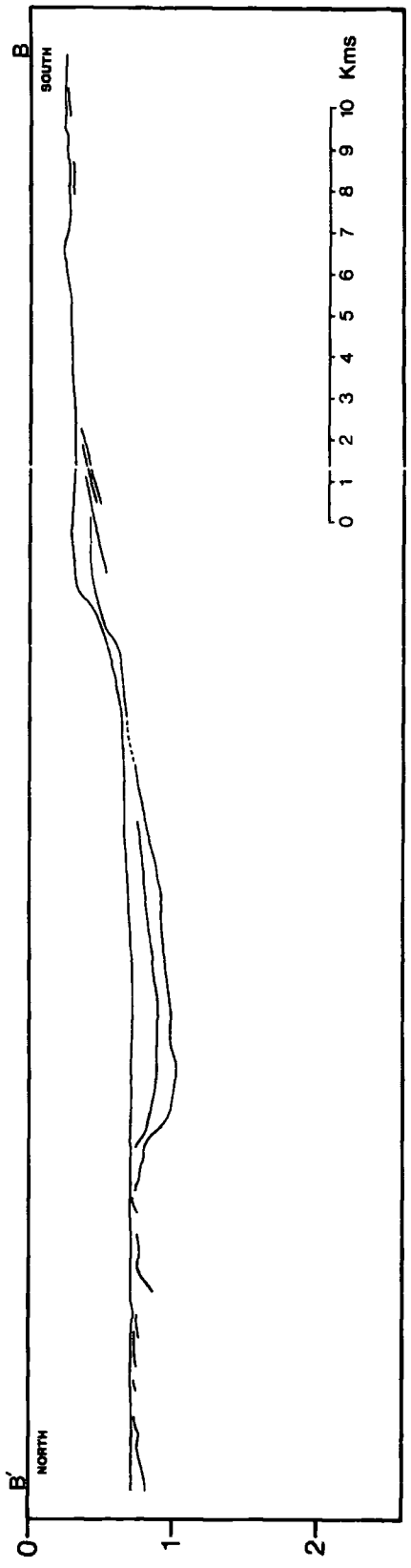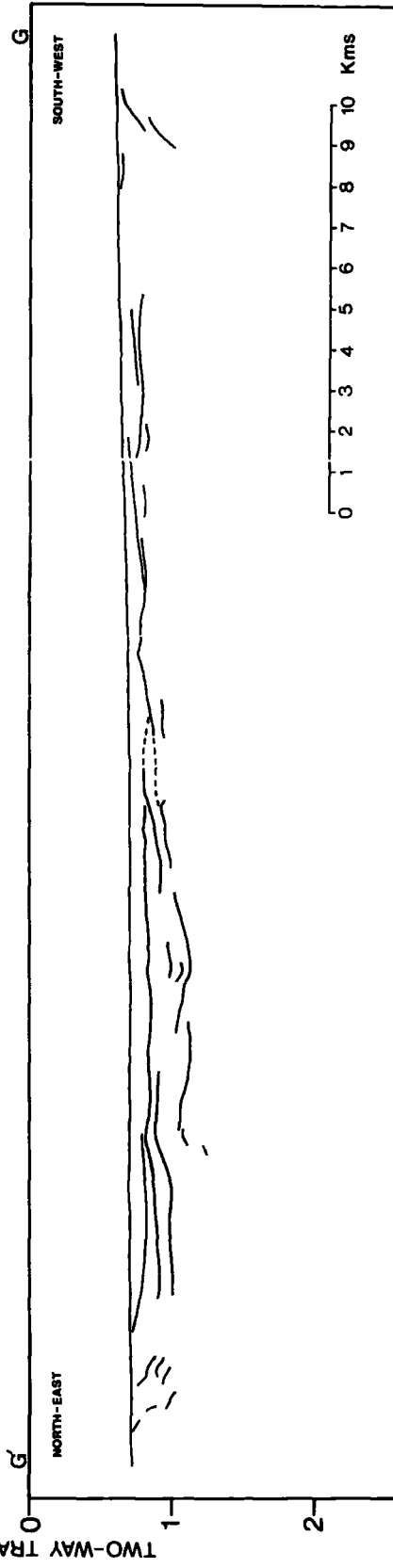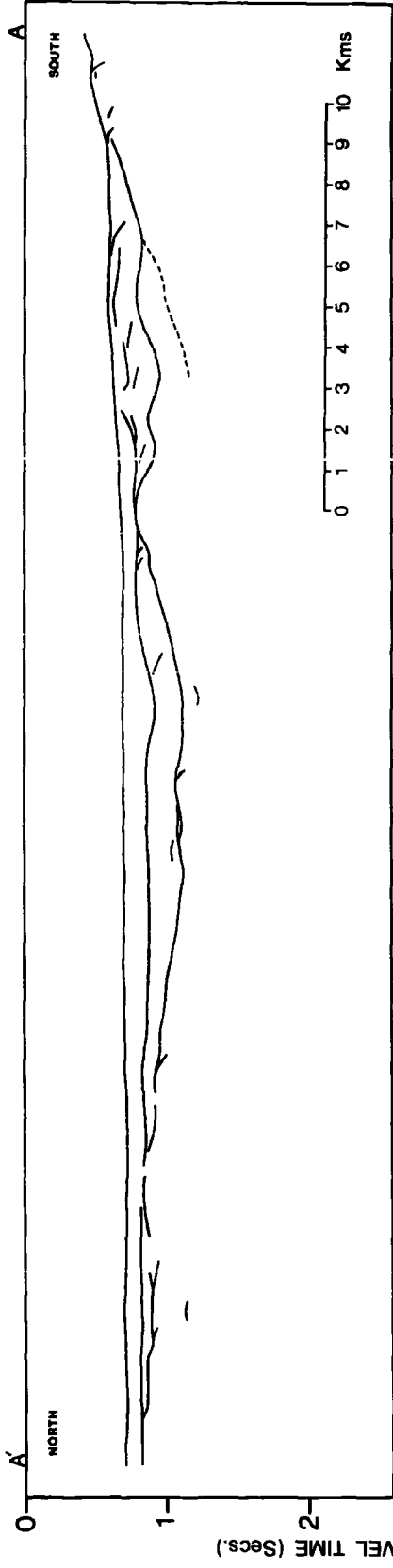
derived sediments. If this structure is truly independent of the other basin then its origin possibly lies with the sinking of the Iceland-Faeroe Ridge. Such structures (normally shown up by medium amplitude gravity anomalies, Bott et.al., 1971) are uncharacteristic of normal oceanic crust and thus indicate the anomalous nature of the Iceland-Faeroe Ridge.

CHAPTER 3

3.1 Summary and conclusions on the sedimentary sequencies

Three major sedimentary sequencies are observed, the uppermost,
Layer A, occurring only in regions close to the Faeroe Islands indicating
that these islands are its possible origin. This layer lies unconformably
with Layer B which appears highly stratified throughout the region. The
positioning of these layers within Layer B indicate a possible turbidite
origin, with associated slumping close to the uplifted areas of the Faeroe
Islands and the Iceland-Faeroe Ridge. The deepest found sedimentary
layering (Layer C) is, like Layer B, found throughout the area of survey.
In this case though Layer C appears acoustically transparent with no major
horizons being found.

The interface between Layers B and C (denoted as horizon R') has
many properties that are similar to horizon R found south of the Faeroe
Islands (Durham 1967 cruise, and Jones et.al., 1970). These similarities
of R' and R include: i) a strong reflective nature whenever observed;
ii) appearance in both instances as an horizon midway down the sedimentary
column; iii) in regions where the basement warps up, such as the Iceland-
Faeroe Ridge and The Faeroe Islands, R and R' also warp up and become
progressively more diffuse, i.e. the distinction between Layer B and Layer C
becomes less apparent; and iv) divides a highly stratified sequence above
from acoustically transparent sediments below.

Results from the reflection profiling and the wide angle data
obtained in the 1972 Durham survey indicate a similarity in the overall
sediment thickness and sediment velocity with those found by Ewing and

Ewing (1959) in regions further north in the Norwegian Sea. This indicates that the deposition of sediments throughout the Norwegian Sea being similar, although irregularities would be expected to occur particularly in regions close to uplifted structures such as the Faeroe Islands and Voring Plateau. Further evidence for this similarity in the Norwegian Sea sediments comes from reflection profiles and a refraction line obtained by Talwani and Eldholm (1972) in regions west of the Faeroe-Shetland and Voring Plateau escarpments. These profiles indicate the presence of two major sedimentary sequencies, the upper sequence having a high level of stratification, and an overall sediment velocity less than 2.0 kms/sec in agreement with the profiling results described in chapter 2.

Thickening of sediments away from the crest of the Iceland-Faeroe Ridge, to a total thickness of 1.36 kms (maximum observed), is seen as the basement dips towards the Norwegian Sea. Sediment cover on the Ridge is rarely greater than about 100 metres, the exception being a sediment filled basin-like structure north-west of the Faeroe Islands. This apparent lack of sedimentary cover on the Ridge must be a result of the current flow of the Atlantic water across it.

3.2 Summary and conclusions on the seismic basement

Basement contours indicate a general increase in depth away from the Faeroes and the Iceland-Faeroe Ridge towards the more oceanic structures of the Norwegian Sea. Steepest slopes of the basement being observed on the rise to the Faeroes block.

The structure causing the gravity 'low' north-west of the Faeroe

Islands is due to an infilled valley of fairly limited aerial extent. This feature is terminated in the west by the Iceland-Faeroe Ridge, although at one stage it may have extended further west but erosional processes may have removed this extension. In the east it is open towards the Norwegian Sea. Basement irregularities in this area appear to have been caused by subaerial erosion followed by later submergence as the Iceland-Faeroe Ridge subsided.

Other processes, such as submarine erosion or faulting may have occurred in conjunction with or independent of subaerial erosion in forming the observed basement topography, but certainly the profiling indicates only subaerial processes. Seismic refraction experiments in this area would help to show if there is any change in crustal structure beneath the basement undulations and therefore possibly helping to explain why they are found in such a confined region.

Tracks across the gravity 'high' immediately north of the Faeroe Islands show no shallow crustal structure or irregularities which might indicate an origin for this gravity anomaly. Sediments thin as they near the Faeroes and are practically absent in this region. Lack of shallow crustal structure or sediment irregularity may indicate the gravity anomaly is caused by a deeper feature. This may be the crust thinning in this area as it changes from the presumed continental crust underlying the Faeroe Islands to the thinner oceanic crust of the Norwegian Sea.

DATA PROCESSING TECHNIQUES

CHAPTER 1

1.1 Introduction

In marine seismic profiling the data obtained will invariably contain the effects of multiple reflections to varying degrees. When this data is to be interpreted, (i.e. a geological representation of the substrata penetrated is required), then the effects of multiples may cause great hindrance in defining a seismic horizon and may also cause the interpreter to 'pick' an arrival that is in fact a multiple. As a consequence it is desirable to remove these multiple reflections and other random noise effects and hence improve the resolution of the true seismic horizons. The basis of this work is the build up of processing techniques that are able to remove these undesirable effects and to produce seismic sections that are realistic of the substrata that are penetrated.

Several sections within this first chapter are concerned with theories and definitions that are relevant to the programs and theories of chapter 2 and chapter 3. In all instances the signal or seismogram is sampled only in the time domain at equally spaced intervals. Thus a wavelet $f(t)$ sampled at times t_0, t_1, t_2, ... t_n will have corresponding measured amplitudes of a_0, a_1, a_2, ... a_n. The analogue signal is that which is continuously recorded and when replayed will give an exact representation of the signal received. The digital signal is, as mentioned above, a series of data values representing sampled points of the analogue signal, which in every case should contain all the relevant information that is required. However it must be stated that the digital signal cannot contain all the information

that is present in the analogue signal (Robinson, 1967a). Since all relevant information should be contained within the analogue signal a limit must be placed on the maximum sampling interval, T. The full mathematics of this constraint is given by Blackman and Tukey (1958) and Hsu (1967), where this constraint is defined as:

$$T < \frac{1}{2f_m}$$

where f_m is the maximum frequency component of a time function $f(t)$. Therefore, if $f(t)$ is uniformly sampled at intervals less than $\frac{1}{2f_m}$ seconds apart, the digitized signal will contain all the information of $f(t)$. (This theorem is sometimes called the Nyquist interval).

A list of the main symbols used throughout this work is given below:-

t   — discrete time, when sampling t=0, 1, 2, ...

w   — angular frequency

f   — frequency (c/s)

$a(t)$, $b(t)$, $f(t)$ — examples of time series such as a wavelet or a seismogram

$A(Z)$, $B(Z)$, $F(Z)$ — Z - transforms of the above signals

$\phi_{ab}(\tau)$ — cross-correlation function of the signal $a(t)$ with signal $b(t)$

$\phi_{aa}(\tau)$ — autocorrelation function of the signal $a(t)$

$\psi_{ab}(t)$ — convolution function of signal $a(t)$ with signal $b(t)$

$\Phi(w)$ — power spectrum

$A(f)$ — amplitude spectrum.

1.2 Concepts of convolution and correlation

a) Convolution:

The convolution of two signals a(t) and b(t) is defined as the function:

$$\psi_{ab}(t) = \int_{-\infty}^{\infty} a(\tau)\, b(t-\tau)\, d\tau$$

In the case of a(t) = 0 and b(t) = 0, for t < 0, i.e. if the signal does not exist for times before sampling is initiated, this equation reduces down to:

$$\psi_{ab}(t) = \int_{0}^{t} a(\tau)\, b(t-\tau)\, d\tau$$

This equation is often expressed as a summation formula:

$$\psi_{ab}(t) = \sum_{\tau=0}^{t} a(\tau)\, b(t-\tau)$$

It may also be shown that: $\psi_{ab}(t) = \psi_{ba}(t)$, Hsu (1967).

Thus it can be seen that this convolution theorem is useful in the formulation of a synthetic seismogram from the source wavelet and spiked impulse response of the earth. An example of this is shown in Fig.1.1. The use of this theorem when applied to spiking filters and other techniques is given in chapter 3.

b) Correlation:

This technique is useful in finding the similarity between two signals. The time shift τ is such that the correlation function $\phi(\tau)$

is at a maximum when the two signals are most similar. This is shown clearly in Fig.1.2, where the peaks in the cross-correlation of the source and seismogram (A, B, C, D, E and F) indicate the positions of similarity.

Mathematically this function may be expressed as (Hsu, 1967):

$$\phi_{ab}(\tau) = \int_{-\infty}^{\infty} a(t)\, b(t-\tau)\, dt$$

which again is often expressed as the summation formula:

$$\phi_{ab}(\tau) = \sum_{t=-\infty}^{\infty} a(t)\, b(t-\tau)$$

and from this it is easily shown that:

$$\phi_{ab}(\tau) = \phi_{ba}(-\tau)$$

A special case is when the signal is correlated with itself, this forms the autocorrelation function:

$$\phi_{aa}(\tau) = \sum_{t=-\infty}^{\infty} a(t)\, a(t-\tau)$$

with the result that we find:

$$\phi_{aa}(\tau) = \phi_{aa}(-\tau)$$

showing that the autocorrelation function is symmetric about $\tau = 0$. This symmetry is clearly shown in Fig.1.2.

Finally the similarity of the correlation and convolution processes can be shown by writing the cross-correlation in the form:

$$\phi_{ab}(\tau) = \sum_{t=-\infty}^{\infty} a(t)\, b\left(-(\tau-t)\right)$$

Fig. 1.1   Convolution theorem

The example shown indicates the application of convolution to the derivation of a synthetic seismogram from the spiked response of the earth and the known source wavelet.

A diagramatic representation of the model used and source wavelet are shown in the upper figures, whilst below is drawn the spiked response of the model and the synthetic seismogram produced by convolving the source wavelet and spiked response.

MODEL

TWO-WAY
TRAVEL TIME (SECONDS)

REFLECTION
COEFFICIENT

0
8 ──────────── Shot/receiver depth

156 ────── · ── · ──────── 0·7

196 ──────────────── 0·5

372 ──────────────── 0·4

SOURCE

Air-gun source (band pass
filtered 20 to 100 c/s)

AMPLITUDE

1·0 ─
0·8 ─
0·6 ─
0·4 ─
0·2 ─
0 ─
−0·2 ─
−0·4 ─
−0·6 ─
−0·8 ─
−1·0 ─
−1·2 ─

AMPLITUDE

0·7 ─
0·6 ─
0·5 ─
0·4 ─
0·3 ─
0·2 ─
0·1 ─
0 ─
−0·1 ─
−0·2 ─
−0·3 ─
−0·4 ─
−0·5 ─
−0·6 ─
−0·7 ─

Spiked response of the model
to a unit spike impulse

AMPLITUDE

1·0 ─
0·8 ─
0·6 ─
0·4 ─
0·2 ─
0 ─
−0·2 ─
−0·4 ─
−0·6 ─
−0·8 ─
−1·0 ─
−1·2 ─

Synthetic seismogram formed by
convolving the source wavelet
with the spiked response of the model
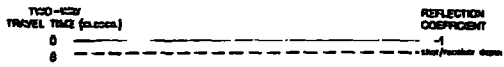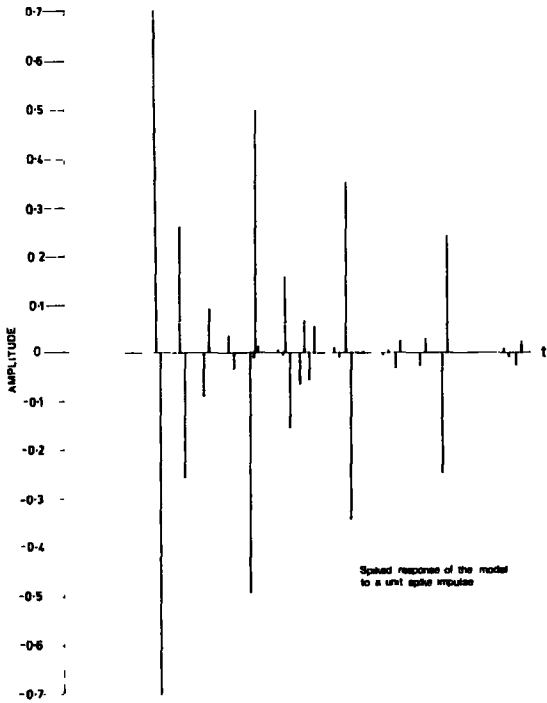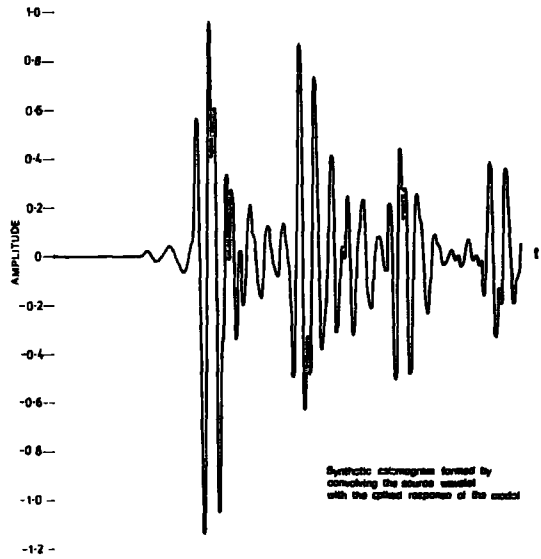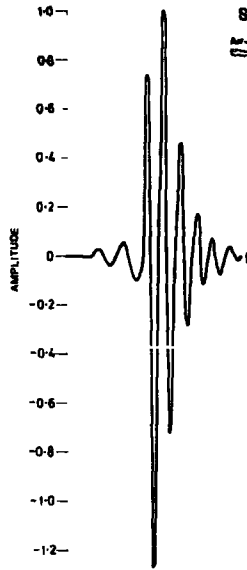
Fig. 1.2 Correlation theorem

These diagrams show the autocorrelation function of the source
wavelet and the cross-correlation function of the source wavelet and
seismogram.

Important features are the symmetry of the autocorrelation
function about $\tau = 0$, and the positions of the signal within the
seismogram which are indicated by the correlation peaks A, B, C, D,
E and F.

Seismogram

Cross-correlation
of
source & seismogram

Autocorrelation
of source

Source
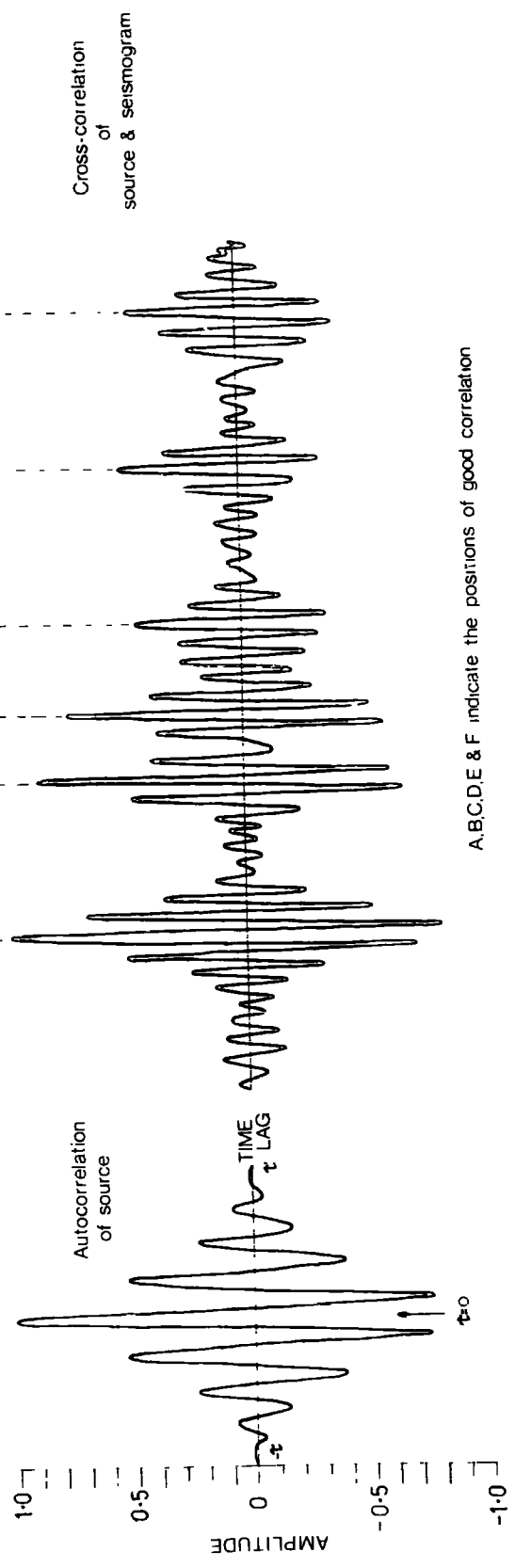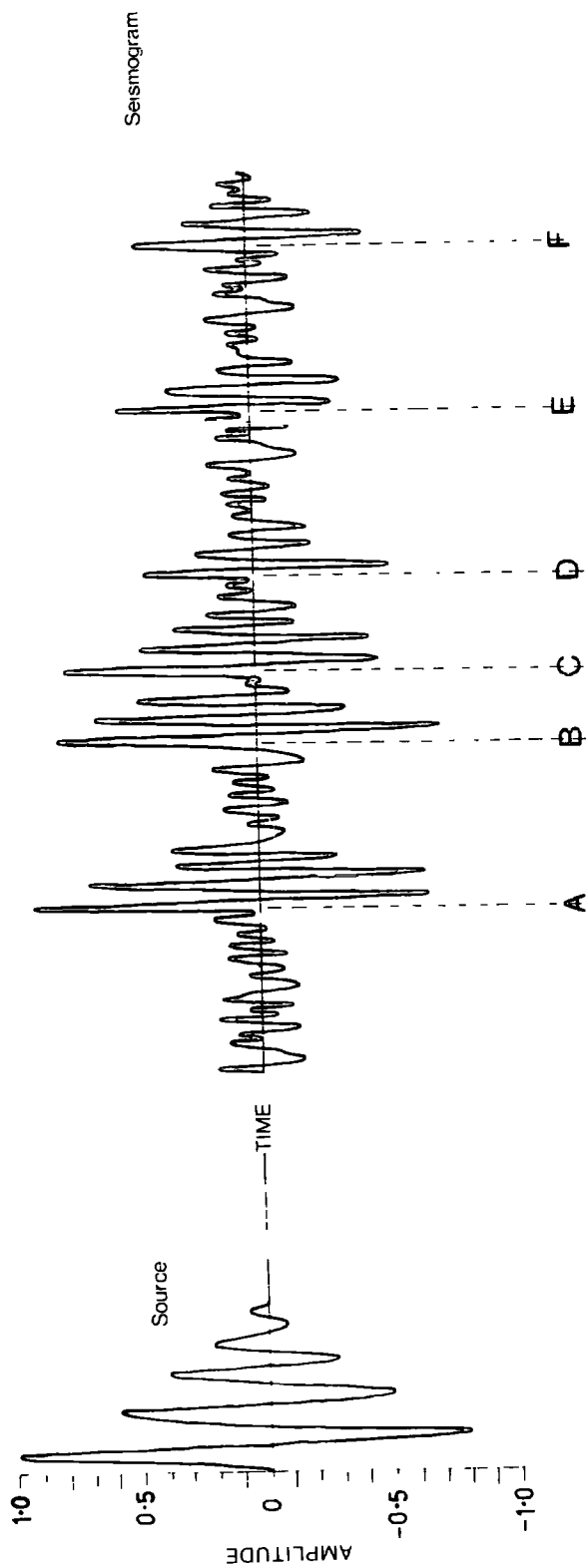
A,B,C,D,E & F indicate the positions of good correlation

AMPLITUDE

TIME

TIME
τ LAG

τ=0

A B C D E F

1·0
0·5
0
-0·5
-1·0

thus the cross-correlation of a(t) with b(t) is the same as the convolution of a(t) with the time reverse of b(t) (Robinson, 1967a).

1.3 Z-transform

The z-transform of an infinite wavelet is the power series in z whose coefficients are the coefficients of the wavelet (Robinson, 1967a). Thus the z-transform of the wavelet f(t) is:

$$F(z) = f_0 + f_1 z + f_2 z^2 + \cdots\cdots + f_n z^n$$
$$= \sum_{t=0}^{n} f_t z^t$$

The application of the z-transform is shown in later sections, where it is used to simplify the convolution of two or more functions of the type f(t).

1.4 Types of wavelet

The concepts of minimum, maximum, and mixed delay wavelets are most clearly explained by considering a couplet (1,k), where the coefficient 1 represents the amplitude at time t = 0, and k is the amplitude at t = τ . We may thus represent the z-transform of this couplet as (1+kz). From this function we may define the various delay wavelets:

$$|k| < 1 \quad - \quad \text{minimum delay}$$
$$|k| > 1 \quad - \quad \text{maximum delay}$$

and the convolution of one wavelet from each type of delay with a mixture of minimum and maximum delay will produce a mixed delay wavelet. An example of this would be:

$$(1,3) * (4,2) * (5,3) \quad = \quad (6, 40, 86, 60)$$

where the asterisk $*$ is used to indicate convolution.

In terms of energy build up the maximum delay wavelet never exceeds the build up of the minimum delay wavelet which is inherent in the fact that the energy of the minimum delay wavelet is concentrated towards the leading edge. With the mixed delay wavelet the energy build up is intermediate between the other two delays (Robinson, 1967a).

1.5 Amplitude and power spectra

a) Amplitude spectra

Considering the Fourier transform pairs of the wavelet a(t) and its frequency spectrum A(f) we have:

$$a(t) = \int_{-\infty}^{\infty} A(f)\, e^{2\pi i f t}\, df$$

and

$$A(f) = \int_{-\infty}^{\infty} a(t)\, e^{-2\pi i f t}\, dt$$

which may be written in polar form as:

$$A(f) = \left| A(f) \right| e^{i\phi(f)}$$

where $\phi(f)$ is the phase spectrum and $\left| A(f) \right|$ is the amplitude spectrum.

For computational purposes this equation is more easily handled in the form:

$$A(f) = \left[\sum_{t=0}^{N} \left[\left(a(t)\cos 2\pi f t \right)^2 + \left(a(t)\sin 2\pi f t \right)^2 \right] \right]^{\frac{1}{2}}$$

(Robinson, 1967a and 1967b).

An example showing the amplitude spectra of an air-gun wavelet is shown in Fig. 1.3.

b) **Power spectra**

The use of the power spectra, a definition of which is given below, is widespread throughout this work. Particularly important are its uses for the derivation and application of the predictive decomposition theory, and for signal recognition in noise where the power spectrum of the source wavelet and seismogram is required. Derivation of the power spectrum is now given.

The Wiener-Khintchne theorem represents the autocorrelation function as:

$$\phi(t) = \int_{-0.5}^{0.5} e^{2\pi i f t} \, d\Lambda(f)$$

where the function $\Lambda(f)$ is called the spectral distribution function, a real monotonically non-decreasing function of frequency f.

It is usual to normalize the spectral distribution function to make the lower value equal to zero, i.e. $\Lambda(-0.5) = 0$, resulting in the upper limit equalling the power.

The limits -0.5 to 0.5 of the above come about from the following: the z-transform of the signal b(t) is defined as:

$$B(z) = \sum_{t=-\infty}^{\infty} b_t z^t$$

letting $z = e^{-2\pi i f}$ we have:

$$B(f) = B\left(e^{-2\pi i f}\right) = \sum_{t=-\infty}^{\infty} b_t e^{-2\pi i f t}$$

Now since t is an integer the exponent function of the above is periodic with period unity, i.e.

$$e^{-2\pi i (f+1)t} = e^{-2\pi i ft}$$

thus the spectrum is also periodic with period unity, i.e.

$$B(f+1) = B(f)$$

Therefore it is only necessary to deal with one period of the spectrum, i.e. confine B(f) to $-0.5 \leqslant f \leqslant 0.5$ (Robinson, 1967a).

If the process is real then $\emptyset(t)$ is real and symmetric which means that $\Lambda(f)$ is real and symmetric, i.e.

$$d\,\Lambda(f) = d\Lambda(-f)$$

Thus the equation above becomes:

$$\emptyset(t) = 2 \int_{-0.5}^{0.5} \cos 2\pi ft \; d\,\Lambda(f)$$

Robinson (1967c) has shown that we may relate the function $\Lambda(f)$ to the power spectrum $\Phi(f)$ by the relationship:

$$\Phi(f) = \frac{d\,\Lambda(f)}{df}$$

thus the equation reduces to:

$$\emptyset(t) = 2 \int_{0}^{0.5} \Phi(f) \cos 2\pi ft \; df$$

Expressing the inverse relationship of this in its most common found form we obtain the relationship for the power spectrum as:

Fig. 1.3 Power and amplitude spectra

In the uppermost diagram is shown the air-gun wavelet from which
are derived its power and amplitude spectra plotted below.

Also shown are the power and amplitude spectra of the same
wavelet after the application of a Hanning window to the source.

Input Wavelet — Air Gun Source

Amplitude Spectra

Amplitude Spectra
with a
Hanning Window

Power Spectra

Power Spectra
with a
Hanning Window
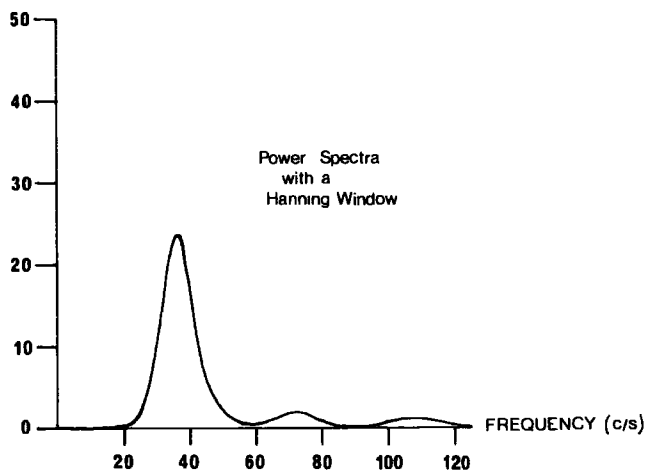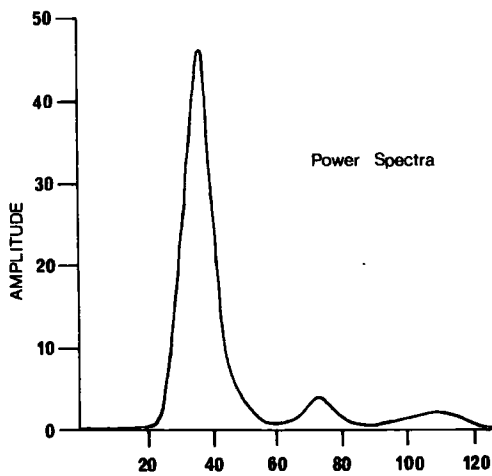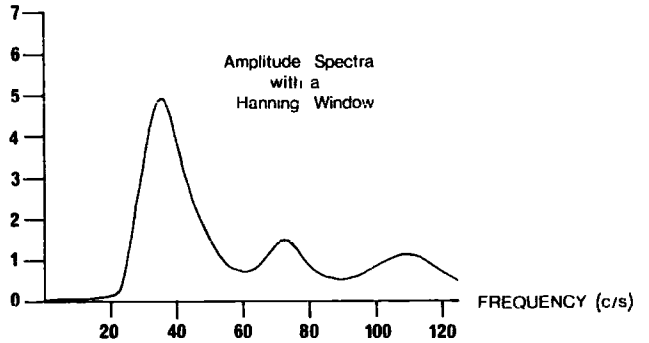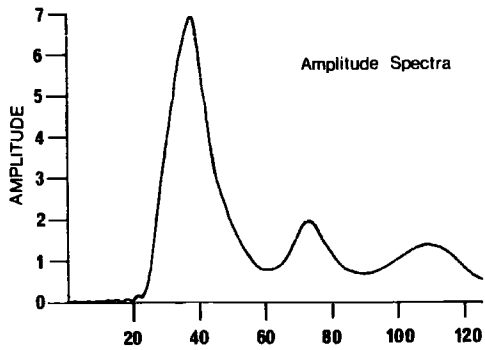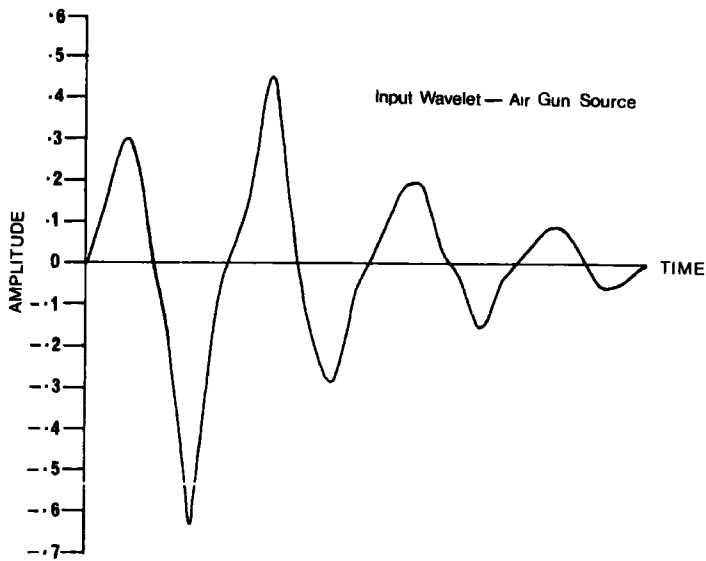
$$\overline{\Phi}(\omega) = \phi(o) + 2 \sum_{t=1}^{\infty} \phi(t) \cos \omega t$$

where:
$$\overline{\Phi}(\omega) \geqslant 0 \ , \ \text{for} \ -\pi \leqslant \omega \leqslant \pi$$

Since the signal that is produced is normally of finite length we may approximate the expression for $\overline{\Phi}(\omega)$ to:

$$\overline{\Phi}(\omega) = \phi(o) + 2 \sum_{t=i}^{T} \left(1 - \frac{t}{T} \right) \phi(t) \cos \omega t$$

(Finetti et.al., 1971)

Examples showing the power spectrum of an air-gun wavelet are shown in Fig. 1.3.

1.6 Truncation errors and the use of windows

These truncation effects were first considered by Blackman and Tukey (1958) and more fully by Jenkins and Watts (1968).

Considering a signal a(t) of infinite length, and its corresponding truncated part that is sampled $a_s(t)$ we have the relationship:

$$a_s(t) = a(t) \ d(t)$$

where d(t) is the data or lag window. Now from the frequency convolution theorem [Hsu (1967), p125] we have:

$$F\left[a_s(t) \right] = \int_{-\infty}^{\infty} A(y) \ Q(f-y) \ dy$$

The function $Q(f)$ is commonly known as the spectral window. Therefore truncating $a(t)$ results in its spectrum being filtered by $Q(f)$. Ideally $Q(f)$ should equal unity so that the filtering effect is minimized, i.e. we should sample an infinite length of $a(t)$.

Diagrams from Jenkins and Watts (1968) and Blackman and Tukey (1958) show several types of spectral window, with two marked features standing out; 1) those approximating to the ideal situation of $Q(f)=1$, i.e. a narrow central peak, having large side lobes causing instability, and 2) windows with a broad peak, having smaller side lobes but loss of finer detail.

Three major types of windows that are commonly applied to seismic data are the Bartlett, Hanning and Hamming windows. The mathematical formulation of these is as follows:

Bartlett:-

$$D_1(\tau) = 1 - \frac{|\tau|}{T_m} \qquad |\tau| < T_m$$

$$= 0 \qquad |\tau| > T_m$$

$$Q_1(f) = T_m \left(\frac{\sin \pi f T_m}{\pi f T_m} \right)^2$$

Hanning:-

$$D_2(\tau) = 0.5 + 0.5 \cos \frac{\pi \tau}{T_m} \qquad |\tau| < T_m$$

$$= 0 \qquad |\tau| > T_m$$

$$Q_2(f) = 0.5 Q_0(f) + 0.25 \left[Q_0 \left(f + \tfrac{1}{2T_m} \right) + Q_0 \left(f - \tfrac{1}{2T_m} \right) \right]$$

Hamming:-

$$D_3(\tau) = 0.54 + 0.46 \cos \frac{\pi \tau}{T_m} \qquad |\tau| < T_m$$

$$= 0 \qquad |\tau| > T_m$$

$$Q_3(f) = 0.54 Q_0(f) + 0.23 \left[Q_0 \left(f + \tfrac{1}{2T_m} \right) + Q_0 \left(f - \tfrac{1}{2T_m} \right) \right]$$

where : $\quad Q_0(f) = 2T_m \cdot \dfrac{\sin 2\pi f T_m}{2\pi f T_m}$

<u>Fig. 1.4   Spectral and lag windows</u>

Examples shown are the Bartlett, Hanning and Hamming windows.
For each is drawn the spectral window $Q_i(f)$ and lag window $D_i(\tau)$.
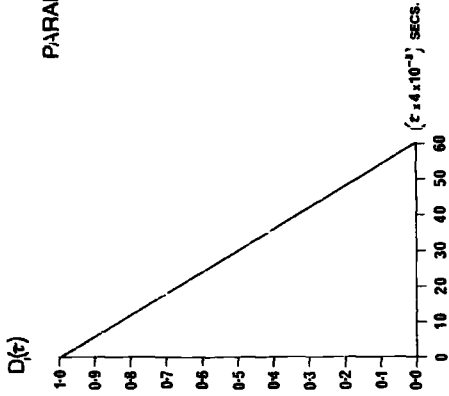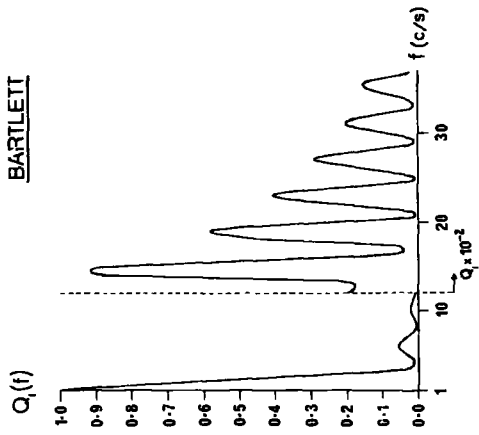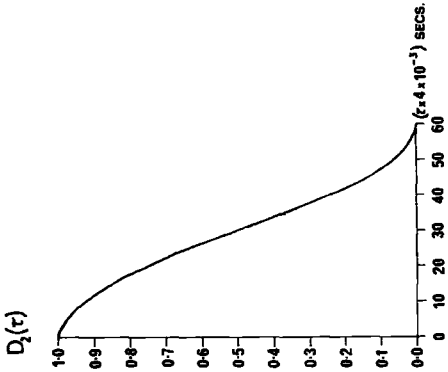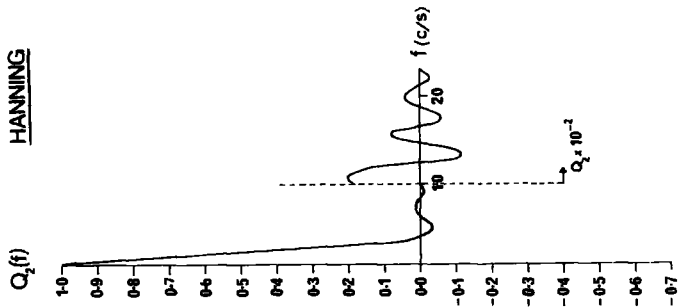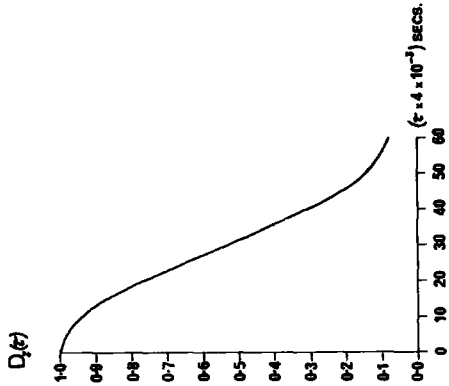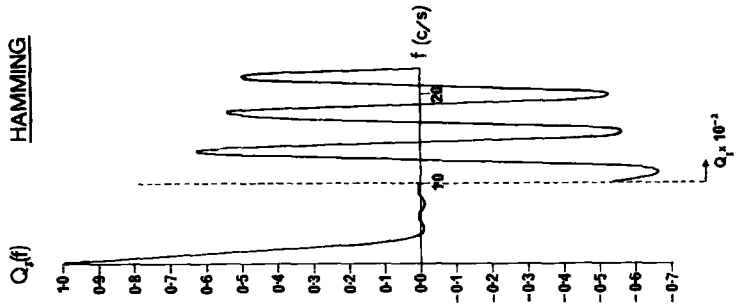
T_m is the window length and τ is the time lag.

$Q_i(f)$, the spectral window, is defined as the Fourier transform of $D_i(\tau)$, the lag window.

Ideally the main lobe $Q_i(f)$ should be close to $f = 0$, whilst side lobes should be as small as possible. To obtain the first condition $D_i(\tau)$ should be flat, but for the second $D_i(\tau)$ should be smooth and gently tapered. Since $D_i(\tau)$ should vanish when $|\tau| > T_m$ a compromise between the two conditions has to be made. The three windows described above try to compromise these two requirements and are shown in Fig.1.4. In all cases the functions $D_i(\tau)$ and $Q_i(f)$ are computed for a window length $T_m = 0.24$ seconds, and a sampling interval of 4 m.secs.

The Bartlett spectral window has the best approximation to the requirement that $Q_i(f)$ should be close to $f = 0$, although it has the highest side lobes of the three. Although the primary side lobes of the Hamming spectral window are smaller than those of the Hanning spectral window they do not fall off so rapidly.

Throughout the remainder of this work the Hanning window is used as it appears to work quite satisfactorily. Examples of the Hanning window applied to a seismic wavelet (air-gun) are shown in Fig.1.3. Also shown is the effect on the autocorrelation function and power spectrum of the wavelet before and after the application of the Hanning window to the seismic wavelet.

1.7 Introduction to noise theory

This section contains some of the concepts and definitions of the types of noise encountered during marine seismic profiling. Also included

is the general characterization of random signals and other factors that
result in the general degradation of the seismic signal.

Noise to varying degrees is an ever present problem in the reception
of signals, the received data consisting of a mixture of signal, s(t),
and noise, n(t). Throughout this, and subsequent work, the noise is
assumed to be additive, i.e. the received data r (t) is of the form:

$$r(t) = s(t) + n(t)$$

(Robinson, 1967a)

1.7.1 The stochastic and ergodic processes

Considering a digital signal x_t , the set or ensemble of all
possible signals is collectively referred to as the process $\{x_t\}$. The
probability distribution of the sample points over the sample space will
determine the probability distribution of sample functions over the
ensemble. The probability system, comprising the sample space, the
ensemble and the probability distribution function is called a random
process. Such a process is commonly known as a stochastic process (Lathi,
1968). The random features may be due to the physical model, or effects
that are undesirable and cannot be treated separately. Another class of
random process is the stationary stochastic process. The process may be
termed 'stationary' if its statistical properties do not change with time.
Thus for a stationary process the probability density function is independ-
ent of time. It is not easy to determine whether or not a process is
stationary; if the probability densities depend upon the choice of a time
origin, then the process is non-stationary.

In the above processes the complete statistics have to be obtained

from an ensemble of sample functions. If the complete statistics can be

determined from any one sample function then the process is called ergodic.

Thus the statistics over a long time interval for any one signal are then

the same as the statistics over the ensemble of all possible signals at

any one time instant (Robinson, 1967a, Lathi, 1968). Since it is possible

to determine only time averages from a single sample function, it is

obvious that in an ergodic process the time averages must be identical

with ensemble averages. The ergodic assumption implies that any given

member of the ensemble takes on all possible values in time with the same

relative frequency that an ensemble will take at any given instant (Lathi,

1968).

1.7.2 Autocorrelation and power spectra

For an ergodic process the power-density spectrum of any sample

function is given by the Fourier transform of the autocorrelation function,

although it must be noted that the power-density spectrum is not a

complete measure of the signal but is just an average parameter of the

signal. This arises because the power-density spectrum by definition

is a power-density averaged over a large time interval. For ergodic

signals all the sample functions have the same averages and hence the

power-density spectra of all sample functions are identical.

If a stationary process is not ergodic then the sample functions

are not statistically equivalent and each sample function has a different

time autocorrelation and hence a different power-density spectrum. For

the ergodic random process each of its sample functions has the same

power density spectrum, and hence the ensemble averages of the power

density is the same as that of any of the sample functions.

For a given process there is a unique autocorrelation function but the converse is not true, the autocorrelation function corresponding to a large number of different processes. This is due to the autocorrelation function not being a complete measure of a random process but rather one of the average parameters (Robinson, 1967a, Lathi, 1968).

1.7.3 Random signals

During seismic profiling many unwanted signals, or noises, are encountered most of which may be regarded as approximations of stationary stochastic processes. Described below are some of these signals.

One special type of noise which is extremely important is white noise. By definition white noise is a stationary stochastic process containing all frequencies in equal strength, thus causing its power spectrum to be uniform over the entire frequency range. White noise (in continuous time) is a physically non-existant phenomenon since it requires infinite power, although it adequately represents broadband noise sources such as thermal noise (Robinson, 1967a). The autocorrelation function of white noise is in principle similar to the time function of a unit pulse. White noise is thus identical to a random sequence of unit pulses (Lange, 1967).

There are two major types of white noise: 1) independent white noise process from which successive observations represent a sequence of independent random variables from a fixed probability distribution function; and 2) uncorrelated white noise process in which the random variables are

assumed to be uncorrelated in pairs. That is, considering the random

variables $\cdots\cdots\cdots x_t \, , \, x_{t+1} \, , \, x_{t+2} \, , \, \cdots\cdots\cdots$, we have:

$$E\left\{x_t x_s\right\} = E\left\{x_t\right\} E\left\{x_s\right\} \qquad t \neq s$$

(Lathi, 1968, Lang, 1967).

A useful definition which follows on from this is prewhitening. Compensation to make the power spectrum of the signal transmitted or recorded more constant to that analysed is called prewhitening. Ideally this would mean bringing the spectrum close to that of white noise, although all that is needed in practice is to make the rate of change of the power spectrum with frequency to be relatively small. Prewhitening of the data after equally spaced digitization helps overcome the problem of the side lobes that are encountered with the spectral windows (Blackman and Tukey, 1958).

Other types of noise which may be included in this work are: 1) thermal noise, which is the result of the random motion of free electrons in a conductor and which may be regarded as the physical realization of the mathematical concept of white noise; 2) shot noise, which is due to the random emission of electrons in the elctronic circuitry (amplifiers and filters); and 3) ship noise, which may be caused by the ship's engines and wave surface noise.

1.7.4 Amplitude considerations

a)   Acoustic impedance:

The acoustic impedance controls the transmission of energy from one

medium to another and the ratio of reflected to incident energy. If the acoustic impedance of two adjacent media differ considerably, almost no energy is transmitted and nearly perfect reflection occurs. The amplitude of a seismic reflection is thus dependent upon the product of its own reflection coefficient with the product of all the two-way transmission coefficients of the interfaces above it. The larger the reflection coefficient, the greater is the transmission loss (Heiland, 1968).

b)   Spherical divergence;

This acts to diminish seismic amplitudes at a distance from the source , but does not involve any loss of seismic energy, merely a spreading of it over a greater area of wavefront. Spherical divergence in itself conveys no geological information and so has to be compensated for normally by multiplying each sample by a factor proportional to the depth to which the arrival has come from (White, 1965, Heiland, 1968).

c)   Dispersion:

Selective scattering is due to reflections and refractions on prominent irregularities. The attenuation due to scattering increases rapidly for high frequencies, since the dimensions of the disturbing objects become a controlling factor compared with the wavelength. This helps explain why some materials invariably act as a high-cut filter to seismic signals, applying a strong attenuation at all frequencies higher than about 100 c/s. If the medium also happens to be slightly dispersive, then the pulse phase velocity also changes progressively as the shorter wavelengths are eliminated. In most cases this results in a gradual increase in velocity as the pulse moves outward (Grant and West, 1965, Heiland, 1968).

d)   Absorption:

Absorption diminishes seismic amplitudes, as a function of the distance travelled, by an irreversible conversion into heat. Such losses are frequency selective. This is due to the absorption coefficient increasing with the second power of the frequency, hence high frequencies are largely eliminated with increasing distance from the source and the low frequencies are left over. Considering a single pulse, two features affect the peak amplitude: i) this decays as the higher frequencies are absorbed; and 2) decays as the pulse is lengthened by dispersion. The latter is due to the propagation velocity of the sinusoidal components being dependent on frequency, these components being in phase at the peak at the onset, but out of phase at later times (Grant and West, 1965, White, 1965, O'Doherty and Anstey, 1971).

Multiple reflection effects which tend to alter the shape and amplitude of the primary reflections from each seismic horizon are dealt with in detail in Chapter 3.

CHAPTER 2

2.1 Introduction

Some of the techniques developed for the removal of water-layer reverberations, more complex inter-layer multiples, and the general enhancing and recognition of signals in the seismogram require a prior knowledge of the source wavelet that is produced by the seismic source generator. In most instances throughout this work an air-gun system is used as the source of seismic energy, and for this air-gun wavelet derivation a program was kindly lent to the author by Mr. J. H. Peacock of the University of Durham. To test whether this derived wavelet was in fact a true representation of the air-gun source the theory of predictive decomposition was applied to a number of digitized seismic traces, which were obtained whilst reflection profiling in the north-east Atlantic. Digitization of these seismograms was performed by means of the facilities available on the IBM 1130 computer at Newcastle University. Finally in chapter 2 the theory and application of 'SIGREC' (Signal recognition in noise) is described, making use of the source wavelet function derived from the previous sections of chapter 2.

2.2 Source wavelet determination from predictive decomposition theory

The mathematics of this theory have been dealt with in great detail by Robinson (1967c), a brief summary of the equations used are given here.

From the previously derived formula for the autocorrelation function

$\phi_{aa}(\tau)$ of the seismogram a(t) we have:

$$\phi_{aa}(\tau) = \lim_{T \to \infty} \frac{1}{2T+1} \sum_{t=-T}^{T} a_{t+\tau} \cdot a_t$$

Using the autocorrelation function $\phi_{aa}(\tau)$ we then wish to determine the power spectrum $\Phi(\omega)$ defined on:-

$$\Phi(\omega) = \phi_{aa}(0) + 2 \sum_{\tau=1}^{T} \left(1 - \frac{\tau}{T}\right) \phi_{aa}(\tau) \cos \omega\tau$$

This function $\Phi(\omega)$ is a real function of ω such that:

$$\Phi(\omega) = \Phi(-\omega) \quad ; \quad \Phi(\omega) \geqslant 0 \quad , -\pi < \omega \leqslant \pi$$

The following conditions must also be satisfied:

$$\int_{-\pi}^{\pi} \Phi(\omega) \, d\omega < \infty$$

and

$$\int_{-\pi}^{\pi} \log \Phi(\omega) \, d\omega > -\infty$$

Under these conditions $\log \left[\Phi(\omega)\right]^{\frac{1}{2}}$ may be expressed in the real Fourier cosine series:-

$$\log \left[\Phi(\omega)\right]^{\frac{1}{2}} = \sum_{t=-\infty}^{\infty} \alpha_t \cos \omega t$$

where α_t , the Fourier coefficients are given by:

$$\alpha_t = \frac{1}{2\pi} \int_{-\pi}^{\pi} \cos \omega t \cdot \log \left[\Phi(\omega)\right]^{\frac{1}{2}} d\omega \qquad - (2.1.)$$

By definition of the z - transform of the signal b(t) $\left(B(z) \right)$, in section 1.3, and the fact that there are no singularities for $|z| \leqslant 1$ (for minimum delay), the function $B(z)$ may be represented in the power series form:

$$\log B(z) = \sum_{t=0}^{\infty} \beta_t e^{-i\omega t} = \beta_0 + \sum_{t=1}^{\infty} \beta_t \cos \omega t - i \sum_{t=1}^{\infty} \beta_t \sin \omega t$$

$$-(2.2.)$$

from equation 2.1 we have:

$$\log \left[\phi(\omega) \right]^{\frac{1}{2}} = \alpha_0 + 2 \sum_{t=1}^{\infty} \alpha_t \cos \omega t \qquad -(2.3.)$$

Thus taking the real and imaginary parts of 2.2 and 2.3, and then equating the Fourier coefficients we have the relationships:

$$\beta_0 = \alpha_0 \qquad \text{and} \qquad \beta_t = 2\alpha_t \qquad\qquad -(2.4.)$$

Now the power spectrum $\phi(\omega)$ of the seismogram a(t) is equal to the energy spectrum $|B(\omega)|^2$ of the wavelet b(t), i.e.

$$\phi(\omega) = |B(\omega)|^2$$

and writing the transfer function of $B(\omega)$ in the form:

$$B(\omega) = |B(\omega)| e^{i\theta(\omega)} = \left[\phi(\omega) \right]^{\frac{1}{2}} e^{i\theta(\omega)} \qquad -(2.5.)$$

we then have:

$$\log B(\omega) = \log \left[\phi(\omega) \right]^{\frac{1}{2}} + i\theta(\omega)$$

$$= \alpha_0 + 2 \sum_{t=1}^{\infty} \alpha_t \cos \omega t + i\theta(\omega) \qquad -(2.6.)$$

Equating the imaginary parts of 2.2 and 2.6:

$$\text{Im}\left(\log B(\omega)\right) = \theta(\omega) = -\sum_{t=1}^{\infty} \beta_t \sin \omega t$$

Using the relationships of 2.4 we are left with the equation for the minimum phase characteristic $\theta(\omega)$:

$$\theta(\omega) = -2 \sum_{t=1}^{\infty} \alpha_t \sin \omega t$$

Substituting 2.5 into the Fourier transform of the wavelet b(t) we have:

$$b(t) = \frac{1}{2\pi} \int_{-\pi}^{\pi} B(\omega) e^{i\omega t} d\omega \qquad b(t)=0 \text{ for } t<0$$

$$= \frac{1}{2\pi} \int_{-\pi}^{\pi} \Phi(\omega)^{\frac{1}{2}} e^{i(\omega t + \theta(\omega))} d\omega$$

This reduces to the equation required for calculating the source wavelet coefficients:

$$b(t) = \frac{1}{\pi} \int_{0}^{\pi} \Phi(\omega)^{\frac{1}{2}} \cos\left(\omega t + \theta(\omega)\right) d\omega$$

On substitution we obtain the equation used in the computer program to calculate the coefficients b(t):

$$b(t) = \frac{1}{\pi} \int_{0}^{\pi} \Phi(\omega)^{\frac{1}{2}} \cdot \cos\left\{ \omega t - \frac{2}{\pi}\left(\sum_{t=1}^{\infty} \left[\int_{0}^{\pi} \cos\omega t \cdot \log\Phi(\omega) d\omega \right] \sin\omega t \right) \right\} d\omega$$

Fig. 2.1 Predictive decomposition theory

In the upper two diagrams an air-gun wavelet has been used to test the theory, the output showing its application has been efficient at reproducing the input.

The lower diagrams verify that the pressure/depth/periodicity relationships of Fig.2.2 are successful in formulating the source wavelet that has been used to derive the recorded input seismogram.

INPUT

AIR-GUN WAVELET
BAND PASS FILTERED
20-100 c/s

AMPLITUDE

5
4 -
3
1
r
-1 -
-2
-3 -
-4 -
-5
-6

t
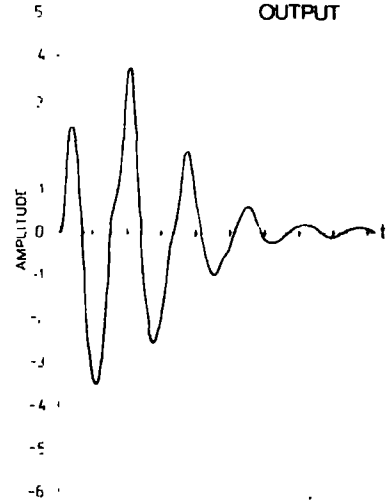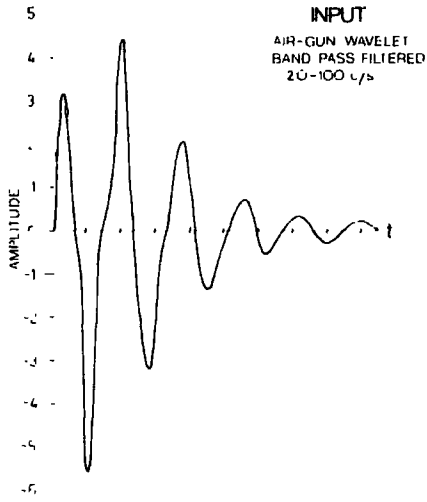
An air-gun wavelet is used as input to predictive
decomposition theory as a test run the output is
shown on the right & shows a good representation
of the input on the left

OUTPUT

AMPLITUDE

5
4 -
2
1
0
-1
-2
-3
-4
-5
-6

t

INPUT

recorded using an air-gun source

AMPLITUDE

50
40
30 -
20 -
10 -
0
-10
-20 -
-30 -
-40 -
-50 -

OUTPUT from pressure depth
relationships of fig 2 2

Parameters used

DEPTH = **18** metres
FREQUENCY = **36** c/s
PRESSURE = **3000** psi

AMPLITUDE

50 -
40
30
20
10
0
-10 -
-20
-30
-40
-50
-60
70

t
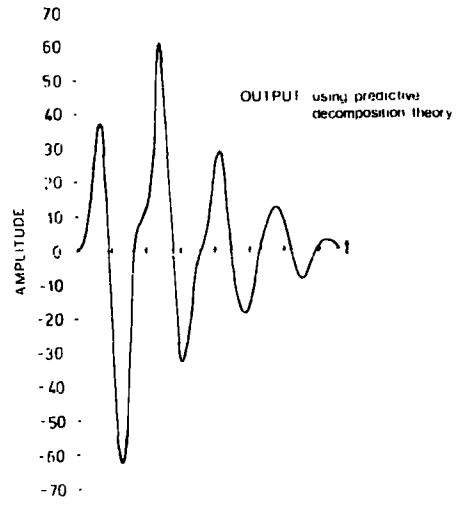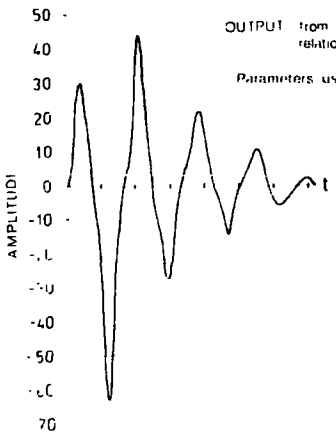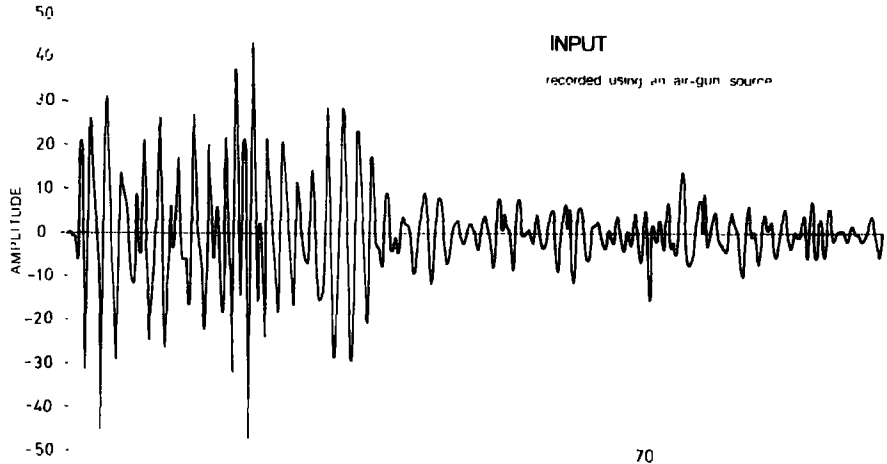
Both outputs show good agreement with one
another thus verifying the pressure-depth
relationship for deriving the source wavelet
is did

OUTPUT using predictive
decomposition theory

AMPLITUDE

70
60
50 -
40 -
30
20 -
10
0
-10 -
-20 -
-30 -
-40
-50 -
-60 -
-70 -

t

A program was developed to test this theory, a number of wavelets of known shape being compared with the output coefficients b(t). In Fig. 2.1 is shown a test signal band-pass filtered 20-100 c/s with the corresponding computed signal which agrees very well to the known characteristics of the signal. Tests were then carried out on digitized seismograms with air-guns as the source of energy (Fig.2.1). The derived wavelet from the pressure/depth/periodicity relationships shown in Fig.2.2 appear similar in character to the wavelet derived from the predictive decomposition theory, thus verifying that these relationships may be used to define the air-gun wavelet. In this case the theory has worked for a wavelet that is not minimum delay, since the air-gun source has been shown by Ziolkowski, 1971, to be a non minimum delay wavelet.

2.3 Pressure/depth/periodicity relationships

These relationships are shown in Fig.2.2 where pressure is plotted against depth for different periodicities. The pressure of the air-gun system will be monitored during the seismic profiling, whilst if the depth to shot/receiver from the sea/air interface is known then the periodicity may be determined from these plots.

Two simple techniques for determining the depth of the shot and receiver are now given, the latter being the most accurate of the two.
a)   As can be seen from the output (Fig.2.1) there appears to be a 'kink' on the second positive lobe of the wavelet which is indicative of the ghosting effect, which in turn is due to the depth of the air-gun and receiver with respect to the water/air interface. This will only give a rough estimate of the mean depth to the shot and receiver from the water/air interface.

b)   In this case use is made of the z - transforms of the signal $A(z)$, time delay due to the shot depth $\left(1-z^{t_1}\right)$, time delay due to the receiver depth $\left(1-z^{t_2}\right)$, and the random response of the earth $\mathcal{S}(z)$. This results in the z - transform of the signal received being of the form:

$$A(z)\left(1-z^{t_1}\right)\left(1-z^{t_2}\right)\mathcal{S}(z)$$

$$= A(z)\mathcal{S}(z) - A(z)\mathcal{S}(z)z^{t_1} - A(z)\mathcal{S}(z)z^{t_2} + A(z)\mathcal{S}(z)z^{t_1}z^{t_2}$$

Now let $A = A(z)$ and $\mathcal{S} = \mathcal{S}(z)$ for simplicity, the autocorrelation of this function is then:

$$F(z) = \left(A\mathcal{S} - A\mathcal{S}z^{t_1} - A\mathcal{S}z^{t_2} + A\mathcal{S}z^{t_1}z^{t_2}\right) * \left(A\mathcal{S} - A\mathcal{S}z^{-t_1} - A\mathcal{S}z^{-t_2} + A\mathcal{S}z^{-t_1}z^{-t_2}\right)$$

$$= (A\mathcal{S})^2 - (A\mathcal{S})^2 z^{-t_1} - (A\mathcal{S})^2 z^{t_1} - (A\mathcal{S})^2 z^{-t_2} + (A\mathcal{S})^2 - (A\mathcal{S})^2 z^{t_2}$$

$$+ (A\mathcal{S})^2 z^{-t_1}z^{-t_2} + (A\mathcal{S})^2 z^{t_1}z^{-t_2} + (A\mathcal{S})^2 z^{-t_1}z^{t_2} + (A\mathcal{S})^2 z^{t_1}z^{t_2}$$

$$- (A\mathcal{S})^2 z^{-t_2} + (A\mathcal{S})^2 - (A\mathcal{S})^2 z^{t_2} - (A\mathcal{S})^2 z^{-t_1} - (A\mathcal{S})^2 z^{t_1} + (A\mathcal{S})^2$$

Since the autocorrelation of the source $B(z) = A(z)A(z)$, and a random response $\mathcal{S}(z)\mathcal{S}(z) = 1$, then on collecting similar terms the equation above reduces to the form:

$$F(z) = B(z)\left[4 - 2z^{t_1} - 2z^{t_2} - 2z^{-t_1} - 2z^{-t_2} + z^{t_1}z^{t_2} + z^{t_1}z^{-t_2}\right.$$
$$\left. + z^{-t_1}z^{t_2} + z^{-t_1}z^{-t_2}\right]$$

The terms $-2z^{t_1}$ and $-2z^{t_2}$ will therefore appear as negative peaks superimposed on the autocorrelation of the received signals at

Fig. 2.2 Pressure/depth/periodicity relationships

A plot is made of the pressure of the air-gun system against depth of the shot/receiver for curves of different periodicity.

These relationships are used for the determination of the source wavelet produced by the air-gun system.

Curves For Different Periodicity In m.secs.

Depth In Metres
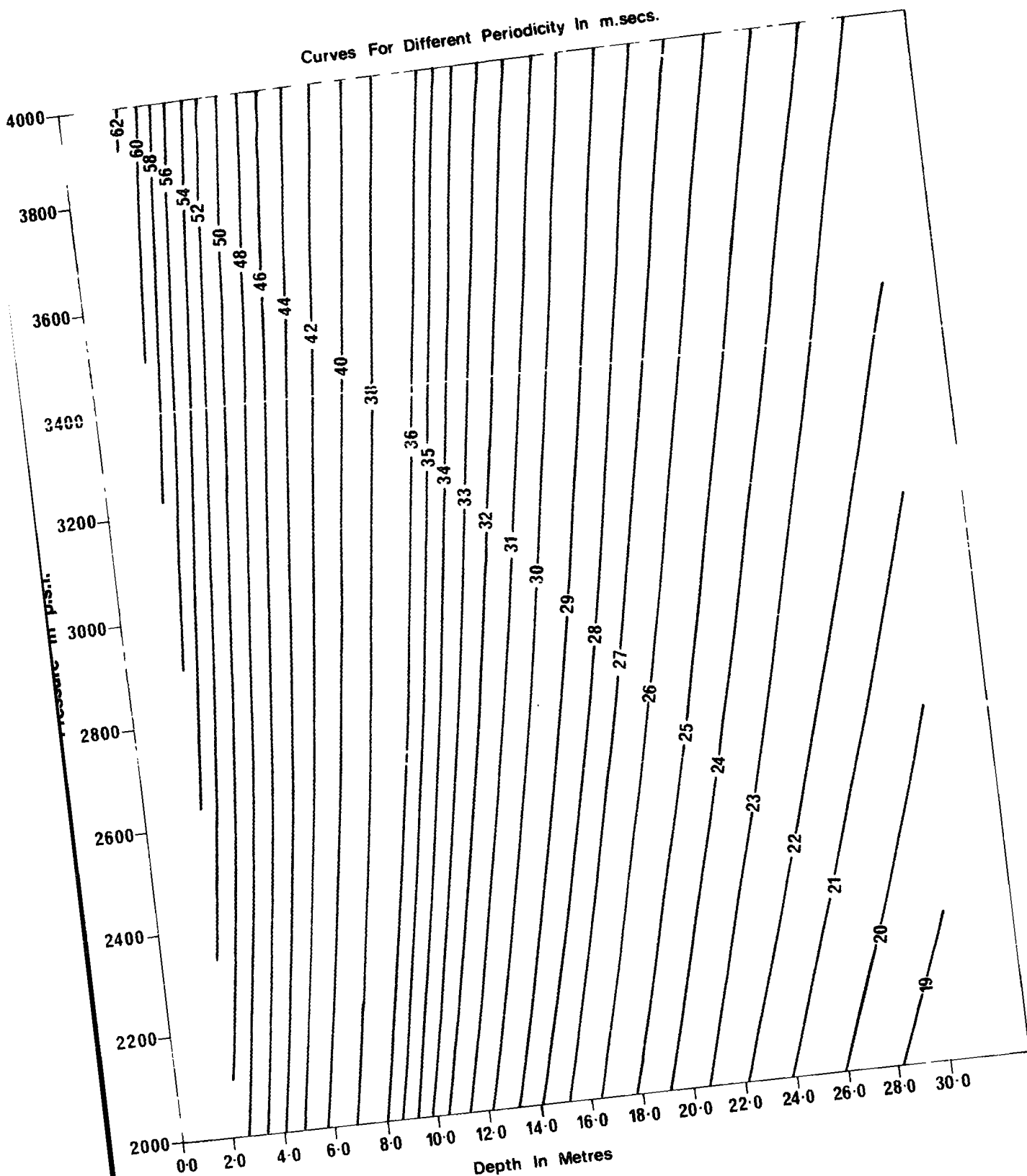
PRESSURE/DEPTH/PERIODICITY RELATIONSHIP

times t_1 and t_2, corresponding to the time delays associated with the depths of shot and receiver respectively. Measurement of these two times will therefore give the depths of the shot and receiver separately, and more accurately than the technique described in a) above.

Thus, having estimates of the depth of the air-guns and receiver, and knowing the pressure of output from the air-guns, it is then possible to optimize to the best wavelet by comparing the output with that derived from the predictive decomposition theory. In the case shown in Fig.2.1 the optimum wavelet was obtained with a pressure of 3000 p.s.i., a depth of 18 metres, and a frequency of 36 c/s.

Since this technique appeared satisfactory on the real data tested it was applied throughout whenever the source wavelet was required from the air-gun system.

2.4 Source wavelet determination using digital template analysis

This was first described by Linsser (1968) and further expanded by Dohr (1971). In both instances the idea is to obtain the best seismic wavelet that can be used to derive the seismogram, in each case there is a set of wavelets (templates) produced which are then tested for coincidence with the recorded wavelet. The template chosen is that which is found to have the greatest coincidence. The theory behind this technique is shown in Fig.2.3. This shows that the wavelet produced is simply the product between an harmonic function and a ramp function. Variation of the eccentricity of the ramp function will produce the required shift of the peak value of the template. In Fig.2.3 the harmonic function is a sine wave and the eccentricity of the ramp function

Fig. 2.3 Digital template analysis

   This indicates how the template may be generated using a

sinusoidal function and a ramp function. Also shown are various

templates that may be produced by varying the eccentricity of the

ramp function.

WAVELET PRODUCTION USING TEMPLATE ANALYSIS

Harmonic Function H(t)

Ramp Function R(t)

Template Wavelet H(t,R(t))
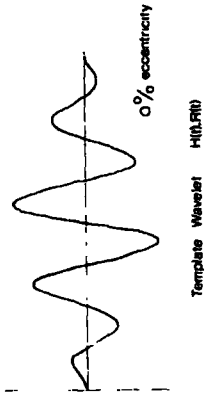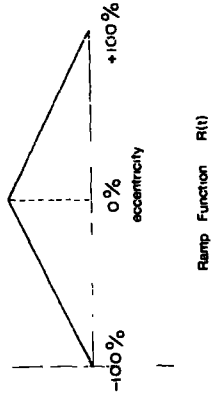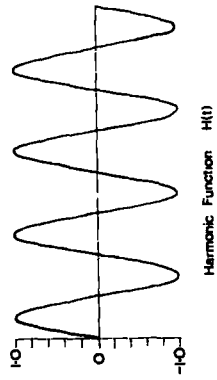
0% eccentricity

OTHER WAVELETS FOR VARIOUS ECCENTRICITIES

-80%   -50%   -20%

+80%   +50%   +20%
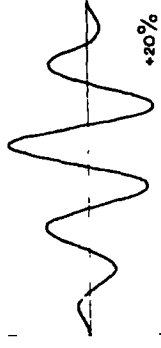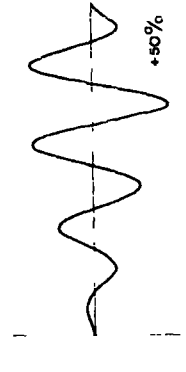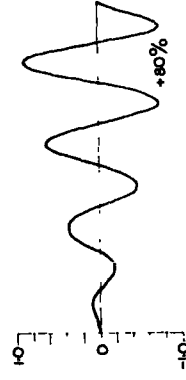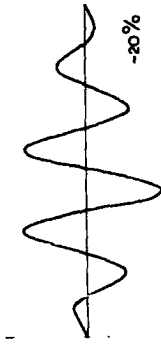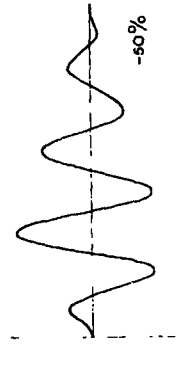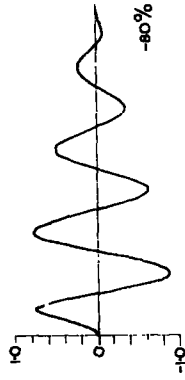
Fig. 2.4 Application of digital template analysis

Digital template analysis theory has been applied to two
examples, in the upper diagram to a smooth monotonic wavelet and
below to an air-gun wavelet. As can be seen the application to
the air-gun wavelet is less successful.

Single frequency wavelet

AMPLITUDE

T, time lag

----- Input function

——— Output from optimized template

Air gun wavelet

AMPLITUDE

T, time lag
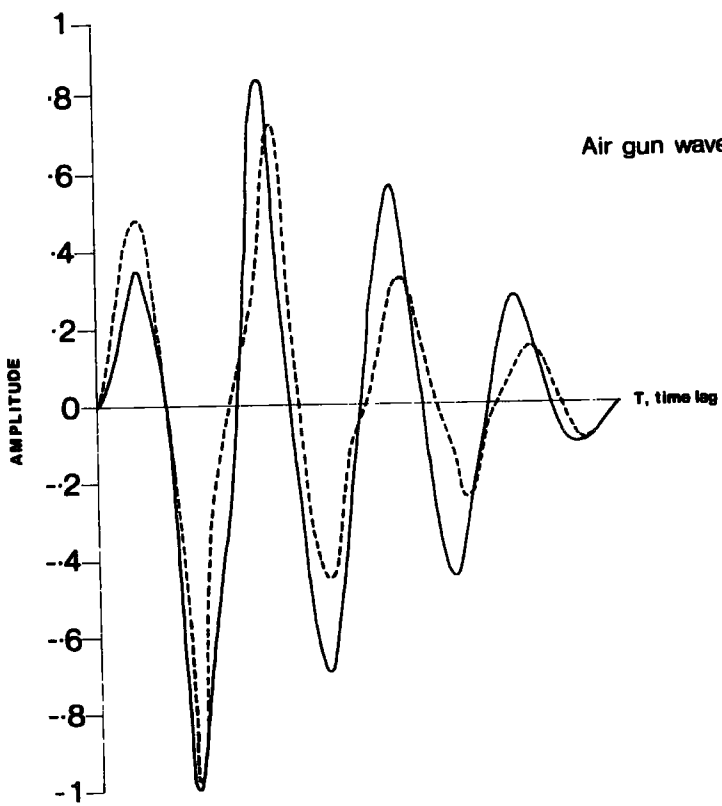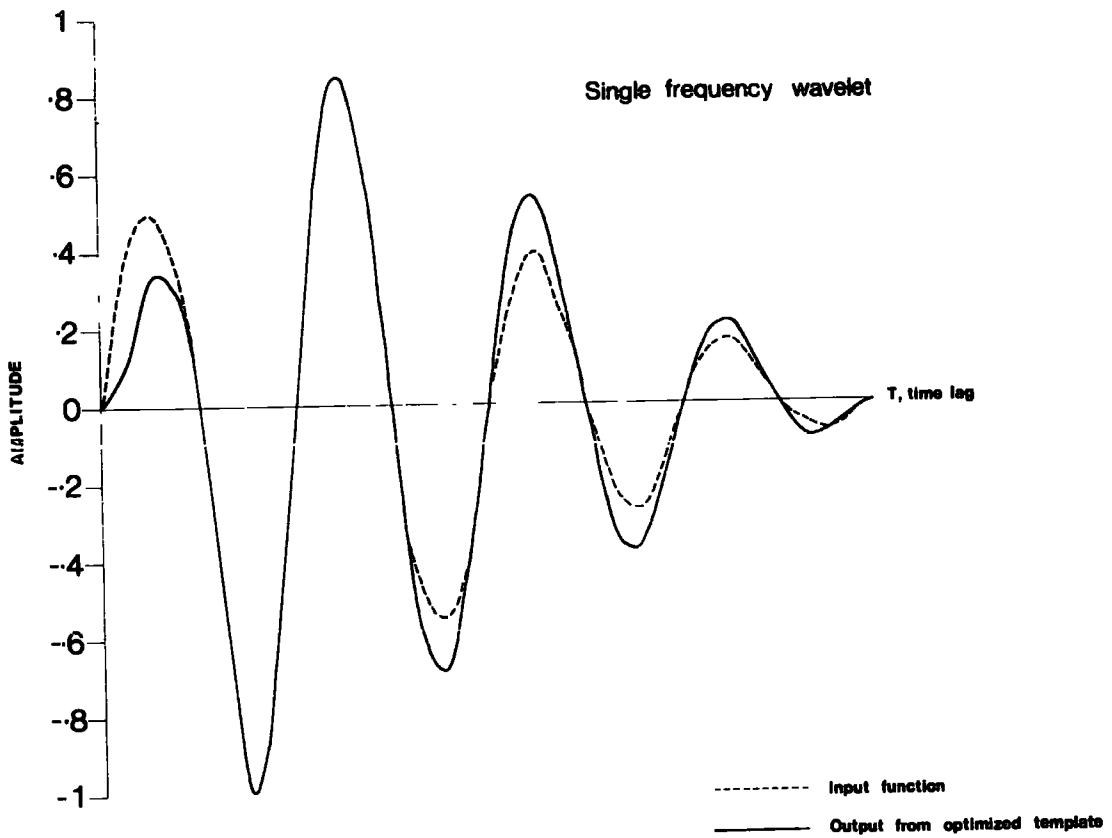
is varied with a constant window length.

In the method described by Dohr all the wavelets produced are compared in turn with each record. An optimization technique was used in this work to obtain the best fit and to replace the comparison test of Dohr. The optimization procedure used being the Rosenbrock technique, which is merely an extension of the simple method of co-ordinate variation (CERN program library, 1969). Parameters which are optimised are the eccentricity of the ramp function and frequency of the sinusoidal function. Having thus obtained these required optimized parameters for describing the template they may then be used as the initializing points for the optimization of templates for other seismograms, i.e. a test for example once every twenty shots of a seismic profiling line.

It was hoped that this method of optimization plus the digital template method of Dohr and Linsser could be used for the derivation of the air-gun source wavelet, but as Fig.2.4 shows, the technique only appears to work successfully with smooth monotonic wavelets. In the upper diagram of Fig.2.4 the wavelet fit is quite successful on the mono-tonic example, whilst in the lower diagram of Fig.2.4 the wavelet fit is not so good. This latter wavelet shows the 'ghosting' effect associated with most of the marine seismic records, obtained using an air-gun source, in the form of a large primary negative peak and a 'kink' in the waveform after this large negative peak. This 'kink' does not appear when the optimized template technique is applied. As a consequence this theory was not used in deriving thesource wavelet produced by an air-gun system, but it must be stated that this optimized template technique appears to have a good application to narrowband or monotonic wavelets.

2.5 <u>Signal recognition in noise ('SIGREC')</u>

This theory does not aim at the removal of multiples from a seismic record but for the recognition of signals within a seismic record. This is particularly important for the low signal to noise ratio cases.

Three functions relating to the properties of the seismic source, noise and seismic record are automatically computed, these are:
1) amplitude γ_1 ; 2) frequency γ_2 ; and 3) power spectrum γ_3 . The functions γ_2 and γ_3 are firstly computed for the seismic source and γ_1 for the noise, then a sampling window of length τ samples is run progressively one sample at a time down the seismogram and the functions γ_1 , γ_2 and γ_3 computed for each window in turn. A comparison is made between the functions for the signal and noise and those of the segmented seismic record to find if a signal is present within the sampled section of the record. (The segmented seismogram is defined as that part of the seismogram that is being considered within the sampling window τ). The resultant output is in the form of a histogram, Fig.2.5, which relates to the presence or absence of a seismic signal within the sampling window. If the signal is present then it is indicated by the shaded segments as shown in Fig.2.5. The mathematical formulation and build up to this histogram output is explained in the next section.

2.5.1 <u>Formulation of the 'SIGREC' functions</u>

The three relevant functions are now considered individually:-
1) <u>Amplitude, γ_1</u>

With γ_1 we have to compare the two basic equations defining the root mean square amplitude of the noise , ζ_0 , and segmented seismogram,

$\mathcal{S}_\nu$. These may be expressed as:

$$\mathcal{S}_\nu = \left[\frac{1}{\tau} \sum_{j=\nu}^{\nu+\tau} y_j^2 \right]^{\frac{1}{2}}$$

$$\mathcal{S}_0 = \left[\frac{1}{N'} \sum_{j=1}^{N'} y_j'^2 \right]^{\frac{1}{2}}$$

where:

y_j = sampled amplitudes of the segmented seismogram.

y_j' = sampled values of the section known only to contain noise.

N = total length of the seismogram to be processed (in samples).

N' = length of the record containing noise (in samples).

τ = length of the sampled segment, this window is moved progressively down the record, (in samples).

ν = 1, 2, 3, ... N-τ

A signal is recognised when $\delta_1 = 1$, defined on the relations:

$$\delta_1 = \begin{cases} 1 & \mathcal{S}_\nu > \mathcal{S}_0 \\ 0 & \mathcal{S}_\nu < \mathcal{S}_0 \end{cases}$$

2)   Frequency, δ_2

The frequency content f_i , of the seismic signal is compared with that of the sampled segmented seismogram, f_j' , to obtain the frequency function δ_2 . In this instance i and j are the spectral maxima. δ_2 is then defined by the relationships:

$$\delta_2 = \begin{cases} 1 & f_j' = f_i \\ 0 & f_j' \neq f_i \end{cases} \qquad i.e.\ j=i\ \text{for}\ i=1, M_s$$

where M_s = number of spectral maxima of the signal being considered.

δ_2 May be regarded as a 'back up test' for the more sensitive test function δ_3 (described below), since δ_2 tests for all the major frequencies, f_i, and not just a compatible dominant frequency.

3) Power spectra, δ_3

The signal power spectrum $\Phi_s(\omega)$ and segmented seismogram power spectrum $\Phi_r(\omega)$ are calculated from the basic equations:

$$\Phi_s(\omega) = \phi_{ss}(0) + 2 \sum_{t=1}^{T} \left(1 - \frac{t}{T}\right) \phi_{ss}(t) \cos \omega t$$

$$\Phi_r(\omega) = \phi_{rr}(0) + 2 \sum_{t=\nu}^{\nu+\tau} \left(1 - \frac{t-\nu}{\tau}\right) \phi_{rr}(t) \cos \omega t$$

where $\phi_{ss}(t)$ and $\phi_{rr}(t)$ are the autocorrelation functions of the signal and segmented seismogram respectively. T is the length of the signal and τ the length of each segment of the seismogram taken, i.e. sampling window length τ . If the total length of the seismogram to be processed is N then $\nu = 1, 2, \ldots N-\tau$

Normalizing $\Phi_s(\omega)$ and $\Phi_r(\omega)$ we then define the function μ_ν by:

$$\mu_\nu = \left| \Phi_r(\omega) - \Phi_s(\omega) \right|_{\omega_i - \Delta\omega}^{\omega_i + \Delta\omega}$$

μ_ν is therefore centred on ω_i , the maximum peak of the power spectrum of the signal, and is a comparison between the two power spectra within the window $2\Delta\omega$. $\Delta\omega$ may be taken as equal to $\omega_i - \omega_i'$ where ω_i' is the frequency value of the signal power spectrum at which the power drops to some percentage of the peak power at ω_i . The value of

$\Delta\omega$ may otherwise be supplied independently to the program by the user. (Polynomial curve fitting over the region $\omega_i \pm \Delta\omega$ is far more rigorous but is more time consuming).

Now we require that μ_ν should be less than some threshold value, i.e. there is a fit of points between the two power spectral curves in the region $\omega = \omega_i \pm \Delta\omega$. This threshold value was chosen to be 1/10th the value of $\overline{\phi}_s(\omega)$. Although this value 1/10th is arbitary it was found suitable when processing the seismic examples described in section 2.5.2.

Thus we have μ_ν defined on the threshold:

$$\mu_\nu < \overline{\phi}_s(\omega)/10 \qquad \text{for} \quad \omega = \omega_i \pm \Delta\omega$$

If we define the function n_ν equal to the number of sampled points within the spectral window $2\Delta\omega$ that obey the criterion above, we may then define the final relationship for γ_3 as:

$$\gamma_3 = \begin{cases} 1 & n_\nu > n_\beta \\ 0 & n_\nu < n_\beta \end{cases}$$

where n_β is the minimum number of points allowed within the window $2\Delta\omega$ for which $\mu_\nu < \overline{\phi}_s(\omega)/10$. The parameter n_β is supplied by the programmer at the onset of processing, and must be less than the number of sampled points within the window

The final displayed output of this technique is in the form of a histogram which is representative of whether all the functions γ_1, γ_2 and γ_3 have been satisfied, within the sampling window τ. If we

define the function that is output, γ_T , by the relationship:

$$\gamma_T = \gamma_1 + \gamma_2 + \gamma_3$$

then if all three functions γ_1 , γ_2 and γ_3 are satisfied, i.e. a signal is present, then $\gamma_T = 1$, otherwise $\gamma_T = 0$. If $\gamma_T = 1$ then a unit spike is output signifying a signal has been recognised, if $\gamma_T = 0$ then there is no output. Examples and description of this output are given in section 2.5.2 below.

2.5.2 Application of the 'SIGREC' technique

In Fig.2.5 the theory of signal recognition, 'SIGREC', has been applied to 20 synthetic seismic records where the signal to noise ratio is high. In all cases the signal has its primary frequency at 20 c/s (at 6dB $\pm$ 8 c/s), and the noise a primary frequency at 30 c/s (at 6dB $\pm$ 5 c/s). Fig.2.5.A. shows the synthetic records from which can be seen four layers, the third clearly showing a 'pinchout' at a depth of 2.4 kms. All seismic traces are fed individually into the program ('SIGREC') the output from which is shown in Fig.2.5.B. The black coloured sections on each individual trace, Fig.2.5.B, indicate the positions and extent over which a signal has been recognised, i.e. all the functions γ_1 , γ_2 and γ_3 have been satisfied for the signal to be present.

Layers 1 and 2 are clearly enhanced by this technique, the signals in both instances having been recognised over most of their extent. Layers 3 and 4 are again well defined, but since the signal to noise ratio is lower than for the first and second layers, they are not so prominent.

Figs. 2.5 & 2.6 Application of 'SIGREC'

These two figures show the application of signal recognition in
noise ('SIGREC') to two seismic sections of varying signal to noise
ratio.

Below each section is drawn the output from 'SIGREC' in the form
of, 1) a histogram representing the positions where the signal has
been recognized, and 2) a comparison of the known synthetic model with
that derived from 'SIGREC' theory.

A

SEISMIC SECTION TO BE ANALYSED
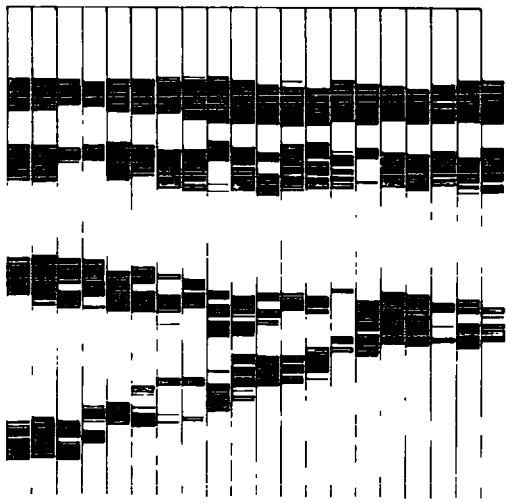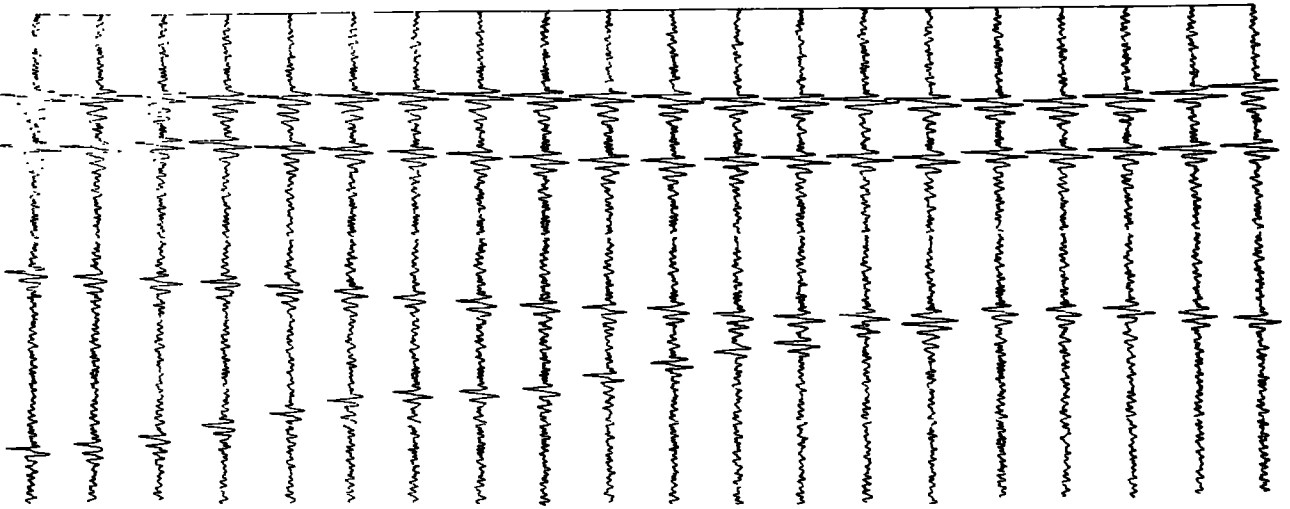
DEPTH
kms

−0−

−1−

−2−

−3−

LAYER 1

LAYER 2

LAYER 3

LAYER 4

B

HISTOGRAM OUTPUT SHOWING THE POSITIONS WHERE
THE SIGNAL HAS BEEN RECOGNIZED

C
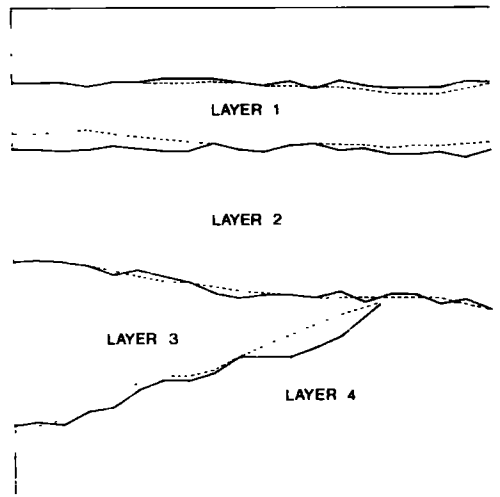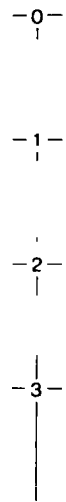
——— MODEL COMPUTED

·· ··· ···· ACTUAL MODEL

A

SEISMIC SECTION TO BE ANALYSED
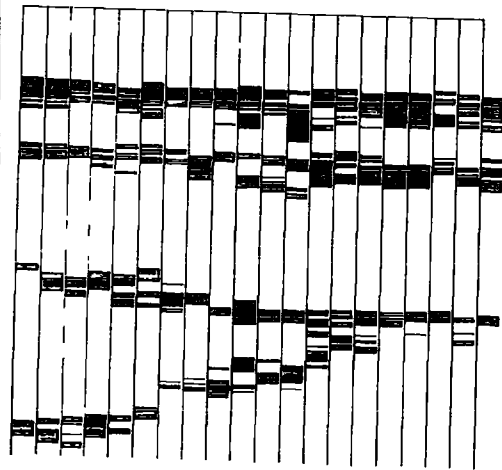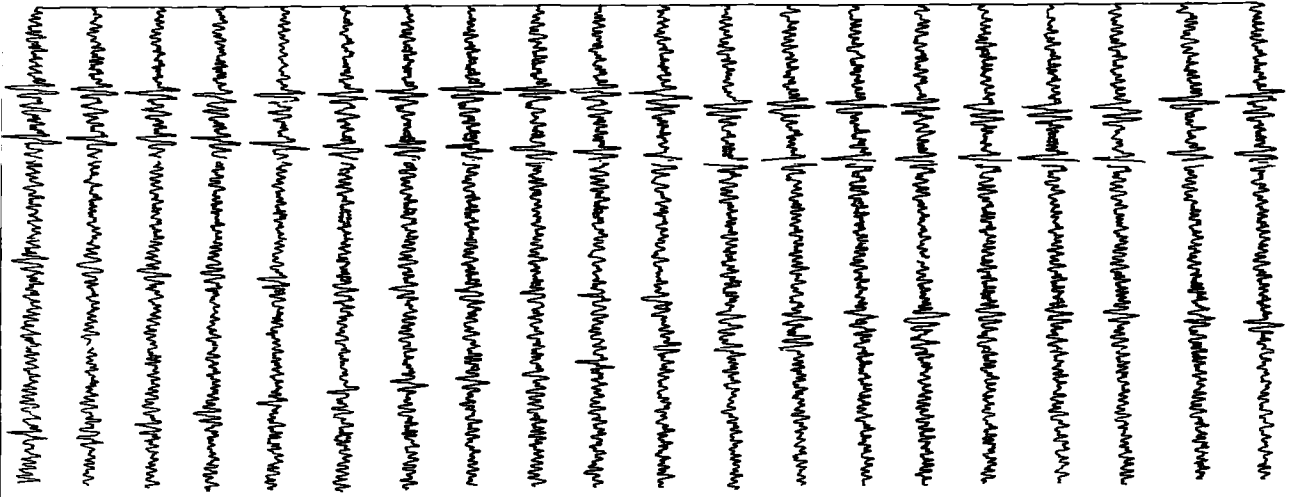
DEPTH
kms

-0-

-1-

-2-

-3-

LAYER 1

LAYER 2

LAYER 3

LAYER 4

B

HISTOGRAM OUTPUT SHOWING THE POSITIONS
WHERE THE SIGNAL HAS BEEN RECOGNIZED

C
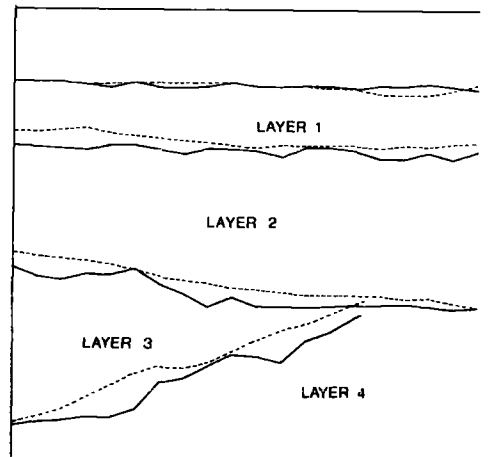
———— MODEL COMPUTED

---------- ACTUAL MODEL

The model that is known, from which the synthetic section was produced, is shown in Fig.2.5.C as the broken line. Unbroken lines indicate the position of the horizons that have been computed from the program. The upper seismic horizon of layer 1 is followed exceptionally well, whilst the layer 1/layer 2 interface has in most instances been recognised a little later. This delay in recognising the signal appears to be due to interference, within the sampling window, of the trailing edge of the first signal with the leading edge of the second. The trailing edge of the first has a slightly lower frequency and as a consequence γ_2 and/or γ_3 are not satisfied. This problem can be overcome by shortening the sampling window τ but in doing so the computation time is also found to increase and there is also a possibility that some of the properties of the signal may be removed from the sampling window. This latter fact becomes very important to consider when the sampling window length is very much less than the known length of the signal. As a consequence these two factors of window length and computation time have to be considered together to find the optimum. In this instant a sampling window close to the length of signal was found most suitable.

With the layer 2/layer 3 interface the computed model again follows the actual model closely, and also shows the 'pinchout' that occurs with layer 3. There is also good agreement with the layer 3/layer 4 interface, but as the layer 2/layer 3 interface is approached there is again a delay in the recognition of the seismic signal.

In the second example the same model for the production of the synthetic section has been used although in this case the overall signal to noise ratio is lower, (Fig.2.6.A). As a consequence of this lower

signal to noise ratio, the characteristics of the noise become more prominent and cause the functions γ_1, γ_2 and γ_3 mentioned in section 2.5.1, to be less readily satisfied. The result of this is clearly shown in Fig.2.6.C where all the horizons, except the first, appear to have the 'recognition' delay.

Fig.2.6.B shows the output from the program. Again all four reflecting horizons are seen, as is the 'pinchout' of layer 3, but the extent over which the signal is recognised has been reduced for all four horizons.

Finally the 'SIGREC' technique has been applied to two records of marine data obtained using an air-gun source (Fig.2.7). For this data a function γ'_T is output in the form of a histogram. The function γ'_T is equal to the function γ_T (section 2.5.2) summed over 20 successive sampling windows, and thus may be expressed in the form:

$$\gamma'_T = \sum_{i=\nu}^{\nu+20} \gamma^i_T \qquad \text{where} \quad \gamma^i_T = \begin{cases} 1 & \text{for } \gamma^i_1 = \gamma^i_2 = \gamma^i_3 = 1 \\ 0 & \text{otherwise} \end{cases}$$

where:

i = the particular window being summed.

$\gamma^i_T = \gamma_1 + \gamma_2 + \gamma_3$ for the ith window.

ν = 1, 2, ... N-τ

τ = window length in number of samples.

N = seismogram length in number of samples.

In the examples shown in Fig.2.7 the major peaks of the histogram have been correlated with those of the seismic record. The closely spaced arrivals P, Q, R, and P', Q', R' are quite clearly brought by this technique of signal recognition.

Fig. 2.7 'SIGREC' applied to marine data

Two marine seismic records are tested with the 'SIGREC' theory, the histogram output for each being shown above. The apparent signals that have been recognized for each record are indicated.

In this case the histogram output is the sum of 20 successive sampling windows.
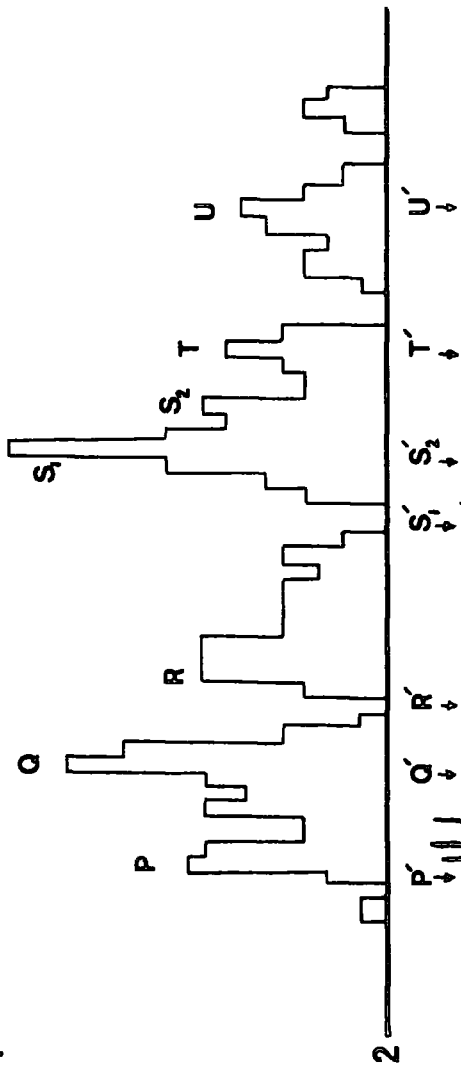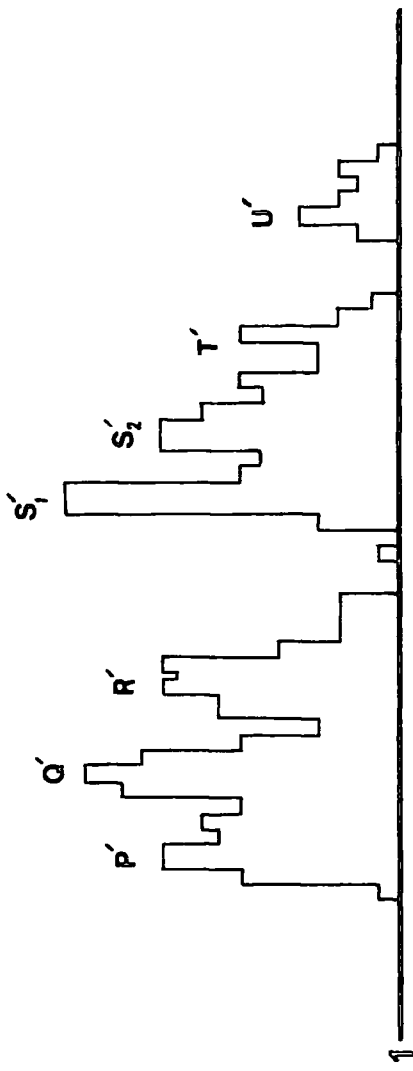
histogram output from
'SIGREC', where the major
peaks have been correlated
with signals on the records
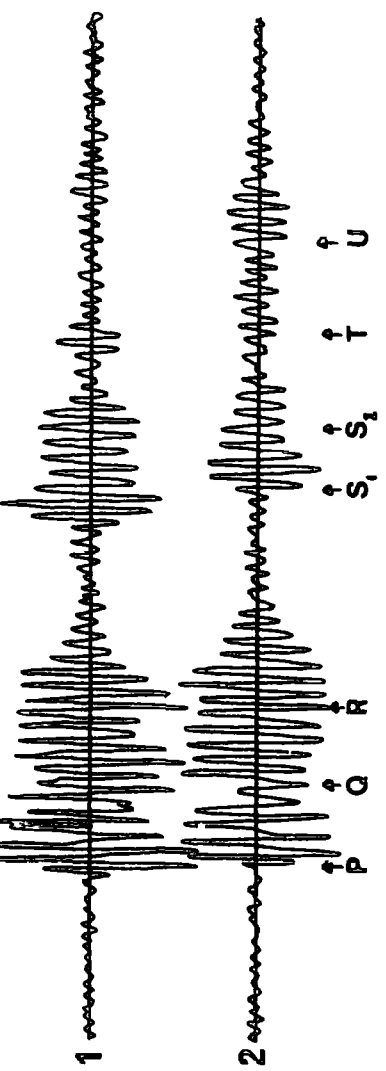
marine seismic records
from an air-gun source

2.5.3 <u>Efficiency of the 'SIGREC' technique</u>

For determining the efficiency of the 'SIGREC' technique a comparison was made between the signal to noise ratio and the extent of signal recognised. (The extent of the signal recognised is the percentage of the known signal length that has been detected by the theory). The relationship between the percentage of signal recognised and the signal to noise ratio is shown in Fig.2.8. The signal to noise ratio, and percentage of recognised signal length for each horizon, have been averaged over the complete length of that horizon for each of the seismic sections in Fig.2.5 and Fig.2.6 separately. As can be seen the most important feature is the exponential character of the curve, showing a slow increase in percentage of signal length recognised with signal to noise ratios greater than about 5 : 1.

Important in deriving this curve is the fact that the noise frequency content has remained constant throughout. If the frequency of noise approaches that of the signal then the functions γ_2 and γ_3 become far less reliable, both may be satisfied even though the signal is not present within the sampling window.

Fig. 2.8 Efficiency of the 'SIGREC' technique

The efficiency is defined by the percentage of the known signal length (time duration) that is recognised by the technique, and is plotted against varying signal to noise ratios.
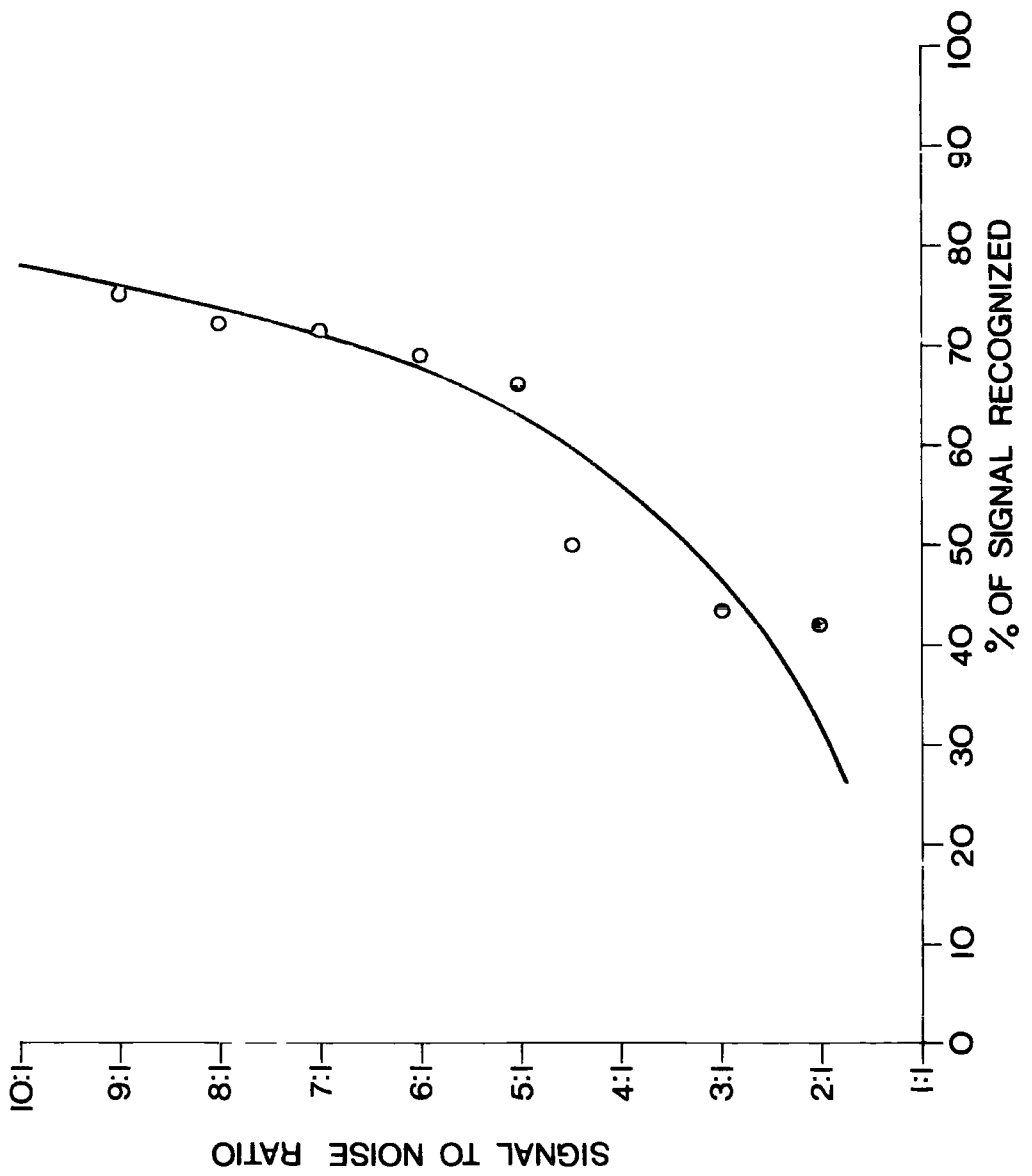
CHAPTER 3

3.1 Introduction

The basis of this chapter is the development and application of marine seismic multiple elimination techniques. An introduction to the inverse filter and spiking filter, which have applications to some of the multiple elimination methods developed is given prior to the formulation of the digital data processing techniques. All the techniques developed were tested on theoretical data and models, in most instances using an air-gun wavelet as the source function for deriving the seismograms. Some of the theories have been tried and tested before by previous workers, but further refinements have been introduced, and in sections 3.6 and 3.7 are described two new techniques for the removal of marine seismic multiples. In every instance these theories may be regarded as continuous digital processes.

Computer programs developed from these theories are listed after chapter 4, indicating the relevant input and output from each along with a simplified flow diagram for the most important methods. All programs are written in FORTRAN IV for use on the IBM 360 computer.

3.2 Inverse and spiking filters

Inverse filtering is a simple method for the removal of multiple reflections from seismic records, and as such is the basis for the development of many other more sophisticated techniques. The inverse filter, as described below, may be regarded as an elementary form of the optimized recursive filter developed in section 3.5, since complex

inter-layer multiples have not been considered in its derivation.
Application of the spiking filter to improve signal resolution is
particularly useful with the 'CHNS' and 'INTERCEPT' techniques
developed in sections 3.6 and 3.7. In both these instances the
efficiency of multiple elimination is found to be improved by applying
a spiking filter prior to processing the seismic trace. Both the inverse
and spiking filter are now considered in detail.

a)   Inverse filtering

Incoherent noise and unwanted coherent signals such as water-layer
multiples, inter-layer multiples and ghosts, are nearly always present
on the seismic traces all of which are required to be removed. The
mathematical expression for this may be represented in the form:

$$x_t = \sum_{\tau=0}^{\infty} a_\tau \, \mathcal{S}_{t-\tau} \qquad\qquad t_1 \leqslant t \leqslant t_2$$
$$t_2 - t_1 = record\ length$$

where x_t is the seismic record, a_t the source wavelet, and $\mathcal{S}_t$ a
stochastic component representative of the response of the earth
(Finetti, et.al., 1971).

As shown with the equation above the reflection seismogram can be
imagined to be formed by the convolution of the response function for a
layered earth with some constant waveform. The basic aim of inverse
filtering (or deconvolution) is to return from the recorded seismogram
to the ground response function $\mathcal{S}_t$. This type of filtering is
normally applied to the elimination of ghosts and water reverberations.
If we consider ghosting we may represent the Z -transform of this
effect as:

$$X(z) = 1 + cz^{\tau}$$

where c is the ghost at time τ . Thus using the convolution formulae
we obtain the ghost elimination filter required, F(Z). (Robinson, 1967a):
(Z - transform of input) (Z - transform of filter)=(Z - transform of
output)

$$\text{i.e.} \quad F(z) = \frac{1}{1 + cz^{\tau}}$$

For water reverberations the signal received represents successive
reflections from the water/air interface of the form:

$$\left(1, -c, c^2, -c^3, \dots \dots \dots \right)$$

where c is the reflection coefficient of the sea bottom. Summing this
in terms of the Z-transform we have:

$$\frac{1}{1 + cz^{\tau}} \qquad \text{for } |c| < 1$$

Thus the Z-transform of the water reverberation elimination filter is:

$$F(z) = \left(1 + cz^{\tau} \right)$$

When considering deep subsurface reflections the water layer acts as a
filter on both the down-going waves and up-going waves coming from the
deep horizons. Hence, a deep reflection is filtered by two cascade
sections representing the water layer. Therefore the overall Z-transform
is the square of the Z-transform due to a single pass, i.e.

$$F(z) = \left(1 + cz^{\tau} \right)^2$$

(Robinson, 1967a, Finetti, et.al., 1971).

As stated by Robinson (1967a) these formulae are far too simple for the true record since the seismic pulse is not a spike and multiples from the record are far more complicated. It must also be noted that the inverse of a finite, discrete, realizable and stable operator $\left(a_t \right)_0^T$ is in general a non-finite operator $\left(f_t \right)_{-\infty}^{\infty}$. This means that it becomes necessary to be able to compute the approximate inverse filter operator (Robinson, 1967a, Finetti, et.al, 1971). This approximation of the inverse filter by means of the least error energy is described in great detail by Robinson, 1967a.

Finally time varying deconvolution may be used to take account of the attenuation of the input waveform as it propagates through the media. On a reflection seismogram this attenuation results in a change with time of the character and frequency of the signal, and as such the seismogram should be treated as a non stationary random process. A fuller description is given by Clarke, 1968.

b) **Spiking filters**

The spiking filter may be regarded as a special case of the shaping filter in that it aims at formulating a spike as the desired output. The basic theory (Robinson, 1967b, 1967a) of these filters is as follows:

Input waveform	a_t	$t = 1, 2 \cdots\cdots\cdots n$
Desired output	d_t	$t = 1, 2 \cdots\cdots\cdots k$
Filter required	f_t	$t = 1, 2 \cdots\cdots\cdots m$
Actual output	b_t	$t = 1, 2 \cdots\cdots\cdots m + n$

As stated previously it is desirable to restrict the filter to a finite length. To obtain this approximation the energy of the error,

Fig. 3.1 Spiking filters

The spiking filter coefficients shown are derived from the
source wavelet and are then convolved with the seismogram to spike
the signals. These are shown at positions A, B, C, D, E and F.

Sea nogram

Spiked Seismogram

Source Wavelet

Spiking Filter
Coefficients
(derived from the source)
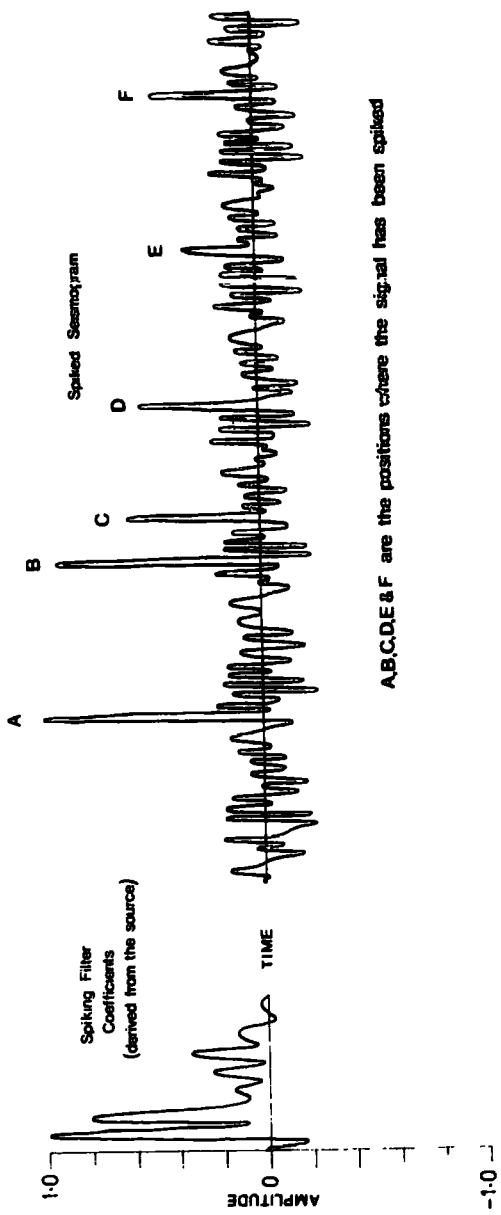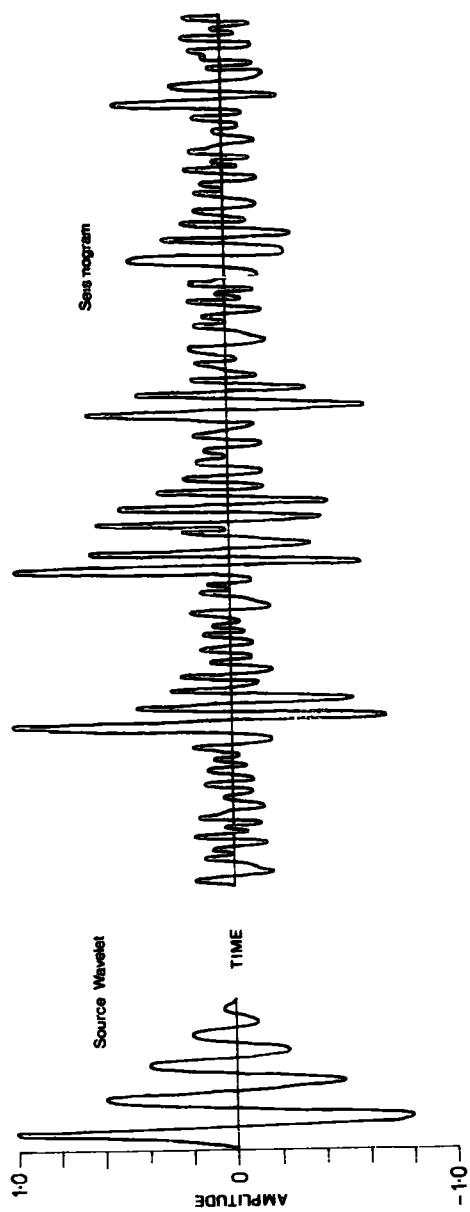
A,B,C,D,E & F are the positions where the signal has been spiked

ϵ_r is minimized according to:

$$\epsilon_r = \sum_{t=0}^{m+n} (d_t - b_t)^2$$

where :

$$b_t = \sum_{\tau=0}^{m} f_\tau a_{t-\tau} \qquad\qquad t = 0,1,\cdots\cdots m+n$$

$$= 0 \qquad\qquad t > m+n$$

therefore:

$$\epsilon_r = \sum_{t=0}^{m+n} \left(d_t - \sum_{\tau=0}^{m} f_t a_{t-\tau} \right)^2$$

Setting the partial derivations of ϵ_r equal to zero we have:

$$\frac{\partial \epsilon_r}{\partial f_j} = \sum_{t=0}^{m+n} 2 \left(d_t - \sum_{\tau=0}^{m} f_t a_{t-\tau} \right)\left(-a_{t-j} \right) = 0 \qquad j=0,1,\cdots m$$

Representing ϕ_{aa} as the autocorrelation of a_t, and ϕ_{da} as the cross-correlation of d_t and a_t, we may express the normal equations for the filter as:

$$\phi_{da} = \sum_{\tau=0}^{m} f_\tau \, \phi_{aa}$$

This theory is extremely useful when trying to improve the signal resolution before performing more complex techniques of multiple elimination. An example showing the use of the spiking filter is given in Fig.3.1.

3.3 Introduction to signal induced noise (multiples)

Multiples are of major concern when seismic records are to be interpreted since they invariably interfere with and distort the wanted signal.

It is therefore important to remove such effects whenever possible, ideally in such a way as to leave only the first arrivals from each horizon. Such multiples include: a) water layer reverberations, b) primary reverberations, c) inter-layer reverberations, d) reverberations at the source.

This, and later sections, deal with some of the multiple elimination techniques, and describe how various types of multiples are produced. A list and description is now given of the various types of multiples mentioned above.

a)   Water Layer reverberations

The water/air interface is a flat, strong reflector, with a reflection coefficient approximately equal to -1 (Backus, 1959). Thus if the water/sea bottom interface is a strong reflector there is a tendency for the formation of an energy trap. As a consequence, a signal generated in this trap, or entering it from below, will be reflected repeatedly from the two boundaries with an associated amplitude decay dependent upon the two relfection coefficients and spreading loss. This effect is particularly strong where basement outcrops occur.

The production and mathematical formulation of water layer reverberations is shown in Fig.3.2.A, and an example showing them recorded at sea is given in Fig.3.3.

b)   Primary reverberations

These are shown by the first two multiples of diagrams B and C in

Fig.3.2. As in the case of water reverberations, they are in effect

reverberations between a reflecting horizon and water/air interface.

In these instances though the amplitude decay is dependent on the

reflection coefficient of the horizon and all intermediate interface

transmission coefficients (Robinson, 1967b). Thus their elimination

becomes somewhat more difficult due to the unknown values of these

reflection and transmission coefficients.

c) Inter-layer reverberations

Under this heading are included all the more complex multiples,

examples of which are shown in Fig.3.2.D. Again, the strength of the

signal received is dependent on the transmission and reflection

properties of the interfaces encountered by the signal. As the number

of interfaces increases so there is a corresponding increase in the

number of different multiples that can be formed, and as the equation

derived by Backus (1959, page 240) shows, their elimination becomes more

complex and lengthy.

d) Reverberations at source (ghosting)

On land this is a result of the shot being below the weathered

layer. Energy produced from the shot travels up as well as down, and

it is this upward travelling energy that is reflected back down again from

the weathered layer to cause the ghosting effect. Similarly, at sea,

the 'ghost' is a result of the upward travelling wave being reflected

back down, this time at the water/air interface, and since this is a

reflection at a higher to lower velocity interface the ghost wave has

a resultant phase change associated with it. There is also a corres-

Fig. 3.2 Mathematical formulation of some specific multiples

Some of the major types of multiples encountered in marine seismic profiling are drawn along with their time of arrival and corresponding amplitudes.

These two functions of the ray, travel time (T) and amplitude (A), are divided into two parts. The first parenthesis contains information concerning the upward travelling ray and the second contains information concerning the downward travelling ray that has been reflected at the water/air interface.

A

$$T = \sum_{n=1}^{\infty} \left\{ (n-1)t_1 + nt_2 \right\} + \left\{ nt_1 + nt_2 \right\}$$

$$A = \sum_{n=1}^{\infty} \left\{ (-1)^{n+1} R_1^n \right\} + \left\{ (-1)^n R_1^n \right\}$$

B

$$T = \sum_{n=1}^{\infty} \left\{ (n-1)t_1 + n(t_2 + t_3) \right\} + \left\{ n(t_1 + t_2 + t_3) \right\}$$

$$A = \sum_{n=1}^{\infty} \left\{ (-1)^{n+1} (1-R_1^2) R_2^n \right\} + \left\{ (-1)^n (1-R_1^2) R_2^n \right\}$$

$$T = \sum_{n=1}^{\infty} \left\{ t_2 + (n+1)t_3 \right\} + \left\{ t_1 + t_2 + (n+1)t_3 \right\}$$

$$A = \sum_{n=1}^{\infty} \left\{ (-1)^n (1-R_1^2) R_1^n R_2^{n+1} \right\} + \left\{ (-1)^{n+1} (1-R_1^2) R_1^n R_2^{n+1} \right\}$$

C

$$T = \sum_{n=1}^{\infty} \left\{ (n-1)t_1 + n(t_2 + t_3 + t_4) \right\} + \left\{ n(t_1 + t_2 + t_3 + t_4) \right\}$$

$$A = \sum_{n=1}^{\infty} \left\{ (-1)^{n+1} (1-R_1^2)^n (1-R_2^2)^n R_3^n \right\} + \left\{ (-1)^n (1-R_1^2)^n (1-R_2^2)^n R_3^n \right\}$$

$$T = \sum_{n=1}^{\infty} \left\{ (t_2 + t_3) + (n+1)t_4 \right\} + \left\{ (t_1 + t_2 + t_3) + (n+1)t_4 \right\}$$

$$A = \sum_{n=1}^{\infty} \left\{ (-1)^n (1-R_1^2)(1-R_2^2) R_2^n R_3^{n+1} \right\} + \left\{ (-1)^{n+1} (1-R_1^2)(1-R_2^2) R_2^n R_3^{n+1} \right\}$$

D

$$T = \sum_{n=1}^{\infty} \left\{ t_2 + t_4 + (n+1)t_3 \right\} + \left\{ t_1 + t_2 + t_4 + (n+1)t_3 \right\}$$

$$A = \sum_{n=1}^{\infty} \left\{ (-1)^n (1-R_1^2)(1-R_2^2) R_2^n R_3^n R_3^n \right\} + \left\{ (-1)^{n+1} (1-R_1^2)(1-R_2^2) R_1^n R_2^n R_3^n \right\}$$

$$T = \sum_{n=1}^{\infty} \left\{ t_2 + (n+1)(t_3 + t_4) \right\} + \left\{ t_1 + t_2 + (n+1)(t_3 + t_4) \right\}$$

$$A = \sum_{n=1}^{\infty} \left\{ (-1)^n (1-R_1^2)(1-R_2^2) R_1^n R_3^{n+1} \right\} + \left\{ (-1)^{n+1} (1-R_1^2)(1-R_2^2) R_1^n R_3^{n+1} \right\}$$

Fig. 3.3 Example of water-layer reverberations

The sea bottom is indicated by the reflection at the two-way travel time of 0.85 seconds. Subsequent water-layer reverberations are clearly indicated.

1 —
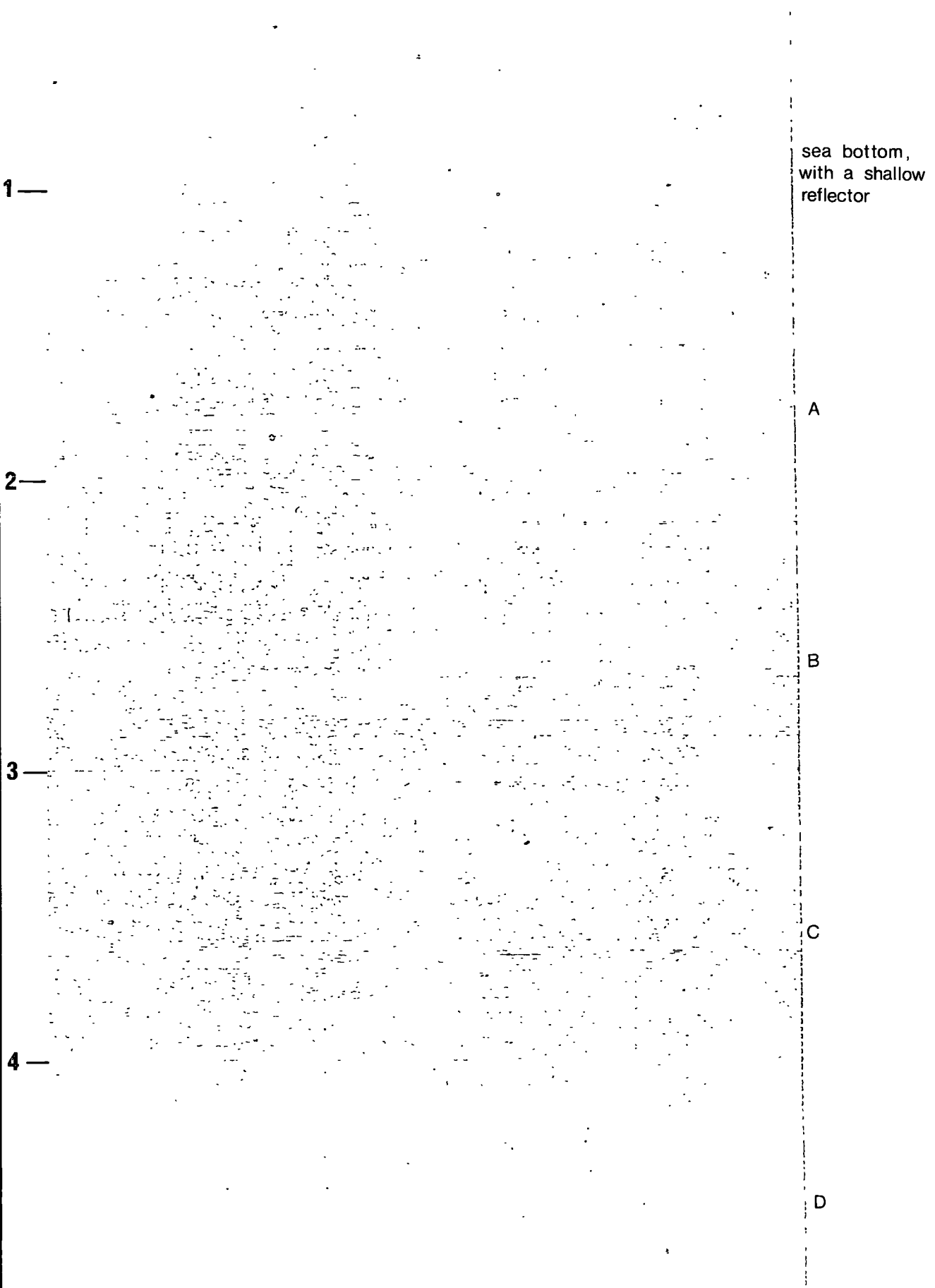
sea bottom,
with a shallow
reflector

A

2 —

B

3 —

C

4 —

D

A,B,C & D indicate sea bottom multiples

ponding 'ghost' effect caused by the depth of the receiver with respect to the water/air interface. Although in most cases ghosting is not a great hindrance, as with other types of multiples described earlier, it is still taken into account when deriving the source wavelet.

3.4 Multiple elimination

With all multiple elimination techniques the basic aim is to remove the signal induced noise and to leave just the primary arrivals from each reflecting horizon. This of course is never entirely possible since most techniques that are used also remove some of the wanted signal, particularly if the signal is completely immersed in a multiple. Another problem that has to be overcome is the determination of the unknown quantities of reflection and transmission coefficient, which will normally have to be estimated. If automatic gain control (A.G.C.) is applied to the received data this will accommodate for the unknown quantities of reflection and transmission coefficient, provided the record does not contain very complex multiples.

A method commonly used in this work is the filter of Backus (1959) which computes the complete range of multiples for n-layers. Once the synthetic seismogram has been produced it is then subtracted from the recorded seismogram to leave the required primary arrivals from each interface. This theory has been simplified for computational purposes and improved upon by applying a cross-correlation optimization technique which obtains the best position of the multiples associated with each interface, and thus the depth to the interface. This technique is described in detail in section 3.5.

Two other techniques for multiple elimination are described in sections 3.6 and 3.7. In one case the method makes use of two consecutive vertical incidence reflection seismograms, and in the other case use is made of the signals received at four active sections of a seismic array system. Neither of these two techniques have been used by previous workers and will therefore be described in detail in these sections.

3.4.1 Previous work on the problem of multiple elimination

Many previous techniques have been developed to overcome the effects of multiples on seismic records. Three important methods which have been applied, and repeatedly refined are: 1) use of velocity logs, 2) the 'Backus' filter; and 3) common depth point techniques. This latter technique is that most commonly used by prospecting companies, although it generally requires the use of expensive seismic array systems for its application.

1) Velocity logging requires the application of some multiple elimination package, although it does produce an insight into the velocity distribution of the layering and hence information about the reflection coefficients required to remove multiple reflection effects. Wuenschel (1960) has shown that exact synthetic seismograms may then be produced from the velocity distribution function obtained from the velocity log data.

2) The 'Backus' filter (Backus, 1959) formulates a synthetic response of the substrata penetrated from several parameters that have to be known. These parameters include shot/receiver depth, two-way travel times to the reflecting horizons and their corresponding reflection

coefficients. The basic equation used in the derivation of the synthetic response is that given by Backus (1959), page 240 equation 14. This is based on plane wave theory and normal incidence reflections. Application of this equation is then made to derive the required inverse filter to remove the effect of multiples.

3) Common depth point techniques provide a series of seismic records which contain information about the substrata layers from one common point of each. After normal moveout and static corrections have been applied the seismic traces are then combined, by horizontal stacking or linear multichannel filtering, into a single record. In this stacked record the primary reflections are enhanced relative to the multiple reflections and random noise since these are reduced by out of phase addition (Marr and Zagat, 1967; Mayne, 1967; Meyerhoff, 1966).

3.5 Optimized recursive filter

Since the filter characteristics to be derived are dependent upon the coefficients of reflection and transmission of the interfaces, it is worthwhile explaining the convention used for both.

Firstly we consider a ray of amplitude A travelling in the ith layer (Fig.3.4) and impinging on the boundary between the ith and $(i+1)^{th}$ layers. The velocity of the $(i+1)^{th}$ layer is assumed to be greater than the ith layer, the reflection coefficient of the boundary being denoted by R_i . With vertical incidence reflection work this ray in the ith layer will, under these velocity constraints, be reflected and transmitted at the boundary. The ray reflected back into the ith layer has an amplitude AR_i and the transmitted ray into the $(i+1)^{th}$ layer

Fig. 3.4 Convention used for the reflection coefficient R_i

i^{th} LAYER

$(i+1)^{th}$ LAYER

INCIDENT
WAVE

REFLECTED
WAVE

TRANSMITTED
WAVE

A

$R_i A$

$(1-R_i) A$

R_i

$(1+R_i) A$

A

$-R_i A$

TRANSMITTED
WAVE

INCIDENT
WAVE
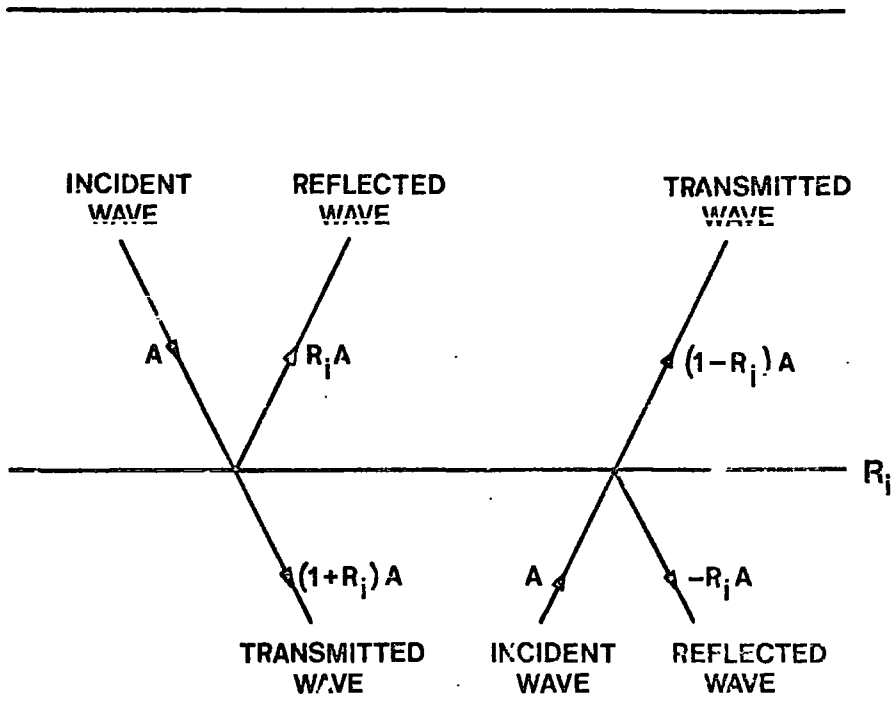
REFLECTED
WAVE

R_i — REFLECTION COEFFICIENT

A — AMPLITUDE OF THE INCIDENT WAVE

an amplitude of $A\left(1 + R_i\right)$.

If we now consider a ray of amplitude A travelling upward in the $(i+1)^{th}$ layer (Fig.3.4) there is again a resultant reflected and trans-mitted ray produced at the boundary with the ith layer. In this case the reflected ray in the $(i+1)^{th}$ layer has an amplitude $-AR_i$, and the transmitted ray into the ith layer an amplitude of $A\left(1-R_i\right)$. This convention is that used by Robinson (1967b) and Backus (1959) and will be used throughout this work.

Using this convention the amplitude of the arrivals and their corresponding travel times are computed from the formulae in Fig.3.2. These formulae are written so that the first parenthesis contains information concerning the upward travelling ray, and the second paren-thesis contains information about the downward ray which has been reflected at the water/air interface. For the purpose of computation of these formulae the amplitude of the source has been normalized, and the water/air interface has an assumed ideal reflection coefficient of -1.

Thus using Fig.3.2.A as an example, and setting t_1 = 20 m.secs; t_2 = 1.20 secs; R_1 = 0.60, there would be arrivals at time, T = (1.20, 1.22, 2.42, 2.44, 3.64, 3.66 ....) secs with corresponding amplitudes of, A = (0.6, -0.6, -0.36, 0.36, 0.216, -0.216, ...).

3.5.1 Computation of the filter

Initial estimates of the reflection coefficients and travel times

to each horizon are provided along with the pre-determined source function. The first calculation involves the determination of the depth to the sea bottom. Since the shot instant is known accurately, and the first large break on the seismic record is generally the first reflection from the sea bottom, it is relatively easy to evaluate the two-way travel time to the sea bottom. The impulse response of the water layer is then produced from the two-way time using the equations shown in Fig.3.2.A, the output being a spiked wave train. This is then convolved with the source function to produce the required water-layer reverberations which are then subtracted from the record.

Multiples associated with the first sub-bottom horizon are then evaluated. These are computed for search points around the original estimate of the depth to the horizon. For each search position the synthetic seismogram (i.e. that containing the computed multiples) and recorded seismogram are correlated to find the optimum depth to the horizon. This optimum depth will occur when the cross-correlation coefficient attains its maximum over the search range. When this maximum has been found the multiples associated with the horizon at this depth are removed from the recorded seismogram in the same manner as the water-layer reverberations.

This procedure is then followed for the next horizon and so on, eventually the final output will be the recorded seismogram less all computed multiples, the efficiency of their removal depending upon the estimates supplied by the programmer for the reflection coefficients and travel times to each horizon.

These optimized values of the depths to each horizon are then used

Fig. 3.5 Stages of multiple elimination for the optimized

recursive filter

In this example the stages of multiple removal from the three

horizons are shown.

The initial multiples that are removed are the water-layer

reverberations and then by means of the cross-correlation coefficients

derived (to find the optimum depths) the second and third layer multiples

are eliminated. The resultant 'multiple-free' record is shown in the

final diagram.

AIR-GUN SOURCE FOR
THE SEISMOGRAM
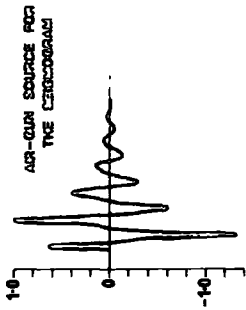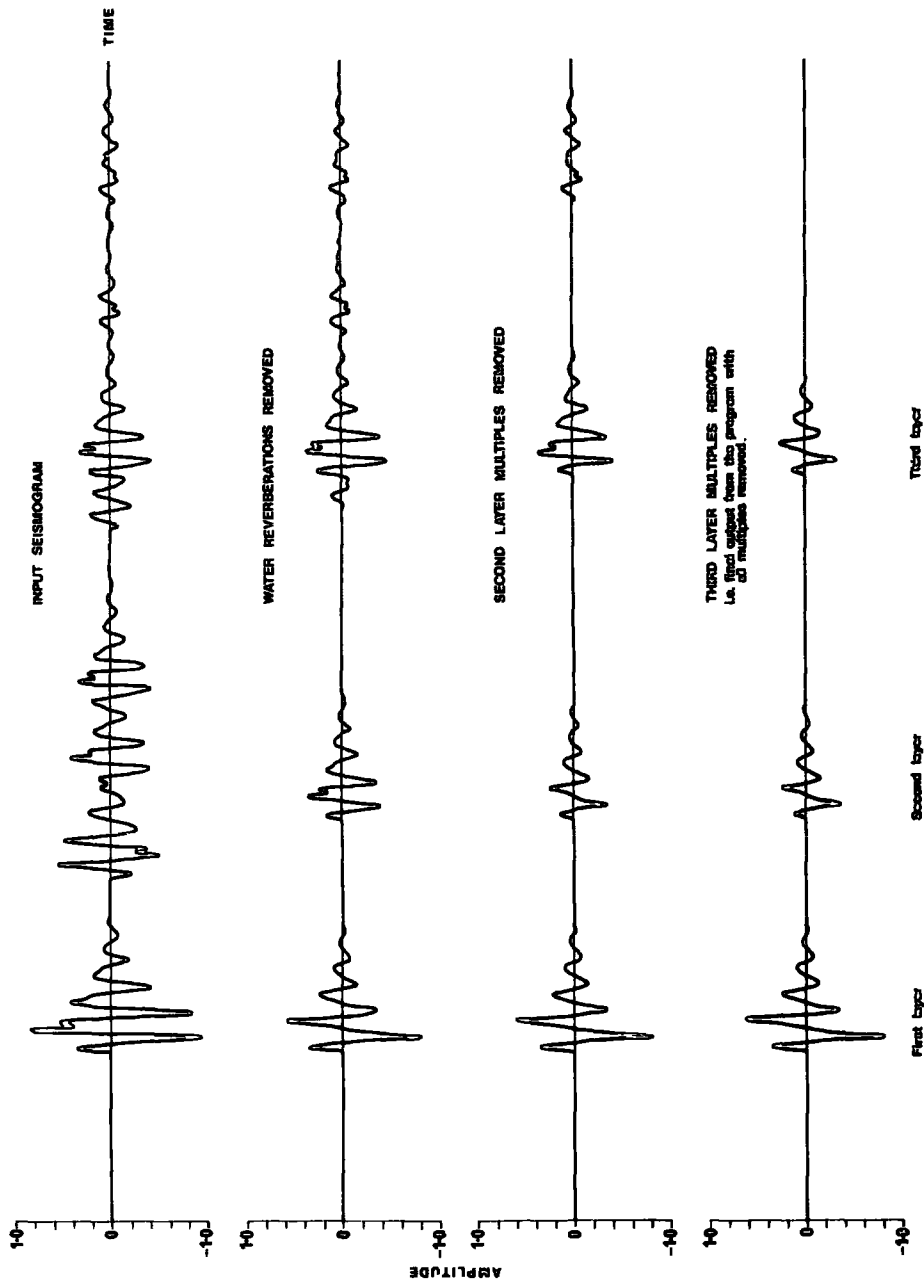
Order in chosen the cross-correlation functions
of the input seismogram is computed multipion,
the cross indicating the position of optimum depth,
i.e. two-way travel time to the layer.

SECOND LAYER

THIRD LAYER

INPUT SEISMOGRAM

TIME

WATER REVERBERATIONS REMOVED

SECOND LAYER MULTIPLES REMOVED

THIRD LAYER MULTIPLES REMOVED
i.e. final output from the program with
all multiples removed.

First layer

Second layer

Third layer

AMPLITUDE
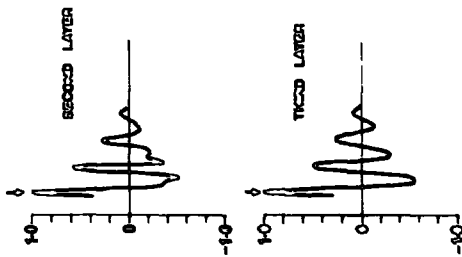
as the starting point of the search routine to find the maximum of the cross-correlation coefficient (i.e. the new optimized depths) for the next incoming seismic record. Thus this program is continuous and does not necessitate the programmer to input new parameters for each seismogram. However, if a new horizon becomes apparent along a seismic section and it is deemed necessary to remove multiples associated with this horizon, new input parameters will then have to be provided to the filter.

Stages of multiple removal from a seismic record by the application of the optimized recursive filter are shown in Fig. 3.5.A. The seismogram can be seen to consist of primary arrivals and multiples from three horizons, which have been generated by using an air-gun source wavelet. The first multiples that are to be removed are the water-layer reverberations which, as can be seen in the second diagram of Fig.3.5, considerably improves the seismogram. For the second layer the cross-correlation coefficients are computed throughout the search range to obtain the optimum depth, and then the multiples computed for this depth removed from the record as shown. Finally, multiples associated with the third layer are computed in a similar manner and removed from the record. This leaves the primary reflections from the three layers as shown in the lowest diagram of Fig.3.5. The shape of these primary wavelets is in very good agreement with the source wavelet used to construct the seismogram. Also shown to the right of these diagrams in Fig.3.5 is the variation of the cross-correlation coefficients for the second and third layers, where the arrows indicate the position of the maximum coefficient.

3.5.2   Application of the filter to a seismic section

The upper diagram of Fig.3.6 shows the seismic section, using an

Fig. 3.6 Application of the optimized recursive filter

The input section shown in the upper diagram contains primary arrivals, primary and inter-layer reverberations.

The output from the optimized recursive filter shows a reduction in the effect of the multiples and has made interpretation of the major horizons much easier.

Input Seismic Section

Output Seismic Section

From The Optimized Recursive Filter
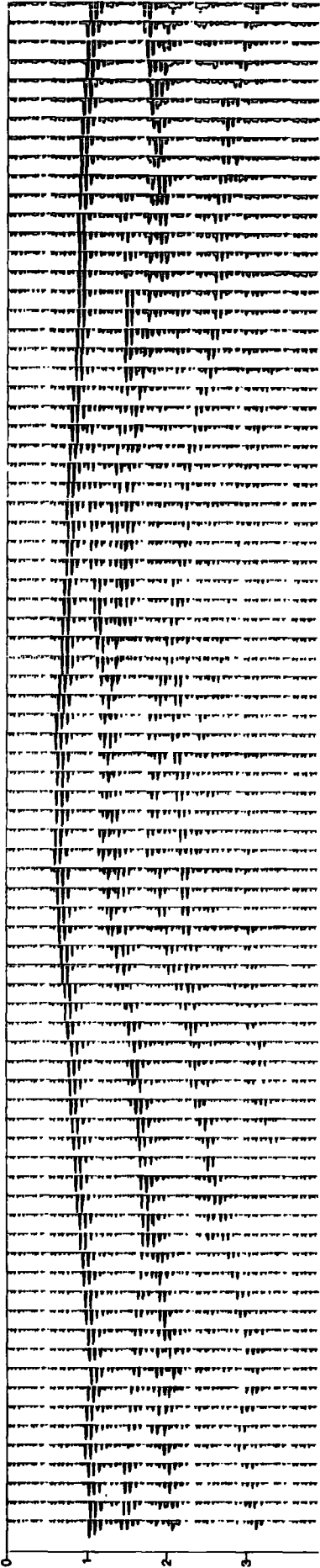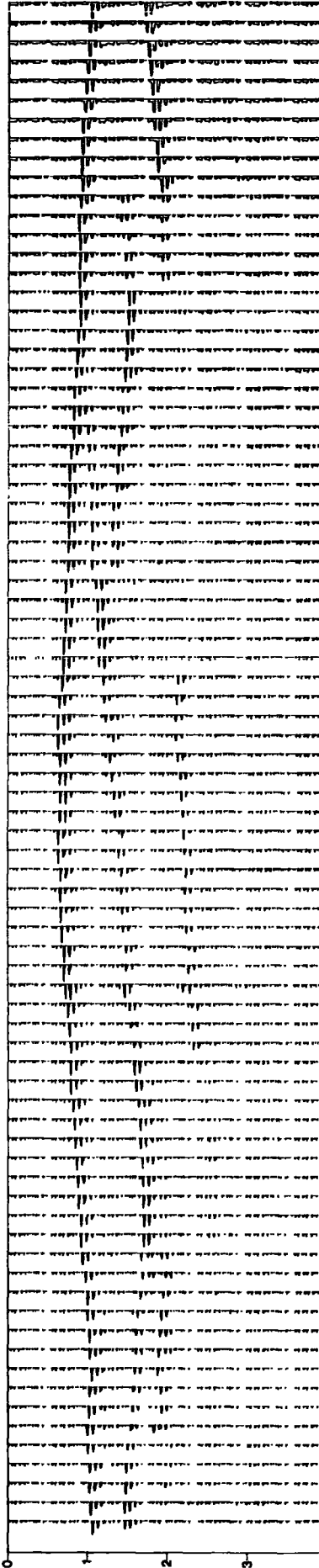
TWO-WAY TRAVEL TIME IN SECS.

air-gun source, that is to be processed using the optimized recursive
filter. This seismic section contains six reflecting horizons and their
associated multiples, and on many of the shots the primary arrivals
from some horizons are immersed in these multiples thus making them
rather indistinct. The process by which the filter is applied has been
described in the previous two sections (3.5 and 3.5.1). Throughout the
signal has a dominant frequency of 18 c/s (at 6dB $\pm$ 5 c/s) and the noise
25 c/s (at 6dB $\pm$ 5 c/s).

As can be seen from the output (lower diagram of Fig.3.6) the
optimized recursive filter has removed the multiples from the seismic
section and has enabled all six horizons to be observed more clearly.
The structure deduced from this output is one containing a sea bottom at
a depth of about 1.0 secs (two-way time), a major structure below this
at a depth varying between 1.0 and 1.5 secs (two-way time), and finally
four other minor horizons at varying depths below this.

The output shows quite clearly that this filter has good application
to seismic sections containing multiples, with the result that the
multiples are filtered out leaving the primary arrivals from the seismic
reflectors. No velocity/depth determination prior to running the filter
is required, however the efficiency of filtering out the multiples is
largely dependent upon the reflection coefficients input to the program
prior to computation. This may however be overcome in some instances,
as mentioned before, by the use of automatic gain control.

It must be noted that throughout this computation the seismic
horizon is assumed to be horizontal over the region where the multiples
are being generated, i.e. the travel times are unaffected by the aperture

of the seismic array. This assumption becomes more valid for dipping interfaces as their depth increases with respect to the shot/receiver depth.

3.5.3 Discussion of the optimized recursive filter

Although this technique has shown that most types of multiples may be formulated, their efficiency of removal is greatly dependent upon the estimates of the reflection coefficients of each seismic horizon. If these coefficients supplied are fairly accurate then the examples show that the filter readily removes the multiples and leaves the primary arrivals from each horizon, clearly making the picking and subsequent interpretation of the seismic horizons easier. Three factors have not been taken account of when deriving the multiples, these are: spherical divergence, absorption and interface transmission losses. Ideally if the degrees to which these factors affect the seismic record are known then they should be compensated for, but in most instances they are unknown quantities.

Apart from the initializing of certain parameters (e.g. source wavelet, reflection coefficients, and times to horizons) this optimized recursive filter may be regarded as an automatic process. However, if new horizons become apparent later on in the seismic section and it is required to remove multiples associated with these horizons, the program should be interrupted and new input parameters supplied to the filter. This testing for new horizons may also be carried out automatically by running a test down the seismic trace and comparing the horizons computed with those computed from the previous seismic trace. A new horizon should be shown up by this comparison test.

The efficiency of this technique compared with other methods of multiple elimination is shown in Chapter 4.

3.6 Removal of multiples by using 4 active sections of an array ('CHNS')

Described below is the theory and its application to examples for the program 'CHNS' listed after chapter 4.

Basically the theory involves the receiving of signals from the same shot at four active sections of a seismic array, which is towed behind the shooting vessel. A fifth channel is required for the accurate recording of the shot instant. Fig.3.7 shows the layout of the system, where A, B, C and D are the four active receiving elements of the array, and x_1, x_2, x_3 and x_4 are the distances of each from the shot point.

The assumption is made that the aperture of each horizon that is producing the reflections for each individual shot is horizontal (i.e. R in Fig.3.7).

3.6.1 Theory of 'CHNS'

From the standard equation for travel time from shot to receiver for a signal reflected from the ith seismic horizon we have for the first active element of the array a travel time given by:

$$t_1^i = \left(\frac{x_1^2}{4} + z_i^2 \right)^{\frac{1}{2}} \cdot \frac{2}{V_i} \qquad -(3.1.)$$

where z_i is the depth to the interface and V_i is the mean velocity of the path travelled by the signal. (The mean velocity of the ray path is used to try and overcome the problem of minimizing the errors in

Fig. 3.7 Physical layout required for the 'CHNS' technique

    In this technique the four active sections of the seismic array

(A, B, C & D) are towed behind the surveying vessel at distances X_1,

X_2, X_3 & X_4 kms. from the shot point S.

    One of the assumptions that is made is that the aperture R,

over which the reflected arrivals from each shot to the seismic array

have occurred, is horizontal for each layer.

DISTANCE FROM SHOT

O kms X_1 X_2 X_3 X_4

S   A   B   C   D

SEA/AIR INTERFACE

i^{th} SEISMIC REFLECTING HORIZON

$(i+1)^{th}$ HORIZON

Z_i
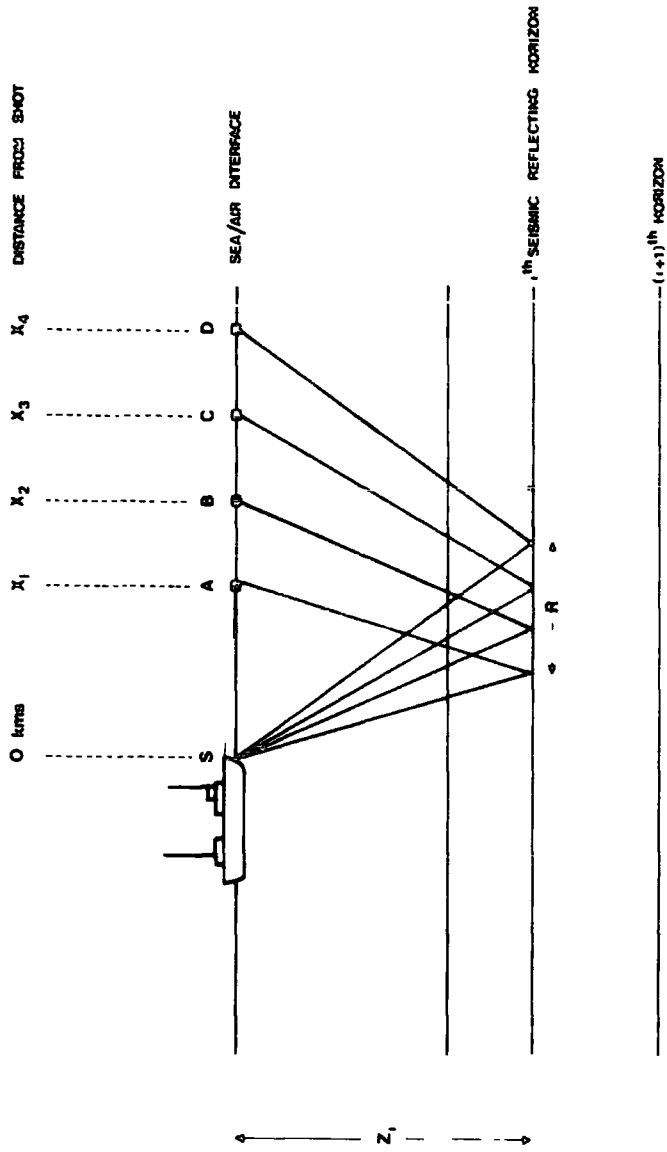
A,B,C & D ARE THE 4 ACTIVE SECTIONS OF
THE SEISMIC ARRAY

S IS THE SHOT POINT

calculating each individual layer velocity).

Similarly for the second active element of the array:

$$t_2^i = \left(\frac{x_2^2}{4} + Z_i^2 \right) \cdot \frac{2}{V_i} \qquad\qquad -(3.2.)$$

Generalizing:

$$t_j^i = \left(\frac{x_j^2}{4} + Z_i^2 \right) \cdot \frac{2}{V_i}$$

where: $\qquad i = 1, 2, 3, \ldots n \quad , \quad$ n = number of seismic horizons

$\qquad\qquad j = 1, 2, 3, 4 \qquad , \quad$ i.e. 4 active elements of the

array

The assumption is made, for equations 3.1 and 3.2 to be valid, that there is no continuous velocity increase with depth in any individual layer. However, the velocity of the $(i+1)^{th}$ layer is assumed greater than the velocity of the ith layer.

Using equations 3.1 and 3.2 to derive Z_i we have:

$$\frac{x_1^2}{4} + Z_i^2 = \left(\frac{t_1^i}{t_2^i} \right)^2 \left(\frac{x_2^2}{4} + Z_i^2 \right)$$

$$\therefore \; Z_i^2 = \left[\left(\frac{t_1^i x_2}{2 t_2^i} \right)^2 - \frac{x_1^2}{4} \right] \frac{(t_2^i)^2}{(t_2^i)^2 - (t_1^i)^2}$$

$$\therefore \; Z_i = \left[\frac{(t_1^i x_2)^2 - (t_2^i x_1)^2}{4 (t_2^i - t_1^i)(t_2^i + t_1^i)} \right]^{\frac{1}{2}} \qquad\qquad -(3.3.)$$

Substituting equation 3.3 back into 3.1 we obtain an expression for V_i , the mean velocity:

$$V_i = 2 \left(\frac{x_1^2}{4} + \frac{\left(t_1^i x_2\right)^2 - \left(t_2^i x_1\right)^2}{4\left(t_2^i - t_1^i\right)\left(t_2^i + t_1^i\right)} \right)^{\frac{1}{2}} \Big/ t_1^i$$

$$\therefore \quad V_i = \left(x_1^2 + \frac{\left(t_1^i x_2\right)^2 - \left(t_2^i x_1\right)^2}{\left(t_2^i - t_1^i\right)\left(t_2^i + t_1^i\right)} \right)^{\frac{1}{2}} \Big/ t_1^i \qquad -(3.4.)$$

Thus if we can successfully pick off corresponding arrivals on the first and second active sections of the seismic array we may compute the quantities Z_i and V_i

For multiples between the ith reflecting horizon and the water/air interface the function V_i will appear less than that of the primary reflection from the ith horizon, and as a consequence this property is used in eliminating such multiples.

3.6.2 Limitations of the 'CHNS' theory

Two major limitations occur when applying this method of multiple elimination. The first of these is that inter-layer reverberations cannot be removed from the record. This deficiency is due to the mean velocity calculated from the multiple appearing greater than that calculated from the primary reflection. The second limitation is due to the resolution of $\left(t_2^i - t_1^i\right)$ which is dependent upon the sampling rate. These will now be treated individually.

a) Inter-layer reverberations

If we consider the simplified case of normal incident reflections as in Fig.3.8 (expanded in the horizontal axis to show ray paths), i.e.

Fig. 3.8 Limitations of the 'CHNS' technique when it is

applied to inter-layer reverberations

s   x,t   s   x,t′   SEA/AIR INTERFACE

V_i Z_i

i^{th} HORIZON

V_{i+1} Z_{i+1}

$(i+1)^{th}$ HORIZON
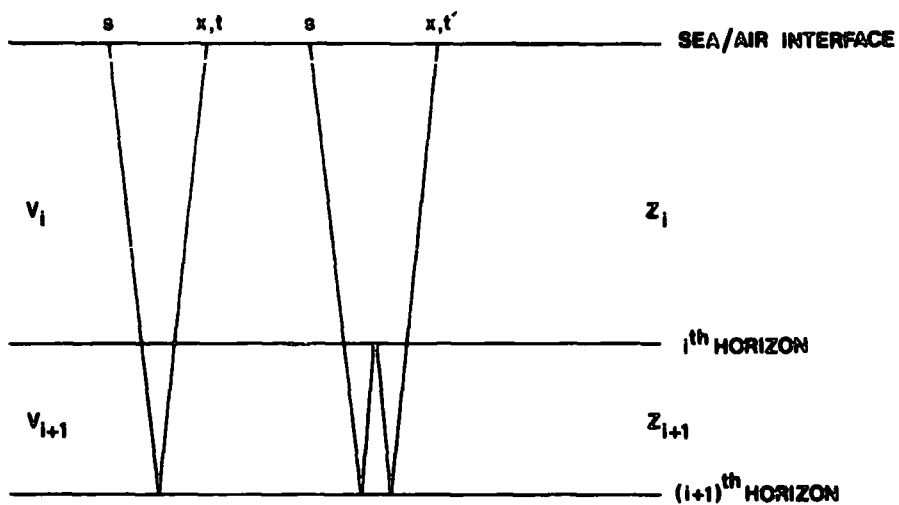
V_i & V_{i+1} ARE THE VELOCITIES , $V_{i+1} > V_i$

Z_i & Z_{i+1} ARE THE DEPTHS

X IS THE DISTANCE FROM SHOT POINT S

t & t′ ARE THE TRAVEL TIMES , $t′ > t$

$x_1^2/4 \ll \left(z_i + z_{i+1}\right)^2$ we obtain the equations for the travel time relationship for the primary reflection and the inter-layer reflection:

$$t = \frac{2z_i}{V_i} + \frac{2z_{i+1}}{V_{i+1}} \quad \text{and} \quad t' = \frac{2z_i}{V_i} + \frac{2nz_{i+1}}{V_{i+1}}$$

where n is the number of reflections from the $(i+1)^{th}$ horizon, (in the example of Fig.3.8 the value of n is 2). The mean velocity in each case is given by:

$$\bar{V}_t = \frac{2z_i + 2z_{i+1}}{t} \quad \text{and} \quad \bar{V}_{t'} = \frac{2z_i + 2nz_{i+1}}{t'}$$

Eliminating z_i from the first two equations we have:

$$\frac{t}{2} = \frac{t'}{2} - \frac{nz_{i+1}}{V_{i+1}} + \frac{z_{i+1}}{V_{i+1}} = \frac{t'}{2} - \frac{(n-1)z_{i+1}}{V_{i+1}}$$

therefore: $\quad z_{i+1} = \frac{V_{i+1}}{2(n-1)} \cdot \left(t' - t\right)$

and substituting back we obtain the expression for z_i :

$$z_i = \frac{V_i}{2(n-1)} \cdot \left(nt - t'\right)$$

Thus using the above expressions we may eliminate z_i and z_{i+1} from $\bar{V}_t$ and $\bar{V}_{t'}$:

$$\bar{V}_t = \left[\frac{V_i}{(n-1)} \cdot \left(nt - t'\right) + \frac{V_{i+1}}{(n-1)} \cdot \left(t' - t\right)\right] \Big/ t$$

$$\bar{V}_{t'} = \left[\frac{V_i}{(n-1)} \cdot \left(nt - t'\right) + \frac{nV_{i+1}}{(n-1)} \cdot \left(t' - t\right)\right] \Big/ t'$$

such that $V_{i+1} > V_i$ and $t' > t$. Subtracting these two equations from one another we have:

$$\bar{V}_{t'} - \bar{V}_{t} = \frac{nV_i}{(n-1)} \cdot \frac{t}{t'} - \frac{V_i}{(n-1)} + \frac{nV_{i+1}}{(n-1)} - \frac{nV_{i+1}}{(n-1)} \cdot \frac{t}{t'}$$

$$- \frac{nV_i}{(n-1)} + \frac{V_i}{(n-1)} \cdot \frac{t'}{t} - \frac{V_{i+1}}{(n-1)} \cdot \frac{t'}{t} + \frac{V_{i+1}}{(n-1)}$$

which reduces to:

$$\bar{V}_{t'} - \bar{V}_{t} = \left(V_i - V_{i+1} \right) \left[\frac{nt}{(n-1)t'} + \frac{t'}{(n-1)t} - \left(\frac{n+1}{n-1} \right) \right]$$

Since $V_{i+1} > V_i$ the term in the first brackets is negative, we there-
fore need to show that the second term is also negative and therefore
$\bar{V}_{t'} > \bar{V}_{t}$. Considering a small time difference Δt , such that
$t' \rightarrow t + \Delta t$ we have:

$$\bar{V}_{t'} - \bar{V}_{t} = \left(V_i - V_{i+1} \right) \left[\frac{nt}{(n-1)(t+\Delta t)} + \frac{t+\Delta t}{(n-1)t} - \left(\frac{n+1}{n-1} \right) \right]$$

Multiplying the above expression out:

$$\bar{V}_{t'} - \bar{V}_{t} = \left(V_i - V_{i+1} \right) \left[nt^2 + (t+\Delta t)^2 - (n+1)(t^2+\Delta t) \right] \Big/ (n-1)(t^2+t\Delta t)$$

$$\therefore \quad \bar{V}_{t'} - \bar{V}_{t} = \left(V_i - V_{i+1} \right) \left(\Delta t^2 - (n-1)t\Delta t \right) \Big/ (t^2+t\Delta t)(n-1)$$

For the inter-layer multiples we have $t > \Delta t$ and the term $\left(\Delta t^2 - (n-1)t\Delta t \right) < 0$
This therefore shows that $\bar{V}_{t'} > \bar{V}_{t}$, verifying that the inter-layer
multiple has an apparent higher velocity than the primary reflection and
will not be removed by this technique.

An example showing how $\bar{V}_{t'} - \bar{V}_{t}$ behaves for different Δt is now
given:

$$\underline{\Delta t \to 0} \qquad \text{i.e. } Z_i \gg Z_{i+1} \qquad \text{then } \Delta t^2 < (n-1)\, t\, \Delta t$$

$$\therefore \; \overline{V}_{t'} < \overline{V}_t$$

(for n = 2 we would have $\overline{V}_{t'} - \overline{V}_t \to 0$)

$$\underline{\Delta t > 0} \qquad\qquad (\text{such that } t'-t \text{ is always less than t})$$

$$\Delta t^2 < (n-1)\, t\, \Delta t$$

$$\therefore \; \overline{V}_{t'} < \overline{V}_t$$

$$\underline{\Delta t \to t} \qquad \text{i.e. } Z_i \ll Z_{i+1} \qquad \text{then } \Delta t^2 < (n-1)\, t\, \Delta t$$

$$\therefore \; \overline{V}_{t'} < \overline{V}_t$$

(for n = 2 we have $\Delta t^2 \to t\, \Delta t$ and hence $\overline{V}_{t'} - \overline{V}_t \to 0$)

b) Resolution of $t_2^i - t_1^i$

The second limitation of the 'CHNS' technique lies in the time difference between t_2^i and t_1^i (times corresponding to the same arrival at the second and first active sections of the seismic array). This time difference $\left(t_2^i - t_1^i\right)$ is dependent upon the sampling rate that is being used for digitization. A sampling rate of 4 m.secs. is used throughout this work and as a consequence $\left(t_2^i - t_1^i\right)$ must be greater than or equal to 4 m.secs. otherwise it cannot be measured.

Fig.3.9.A shows how $\left(t_2^i - t_1^i\right)$ varies for a varying depth of water (the velocity of water assumed to be 1.50 kms/sec.), i.e. the depth below which the sea bottom will not show $\left(t_2^i - t_1^i\right)$ to be greater than 4 m.secs. This critical depth is, for the array dimensions shown in Fig.3.9.A, found to be 3.3 kms. below the water/air interface. (In the calculations the shot point is assumed to be close to the water/air interface).

Fig. 3.9 Limitations of the 'CHNS' technique for the time

difference $\left(t_2^i - t_1^i \right)$

Diagram A shows the variation of $\left(t_2^i - t_1^i \right), \left(t_3^i - t_2^i \right)$ and $\left(t_4^i - t_3^i \right)$ for varying sea bottom depths, where t_1^i, t_2^i, t_3^i and t_4^i are the arrival times for corresponding signals at the four active sections of the seismic array.

Diagrams B and C show how these functions vary for changes in combined depth of water and depth of sediment.

A

MODEL:-

VELOCITY OF WATER = 1 5 Kms/sec
VELOCITY OF SEDIMENTS = 2 0 Kms/sec

SHOT POINT   4 ACTIVE SECTIONS
                    OF THE ARRAY
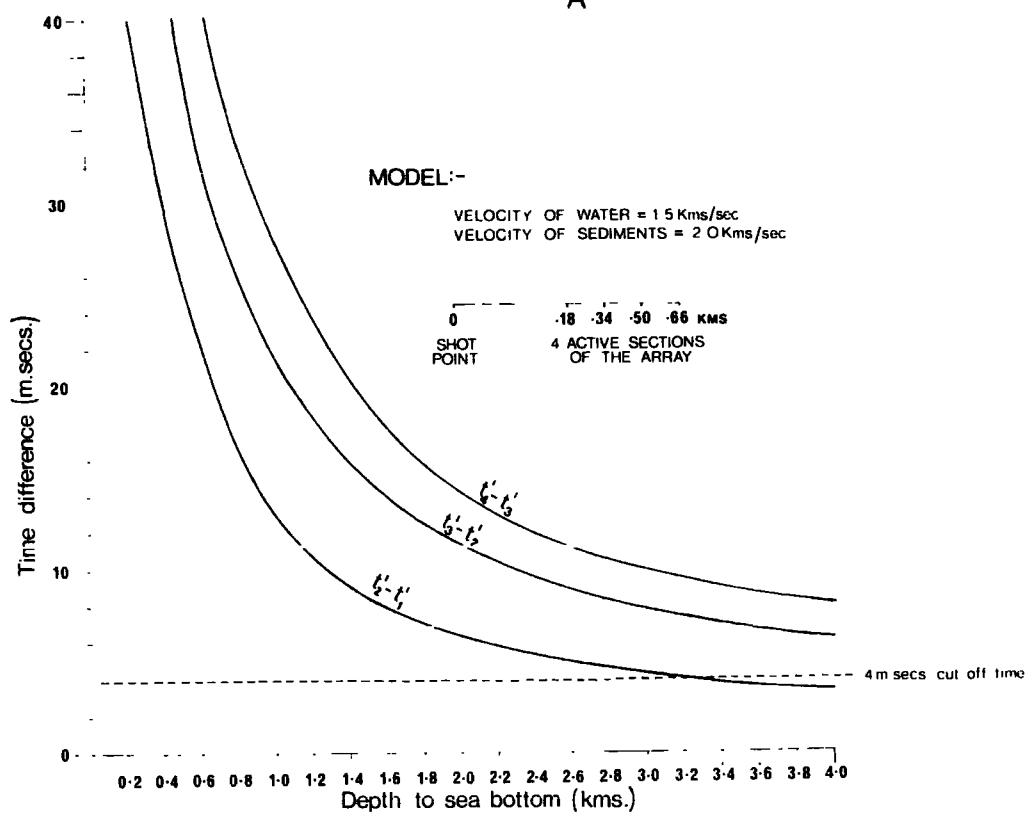
B
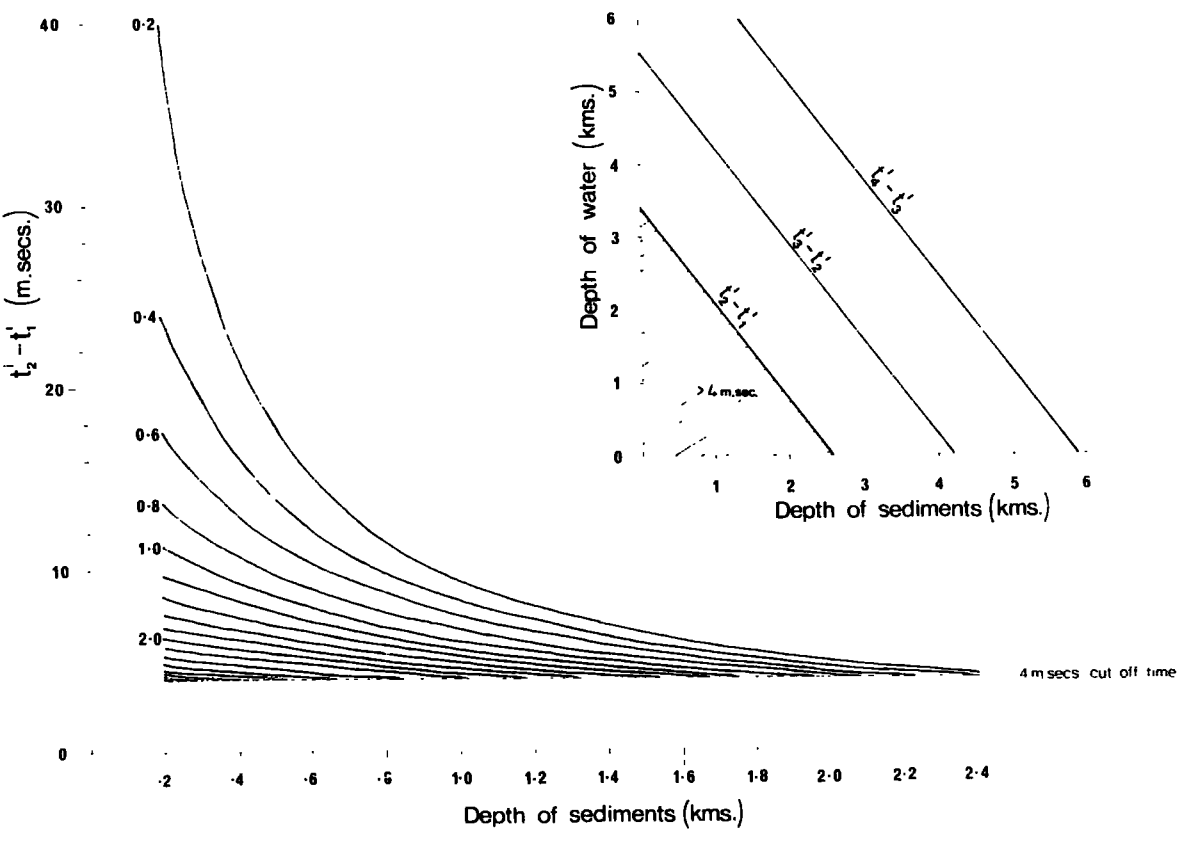
C
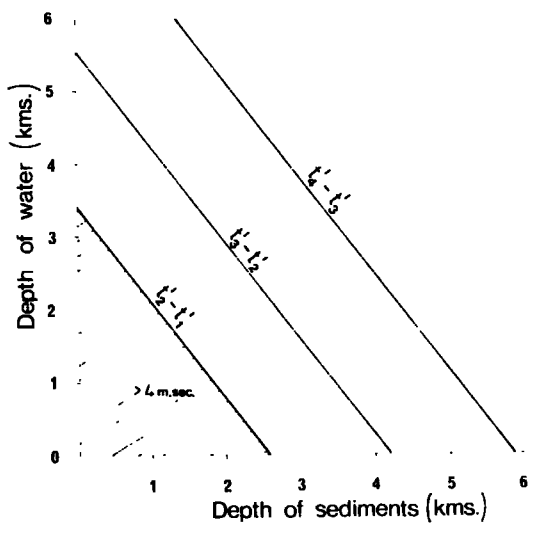
Fig. 3.10 Requirements on the overall length of the seismic array for varying depths of water

In deriving the total length of the seismic array the conditions that $\left(t_2^i - t_1^i\right)$, $\left(t_3^i - t_2^i\right)$ and $\left(t_4^i - t_3^i\right)$ are greater than the sampling rate are the only requirements. The sampling rate in this instance is 4 m.secs.

Curves are drawn for different towing lengths X_1 (kms), i.e. the distance from the shot to first active section of the seismic array.

Curves for various X_1, i.e. towing length

ARRAY ELEMENTS

SHOT X_1 X_2 X_3 X_4

0·05
0·10
0·15
0·20
0·25
0·30
0·40
0·50

Ratio of depth of water to array length:

— · — · —   5:1
— — — —   10:1
·········   15:1

Length of array required in kms.

Depth of water in kms.
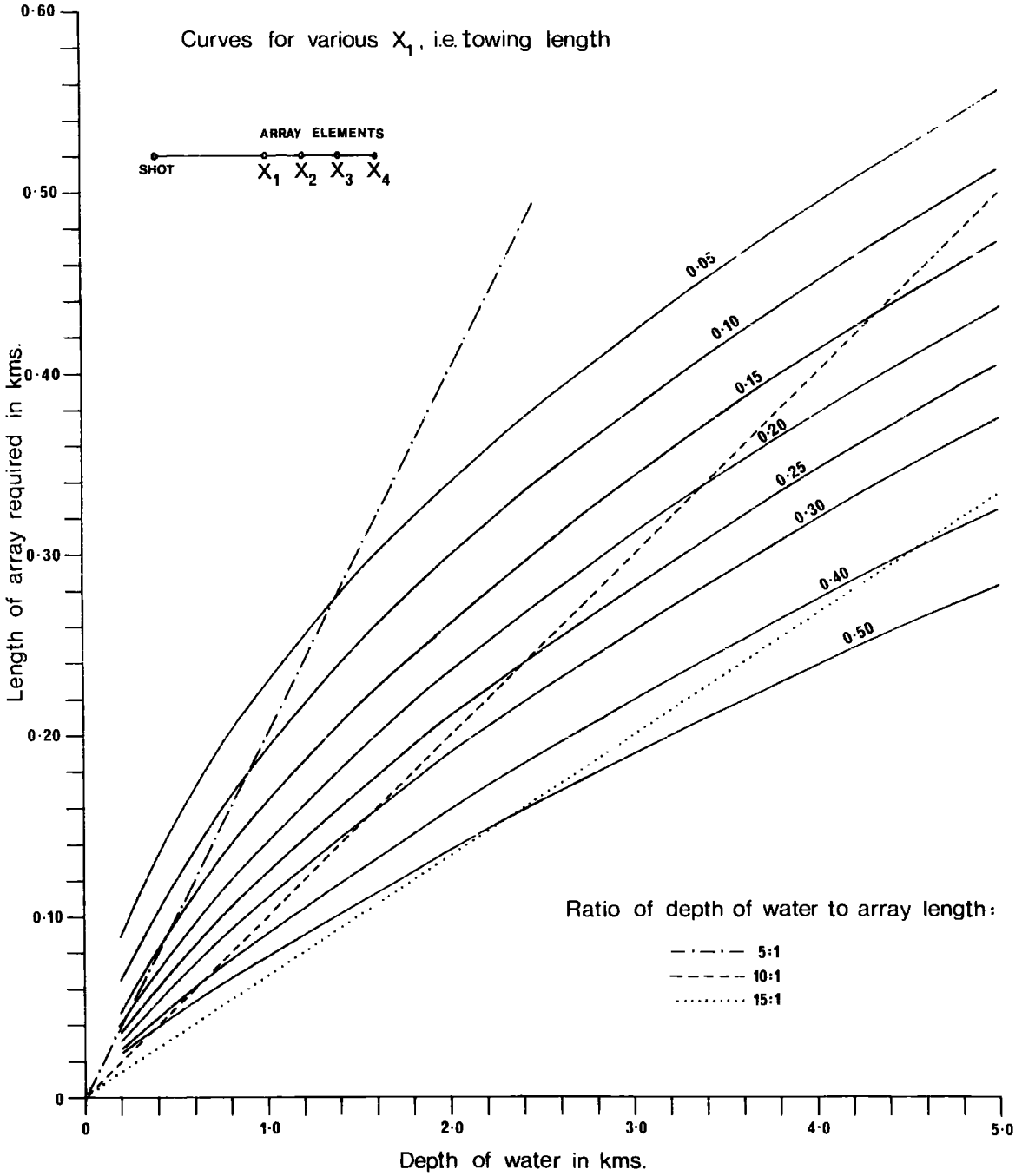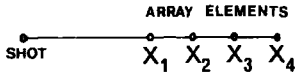
More important is the overall depth of water and sediment that can

be penetrated before $\left(t_2^i - t_1^i \right)$ falls below the 'cut-off' time of 4 m.secs.

Results for this, using the same array dimensions, are given in Fig.3.9.B

and C. The velocity of water and sediments are assumed to be 1.50 and

2.00 kms/sec. respectively. In Fig.3.9.B the depth of sediment is varied

for a fixed depth of water and $\left(t_2^i - t_1^i \right)$ calculated for each combination

of water and sediment depth, Fig.3.9.C shows these variations. Provided

that the combination of sediment and water depths lie within the range

that is shaded in Fig.3.9.C then $\left(t_2^i - t_1^i \right)$ will be greater than 4 m.secs.

It is clear from Figs.3.9.A and C that provided the condition $\left(t_2^i - t_1^i \right)$

is greater than the sampling rate then the other functions $\left(t_3^i - t_2^i \right)$ and

$\left(t_4^i - t_3^i \right)$, for these array dimensions, will also be greater than

the sampling rate.

Since there is a criterion that $\left(t_2^i - t_1^i \right), \left(t_3^i - t_2^i \right)$ and $\left(t_4^i - t_3^i \right)$

should be greater than the sampling rate it is worthwhile showing how the

overall length of the seismic array varies for this to be valid at a

particular depth of water. In Fig.3.10 the total length of array required

is plotted against depth of water, each curve representing a different

distance from the shot prior to first active section of the array in kms

$\left(X_1 \right)$. The total length of the array is defined as $\left(X_4 - X_1 \right)$. In each

instance the sampling rate used in deriving the array length was 4 m.secs.

As can be seen in Fig.3.10 there is a large dependence of the length of

the array upon the towing length X_1 , the larger X_1 becomes the

smaller the array length required becomes for a fixed depth. However,

it must be remembered that as X_1 is increased the strength of the

signals received at each active section of the array is decreased accord-

ingly. The dotted lines in Fig.3.10 represent 5 : 1, 10 : 1 and 15 : 1

ratios of depth of water to total array length required.

3.6.3 Computation procedure

The digitized data from each of the four active sections of the array are read into the program along with the shot instant. A noise level for each of the four sections is computed using a sample window which contains noise only, and then all peak values above these noise levels determined for each section in turn. (The four active sections will be given the notation Chn1, 2, 3 and 4, numbering away from the shot point).

A search is then made down Chn1 to find the position of the first peak above the noise level. The time of its arrival t_1^{i} (i.e. travel time), amplitude and phase characteristics are then determined and stored. Within the time window of $t_1^{i} \pm \Delta t$ a search is made on Chn2 to find a corresponding peak having similar amplitude and phase characteristics as that found on Chn1. (The search window of $\pm \Delta t$ is supplied by the programmer at the onset). If a peak is found within this range $t_1^{i} \pm \Delta t$ with the required characteristics, then $\left(t_2^{i} - t_1^{i}\right)$ is calculated and then used to determine the depth Z_i and mean velocity V_i . If no arrival is found about $t_1^{i} \pm \Delta t$, or does not have the correct amplitude and phase then the arrival picked on Chn1 will be assumed as being noise.

Having found an acceptable arrival on Chn2, the travel times for its arrival on Chn's 3 and 4 (t_3^{i} and t_4^{i} respectively) are computed and similar tests as were performed on Chn2 are performed to detect such arrivals about $t_3^{i} \pm \Delta t$ and $t_4^{i} \pm \Delta t$. These tests on Chn's 3 and 4 are aimed at reducing the possibility of noise being picked up. If the peak can be followed across from Chn1 to Chn's 2, 3 and 4 then

the calculated functions Z_i and V_i are stored, otherwise they are deleted.

This whole procedure is then repeated starting with the search down Chn1 for the next peak. Again if the peak can be followed across all Chn's then Z_{i+1} and V_{i+1} are computed and stored.

A comparison is then made between V_{i+1} and V_i, and Z_{i+1} and Z_i; such that we require $V_{i+1} > V_i$ and $Z_{i+1} > Z_i$. If this is the case then the arrival picked on Chn1 is a primary arrival from a seismic horizon and will be stored, otherwise it is regarded by the program as a multiple and will be removed.

When all the peaks on Chn1 have been tested in this manner then the next four records, from the elements of the seismic array for the next shot, are read into the program along with the new shot instant. The process of searching for corresponding arrivals from Chn1 through to Chn4 described above is then repeated on the new set of data.

3.6.4 Application of 'CHNS' to seismic sections

This technique has been applied to three seismic sections (Figs. 3.11.A, B and C), where the signal has a maximum frequency at 38 c/s (at 6dB $\pm$ 12 c/s) and the noise 40 c/s (at 6dB $\pm$ 8 c/s).

In the first example Fig.3.11.A the synthetic section contains only the sea bottom signal and its associated reverberations, the input to the program being that shown in the diagram on the left (only Chn1 displayed). To the right is drawn the output from the computer program,

<u>Figs. 3.11 A, B & C</u> Application of the 'CHNS' technique to

seismic sections

In each case the seismic section to be analysed is drawn on the

left, the output from 'CHNS' is drawn on the right.

The phase, amplitude, and time of arrival of each peak which is

chosen by the program to be a first arrival is output for each record

in turn, the dotted lines delineate the model derived from the first

onsets.

A

Output showing the phases (in the form of spikes) that have been recognized as first arrival. In this case only one layer, the sea bottom, has been found to satisfy the conditions of the theory

The dotted line delineates the model derived from first onsets

Synthetic section to be analysed.

This shows the sea bottom at a depth of between 0 5 & 1 0 secs (two—way time),and its associated reverberations

TWO-WAY TRAVEL TRAVEL TIME (secs.)

0   1   2   3   4

B

Output showing the 3 layers picked
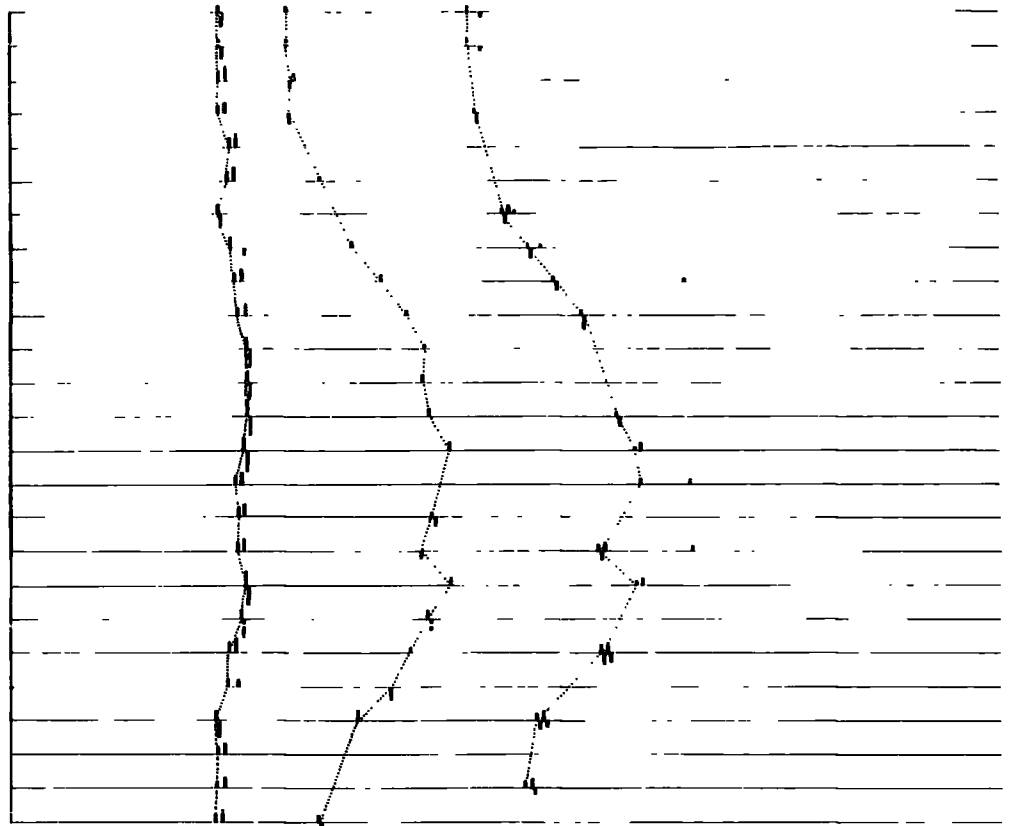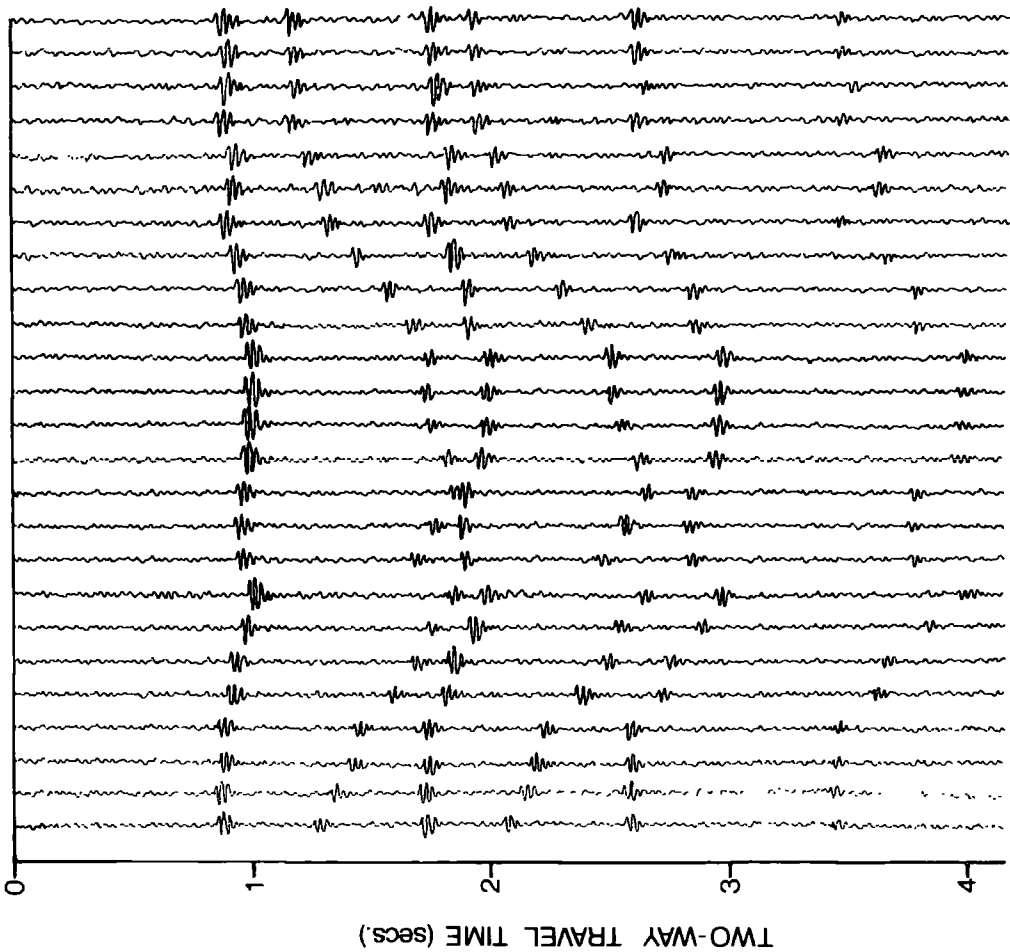
Synthetic section to be analysed.

This contains 3 layers and multiples.

TWO-WAY TRAVEL TIME (secs.)

C

Output clearly showing the 3 seismic horizons

The technique has been very efficient at picking the second
horizon from the sea bottom multiple

Synthetic section to be analysed

The second layer is immersed in the first
sea bottom multiple

TWO-WAY TRAVEL TIME (secs.)

0

1

2

3

4

which indicates the peaks that have been allowed through under the restrictions described in section 3.6.1. Each spike represents the amplitude, phase and time of arrival that has been accepted on Chn1. It can be seen that all primary arrivals from the sea bottom have been output, whilst all the reverberations and noise peaks have been removed. The dotted line represents the model that has been derived from the first onsets.

Fig.3.11.B shows the synthetic section derived from the sea bottom and two deeper structures, both these deeper structures appear throughout the entire section. The right hand diagram shows the output which has picked all three horizons, this model again fits the real structure.

The third example shown in Fig.3.11.C contains three seismic reflectors: a) the sea bottom; b) a second layer at a fairly constant depth beneath the sea bottom but immersed in the first sea bottom reverberation over much of the section of Chn1; and c) a deeper layer dipping downwards over the later part of the section. The sea bottom is picked throughout its entirety and fits the model accurately. Even though the second layer is completely immersed in the first sea bottom multiple over most of the section it has been brought out most satisfactorily, as has the deeper third layer. Again noise and multiples have not been chosen by the program.

3.6.5 <u>Discussion of the 'CHNS' technique</u>

a)   This method has been successful in removing multiples from the seismic sections shown, and also in removing noise peaks that occur above a certain level.

b) The models that have been derived from the seismic sections have been in good agreement with the known models. The technique has thus been shown to be applicable to horizontal and dipping interfaces, and for signals immersed in noise or multiples.

c) A major difficulty that is found with this technique is the picking of corresponding arrivals across all four seismic recording channels, although the seismic sections tested show this does not produce large scale errors (i.e. multiples are not picked throughout the entire seismic section). In Chapter 4 it is shown that pre-spiking of the seismogram enables the efficiency of picking corresponding arrivals to be improved.

3.7 'INTERCEPT' technique of multiple elimination

Two seismic traces derived from two different shots are required for the theory of the 'INTERCEPT' technique. The basic aim being to draw an imaginary line through corresponding arrivals on the two traces and to obtain the co-ordinates at which this line intersects lines drawn through other corresponding arrivals. The two assumptions that are made throughout this theory are that the acoustic interfaces should ideally have a finite dip, and the aperture over which the reflections (primary arrivals and multiples) have been produced for each layer is assumed flat for each shot. This latter assumption becomes more valid for vertical incidence work as the depth to the seismic horizon increases since 'moveout' is reduced. In the theory that follows it will be shown that the first assumption of a finite dip is a requirement for the removal of primary reverberations.

<u>Fig. 3.12   Theory of the 'INTERCEPT' technique</u>

Diagram A shows the build up required for the general equations

derived for the 'INTERCEPT' technique.   In diagrams B and C are shown

the intersection points of the imaginary lines drawn through primary

reverberations and interface reverberations respectively.

A

rth record   sth record

$\mathcal{S}_1 r_1$ $\mathcal{S}'_1 s_1$

$\mathcal{S}_2 r_2$ $\mathcal{S}'_2 s_2$

$\mathcal{S}_3 r_3$ $\mathcal{S}'_3 s_3$

$\mathcal{S}_n r_n$ $\mathcal{S}'_n s_n$
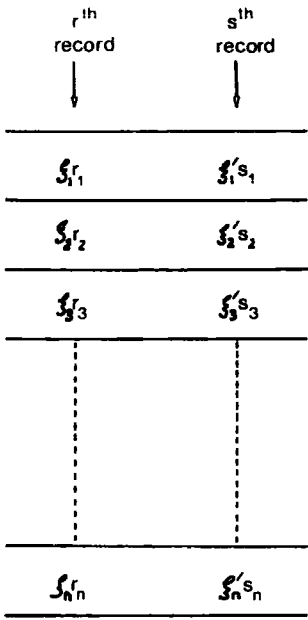
r_i = 2−way travel time in the
i^{th} layer . i = 1,2,3,···· ·n

$\mathcal{S}_1, \mathcal{S}_2, \mathcal{S}_3, \cdots \mathcal{S}_n$ & $\mathcal{S}'_1, \mathcal{S}'_2, \mathcal{S}'_3 \cdots \mathcal{S}'_n$ are the number of passes of the ray in each layer for the rth & s^{th} seismograms.

B

TIME Y

rth record   sth record

$(k+1)\sum s$

$(k+1)\sum r$

$k\sum s$

$k\sum r$

C_{k+1}

C_k

$\sum r$

$\sum s$

C_m

X(m,k),Y(m,k)
&
X(m,k+1),Y(m,k+1)

0   X_1 X_2 X

←Δx→
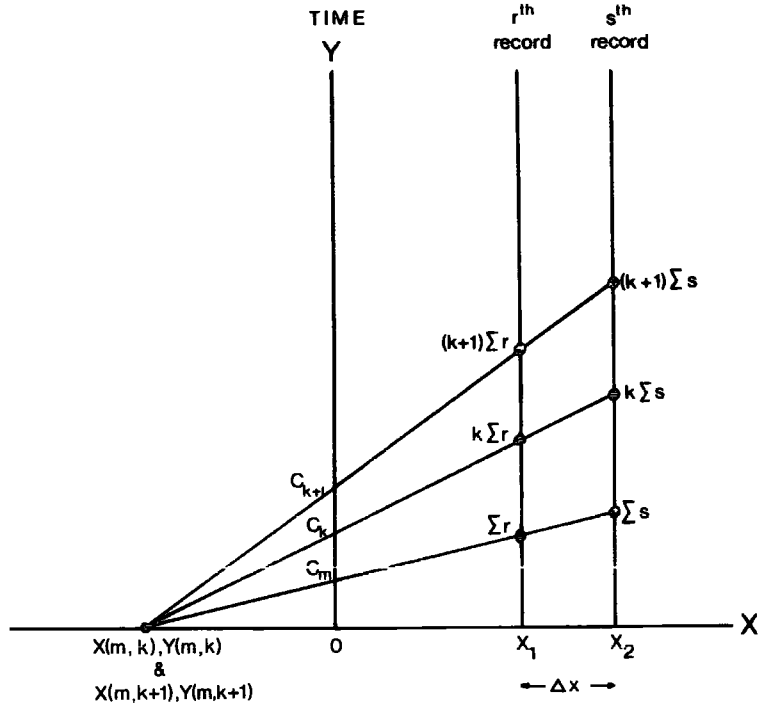
PRIMARY REVERBERATIONS

k = order of primary = 2,3,4,········

C

TIME Y

rth record   sth record

$2\xi + \sum \xi s$

$2r_\xi + \sum \xi r$

$s_\xi + \sum \xi s$

$\xi + \sum \xi r$

$\sum \xi s$

C_{n_1}

C_{n_2}

$\sum \xi r$

C_{n_3}

X(n₁,n₂),Y(n₁,n₂)
&
X(n₁,n₃),Y(n₁,n₃)

0   X_1 X_2 X

← Δx →
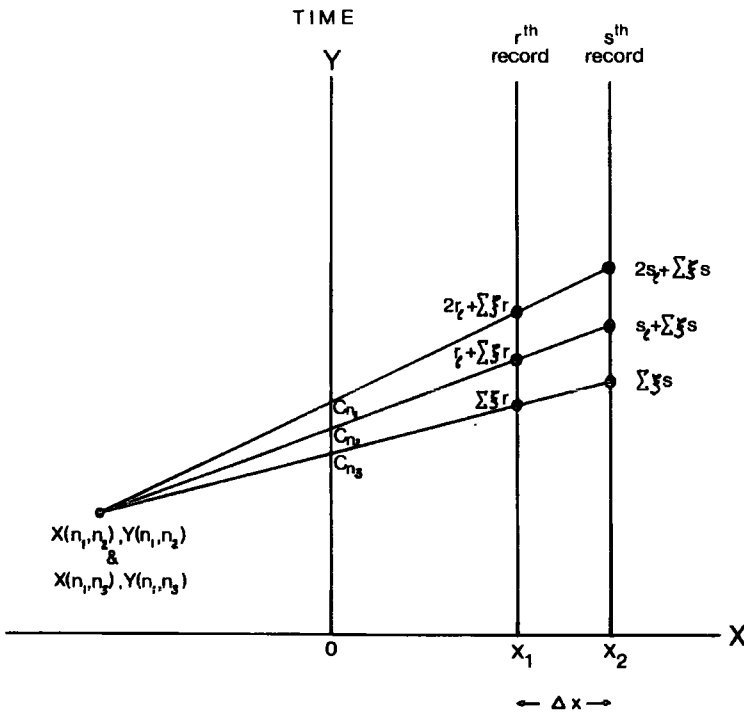
INTERFACE REVERBERATIONS

ξ, s_ξ = layer reverberation is being produced in.

3.7.1 Theory of the 'INTERCEPT' technique

Considering the rth and s^{th} seismic traces (Fig.3.12.A) we initially require to derive the general equations defining the x and y co-ordinates of the intersection points of the imaginary lines drawn through corresponding arrivals on these r^{th} and s^{th} records. If we consider n-layers it is necessary to determine the relationships between the primary arrivals and the reverberations, i.e. consider the nth reverberation and the mth primary arrival.

From Fig.3.12.A we have for the rth seismic trace:

$$\mathcal{S}_1 r_1 + \mathcal{S}_2 r_2 + \mathcal{S}_3 r_3 + \cdots\cdots + \mathcal{S}_n r_n \qquad (n^{th} \text{ reverberation})$$

$$r_1 + r_2 + r_3 + \cdots\cdots\cdots + r_m \qquad (m^{th} \text{ primary})$$

where $\mathcal{S}_1, \mathcal{S}_2, \mathcal{S}_3, \cdots\cdots \mathcal{S}_n$ are the number of passes within any one layer and will be integer valued. $r_1, r_2, r_3, \cdots\cdots r_n$ are the two-way travel times for each layer.

These equations may be summed in the form:

$$n^{th} \text{ reverberation} = \sum_{j=1}^{n} \mathcal{S}_j r_j$$

$$m^{th} \text{ primary} = \sum_{i=1}^{m} r_i$$

Similarly for the sth seismic trace we have:

$$\zeta_1' s_1 + \zeta_2' s_2 + \zeta_3' s_3 + \cdots \cdot \zeta_n' s_n \qquad n^{th} \text{ reverberation}$$

$$s_1 + s_2 + s_3 + \cdots \cdot + s_m \qquad m^{th} \text{ primary}$$

Assuming we are able to pick off corresponding arrivals on each seismic trace then:

$$\zeta_1' = \zeta_1 \quad , \quad \zeta_2' = \zeta_2 \quad , \quad \zeta_3' = \zeta_3 \quad , \quad \cdots \quad \zeta_n' = \zeta_n$$

therefore: n^{th} reverberation $= \displaystyle\sum_{j=1}^{n} \zeta_j s_j$

m^{th} primary $= \displaystyle\sum_{i=1}^{m} s_i$

Now from the equation for a straight line, the intercepts of the imaginary lines drawn through the nth reverberation and m^{th} primary may be determined, (i.e. points on the Y axis at X = 0):

Intercept for the primary
$$C_m = \sum r_i - \frac{\sum s_i - \sum r_i}{\Delta x} \cdot x_1$$

$$= \sum r_i - \frac{\sum (s_i - r_i)}{\Delta x} \cdot x_1 \qquad \text{---} (3.5.)$$

Intercept for the reverberation
$$C_n = \sum_j \zeta_j r_j - \frac{\sum \zeta_j (s_j - r_j)}{\Delta x} \cdot x_1 \qquad \text{---} (3.6.)$$

where $x_1 = x$ co-ordinate of the rth seismic trace and $\Delta x = x_2 - x_1$
where $x_2 = x$ co-ordinate of the sth seismic trace (n.b. for convenience the i's and j's are dropped from the $\sum$).

The intersection point of these two imaginary lines may then be determined from the straight line formulae:

$$Y(n,m) = \frac{\sum S_i - \sum r_i}{\Delta x} \cdot X(n,m) + C_m \qquad —(3.7.)$$

$$Y(n,m) = \frac{\sum \ell_j S_j - \sum \ell_j r_j}{\Delta x} \cdot X(n,m) + C_n \qquad —(3.8.)$$

Eliminating $Y(n,m)$ from 3.7 and 3.8 we have:

$$\frac{\sum (S_i - r_i)}{\Delta x} \cdot X(n,m) + C_m = \frac{\sum \ell_j (S_j - r_j)}{\Delta x} \cdot X(n,m) + C_n$$

$$\therefore \quad X(n,m) = \frac{\Delta x \cdot (C_m - C_n)}{\sum \ell_j (S_j - r_j) - \sum (S_i - r_i)} \qquad —(3.9.)$$

Substituting 3.9 back into 3.7 we have:

$$Y(n,m) = \frac{(C_m - C_n) \sum (S_i - r_i)}{\sum \ell_j (S_j - r_j) - \sum (S_i - r_i)} + C_m \qquad —(3.10.)$$

Thus we may define the required intersection points from the equations 3.5, 3.6, 3.9 and 3.10. All corresponding values of $X(n,m)$ and $Y(n,m)$ are then stored by the program.

Since equations 3.9 and 3.10 have an infinite number of solutions four important general cases will be considered: a) horizontal layering; b) primary reverberations (definition in section 3.3); c) inter-layer reverberations (definition in section 3.3); and d) horizontal layering for inter-layer reverberations.

a) Horizontal layering

Considering the nth layer we cannot have all layers n, n-1, n-2,

.... horizontal. If this were the case we would have $S_j = \Gamma_j$ and $S_i = \Gamma_i$ for all $j = n$, n-1, n-2, ... and $i = n$, n-1, n-2, ..., and as a consequence the denominator in equation 3.9 would equal zero. This fact would therefore mean $X(n, m) \rightarrow \pm \infty$, and as such would be indeterminate.

b)   <u>Primary reverberations</u>

Primary reverberations from the nth layer will always intersect the primary arrival from the nth layer on the X-axis, i.e. at Y = 0. The intersection point for the mth layer primary arrival and reverberations will also occur at Y = 0 but at a different value along the X-axis to the nth layer (Fig.3.12.B). This distinguishing property of the primary reverberations is used in their removal from the seismic record.

Verification of the above statement is now given:

for primary reverberations we require:

$$S_1 = S_2 = S_3 \ldots\ldots = k \qquad , \text{ where } k = 2, 3, 4, \ldots\ldots$$

(Fig.3.12.A)

and we also require m = n in equations 3.9 and 3.10, i.e. we consider primary multiples from the nth layer.

therefore:
$$\sum_{j=1}^{n} S_j r_j = k \sum_{j=1}^{n} r_j \qquad \text{and} \qquad \sum_{i=1}^{m} r_i = \sum_{j=1}^{n} r_j$$

(for convenience let $\sum = \sum_{j=1}^{n}$)

Equation 3.5 therefore becomes:

$$C_m = \sum r_j - \frac{\sum(s_j - r_j)}{\Delta x} \cdot x_1 \qquad \text{(primary)}$$

and
$$C_k = k \left[\sum r_j - \frac{\sum(s_j - r_j)}{\Delta x} \cdot x_1 \right] \qquad \text{(primary multiple)}$$

Thus: $$C_m - C_k = (1-k)\left[\sum r_j - \frac{\sum(s_j - r_j)}{\Delta x}\cdot x_1\right]$$

with the result that equation 3.9 becomes:

$$X(m,k) = \frac{\Delta x \cdot (1-k)\cdot\left[\sum r_j - \frac{\sum(s_j - r_j)}{\Delta x}\cdot x_1\right]}{(k-1)\cdot\sum(s_j - r_j)}$$

$$= \frac{x_1\sum(s_j - r_j) - \Delta x\sum r_j}{\sum(s_j - r_j)} \qquad —(3.11.)$$

and equation 3.10 becomes:

$$Y(m,k) = \frac{\sum(s_j - r_j)}{k\sum(s_j - r_j) - \sum(s_j - r_j)}\cdot\left[\sum r_j - \frac{\sum(s_j - r_j)}{\Delta x}\cdot x_1\right](1-k) + C_m$$

$$= \frac{\sum(s_j - r_j)}{(k-1)\sum(s_j - r_j)}\cdot\left[\sum(s_j - r_j)\cdot\frac{x_1}{\Delta x} - \sum r_j\right](k-1) + \sum r_j - \frac{\sum(s_j - r_j)x_1}{\Delta x}$$

$$= 0 \qquad —(3.12.)$$

Now considering the $(k+1)^{th}$ multiple

$$C_{k+1} = (k+1)\sum r_j - \frac{(k+1)\sum(s_j - r_j)}{\Delta x}\cdot x_1$$

$$\therefore \quad C_m - C_{k+1} = (-k)\left[\sum r_j - \frac{\sum(s_j - r_j)}{\Delta x}\cdot x_1\right]$$

which results in equation 3.9 becoming:

$$X(m, k+1) = \Delta x\cdot(-k)\cdot\left[\sum r_j - \frac{\sum(s_j - r_j)}{\Delta x}\cdot x_1\right]\Big/ k\sum(s_j - r_j)$$

$$= \frac{x_1\sum(s_j - r_j) - \Delta x\sum r_j}{\sum(s_j - r_j)} \qquad —(3.13.)$$

and equation 3.10 becomes:

$$Y(m, k+1) = \frac{\Sigma(s_j - r_j)}{k\,\Sigma(s_j - r_j)} \left[\Sigma r_j - \frac{\Sigma(s_j - r_j)}{\Delta x} \cdot x_1 \right] \cdot (-k) + \Sigma r_j - \frac{\Sigma(s_j - r_j)}{\Delta x} \cdot x_1$$

$$= 0 \qquad - (3.14.)$$

Therefore comparing equation 3.11 with 3.13, and equation 3.12 with 3.14, we see that:

$$X(m,k) = X(m,k+1)$$

and

$$Y(m,k) = Y(m,k+1) = 0$$

which verify the previously stated conditions required for primary arrivals and primary reverberations. Thus considering the primary arrival to have the smallest time lag all subsequent intersections at the above points are considered to be multiples and will be removed by the program.

c)   Inter-layer reverberations

This type of reverberation may also be removed from the record since as for primary multiples, inter-layer reverberations from a particular layer will always intersect at the same point (Fig.3.12.C). Verification of this statement is now given.

If we consider the reverberation sequence:

$$S_1 r_1 + S_2 r_2 + \cdots\cdots + S_\ell r_\ell + \cdots\cdots + S_n r_n \qquad (r^{th} \text{ record})$$

$$S_1 s_1 + S_2 s_2 + \cdots\cdots + S_\ell s_\ell + \cdots\cdots + S_n s_n \qquad (s^{th} \text{ record})$$

then we have for the $(\ell+1)^{th}$ and $(\ell+2)^{th}$ reverberations in the ℓth layer, the sequencies:

$$S_1 r_1 + S_2 r_2 + \cdots + (S_\ell+1) r_\ell + \cdots + S_n r_n$$

$$S_1 s_1 + S_2 s_2 + \cdots + (S_\ell+1) s_\ell + \cdots + S_n s_n$$

and

$$S_1 r_1 + S_2 r_2 + \cdots + (S_\ell+2) r_\ell + \cdots + S_n r_n$$

$$S_1 s_1 + S_2 s_2 + \cdots + (S_\ell+2) s_\ell + \cdots + S_n s_n$$

These may be simplified to the expressions (Fig.3.12.C):

$$\sum \mathcal{f}_j r_j \quad ; \quad r_\ell + \sum \mathcal{f}_j r_j \quad ; \quad 2r_\ell + \sum \mathcal{f}_j r_j \qquad (r^{th}\ \text{record})$$

$$\text{and} \quad \sum \mathcal{f}_j s_j \quad ; \quad s_\ell + \sum \mathcal{f}_j s_j \quad ; \quad 2s_\ell + \sum \mathcal{f}_j s_j \qquad (s^{th}\ \text{record})$$

Equations 3.5 and 3.6 then take the form:

$$C_{n_1} = \sum \mathcal{f}_j r_j - \frac{\sum \mathcal{f}_j (s_j - r_j)}{\Delta x} x_1$$

$$C_{n_2} = r_\ell + \sum \mathcal{f}_j r_j - \frac{s_\ell - r_\ell + \sum \mathcal{f}_j (s_j - r_j)}{\Delta x} \cdot x_1$$

$$C_{n_3} = 2r_\ell + \sum \mathcal{f}_j r_j - \frac{2s_\ell - 2r_\ell + \sum \mathcal{f}_j (s_j - r_j)}{\Delta x} \cdot x_1$$

Thus we have the relationships:

$$C_{n_1} - C_{n_2} = \frac{x_1 s_\ell - x_1 r_\ell - \Delta x . r_\ell}{\Delta x} \quad ; \quad C_{n_1} - C_{n_3} = \frac{2(x_1 s_\ell - x_1 r_\ell - \Delta x . r_\ell)}{\Delta x}$$

Substituting these into equations 3.9 and 3.10 we have:

$$X(n_1, n_2) = \frac{x_1 s_\ell - x_1 r_\ell - \Delta x . r_\ell}{\sum \mathcal{f}_j (s_j - r_j) - r_\ell + s_\ell - \sum \mathcal{f}_j (s_j - r_j)} = \frac{x_1 s_\ell - x_1 r_\ell - \Delta x . r_\ell}{s_\ell - r_\ell}$$

$$Y(n_1, n_2) = \frac{[\sum \mathcal{f}_j (s_j - r_j)] . [x_1 s_\ell - x_1 r_\ell - \Delta x . r_\ell]}{\Delta x . (s_\ell - r_\ell)} + \sum \mathcal{f}_j r_j - \frac{\sum \mathcal{f}_j (s_j - r_j)}{\Delta x} . x_1$$

and similarly:

$$X(n_1, n_3) = \frac{2(x_1 s_\ell - x_1 r_\ell - \Delta x . r_\ell)}{\sum \mathcal{f}_j (s_j - r_j) - 2r_\ell + 2s_\ell - \sum \mathcal{f}_j (s_j - r_j)} = \frac{x_1 s_\ell - x_1 r_\ell - \Delta x . r_\ell}{s_\ell - r_\ell}$$

$$Y(n_1, n_3) = \frac{[\sum \mathcal{f}_j (s_j - r_j)] . [x_1 s_\ell - x_1 r_\ell - \Delta x . r_\ell]}{\Delta x . (s_\ell - r_\ell)} + \sum \mathcal{f}_j r_j - \frac{\sum \mathcal{f}_j (s_j - r_j)}{\Delta x} . x_1$$

Thus comparing $X(n_1,n_2)$ with $X(n_1,n_3)$, and $Y(n_1,n_2)$ with $Y(n_1,n_3)$ we see that:

$$X(n_1,n_2) = X(n_1,n_3) \text{ and } Y(n_1,n_2) = Y(n_1,n_3)$$

which proves that these types of inter-layer reverberations intersect one another at the same point, and knowing this property they may be removed from the seismic record.

d)   Horizontal layering for inter-layer reverberations

Considering the type of inter-layer reverberations described above we require, for the ℓth layer reverberation sequence to have points of equal intersection, the depths r_ℓ and s_ℓ not to be equal. If r_ℓ does equal s_ℓ then the equations above defining $X(n_1,n_2)$, $X(n_1,n_3)$, ... would have infinite values since $s_\ell - r_\ell = 0$. This means that the X-values would be indeterminable and as such the inter-layer reverberations would not be removed from the seismic record.

Generalizing the above examples we require to determine all the X and Y -values of intersection for every imaginary line that has been 'drawn' through corresponding arrivals on the rth and s^{th} seismic records. Having obtained these values the program will then: 1) store all the lines (i.e. arrivals) that have intersected at a common X and Y point; 2) keep the arrival with the lowest time lag (with respect to the shot instant) and remove the later arrivals passing through the same X and Y, these being regarded by the program to be multiples of the lowest time lag arrival; and 3) all arrivals that do not have a common X and Y with any other arrivals are regarded as primary arrivals and stored. This latter point makes the assumption that corresponding arrivals on the rth and s^{th} seismic traces have been correlated correctly. If correlation

becomes difficult then the efficiency of this technique is reduced, although the application of spiking filter to the rth and s^{th} records prior to processing increases the resolution of the seismic signal and hence improves the correlation.

To obtain corresponding arrivals on the rth and s^{th} seismic records the program compares the time, phase and amplitude characteristics, of each arrival above a certain discriminating level. This level is obtained by taking the root mean square or absolute value of a section containing noise only. To increase the efficiency of this procedure when there is a low signal to noise ratio a spiking filter may be applied to the records to help resolve the signal.

3.7.2 Application of the 'INTERCEPT' technique

Two theoretical examples are used to apply this theory, the first a simple section having no noise, the second having noise and also using a pre-spiking filter.

a)   No noise

The noise free case shown in Fig.3.13 is used to test the validity of the theory described in section 3.7.1, Fig.3.13.A is the synthetic section and Fig.3.13.B the resultant seismogram. Also included within this synthetic section are multiples which are to be removed. The model used has four layers, three of which show a synclinal structure, whilst the fourth, layer 2, 'pinches out' against layer 1 in two places.

Output in Fig.3.13.C shows the positions, phase and amplitude of

Fig. 3.13 Test of the 'INTERCEPT' theory on a synthetic

    seismic section containing a zero noise level

DEPTH IN KMS.

A
INPUT MODEL

LAYER 2
LAYER 2
LAYER 1
LAYER 3
LAYER 4

B
SEISMIC
SECTION

C
OUTPUT
MODEL
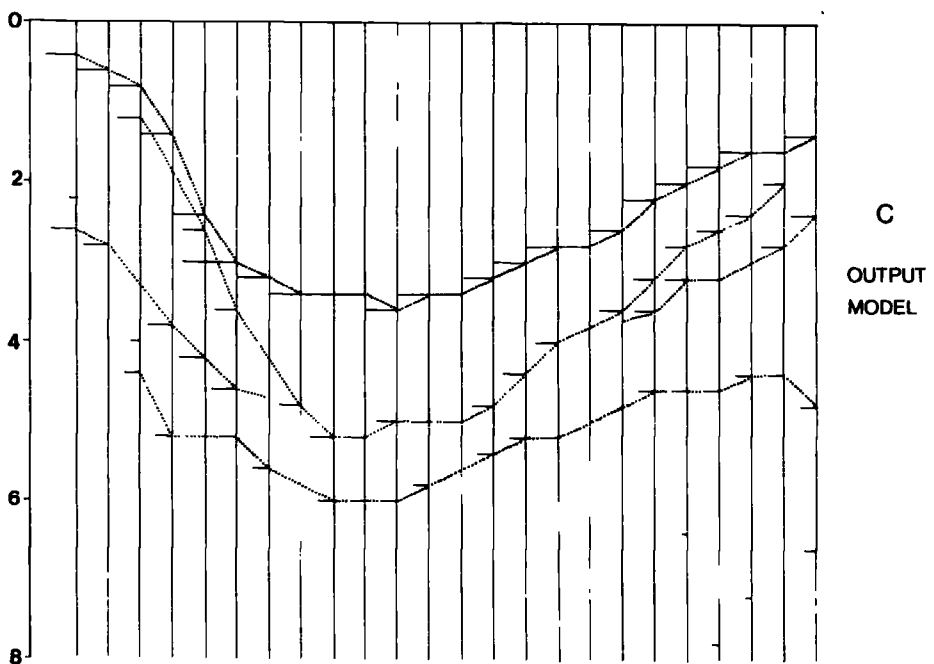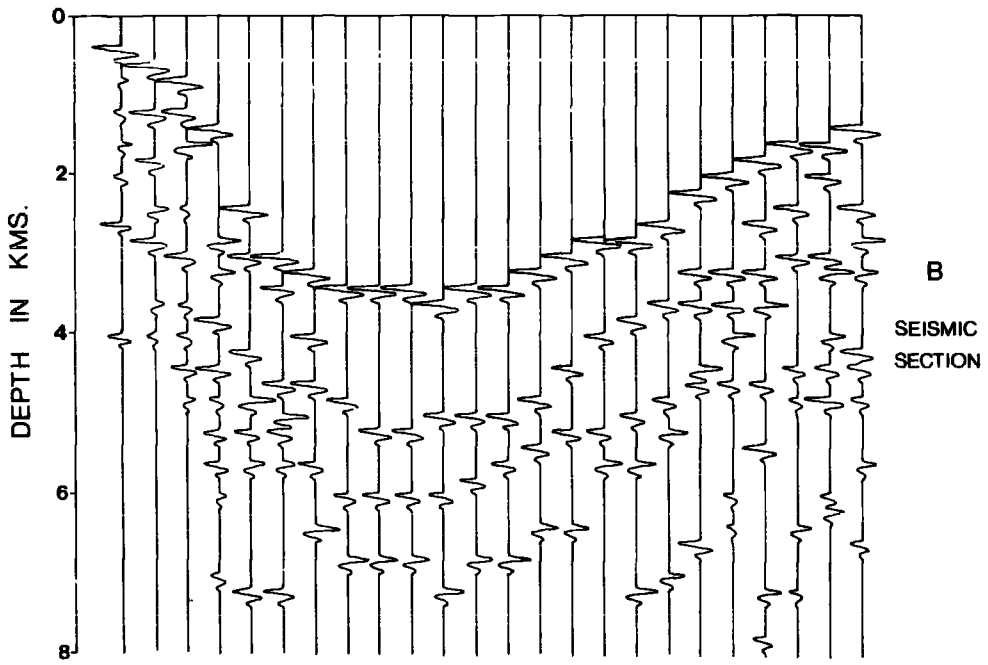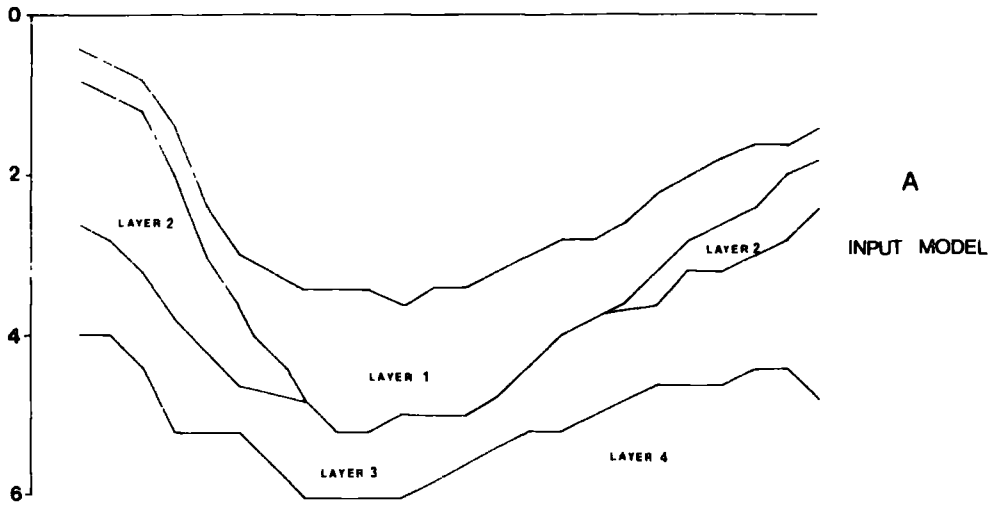
Fig. 3.14 Application of the 'INTERCEPT' technique to a

seismic section

A spiking filter is applied to the input seismic section to help

resolve the signals. The output, showing the position of each peak

chosen by the program to be primary arrivals, is shown to the right.

The model produced by pre-spiking and application of the 'INTERCEPT'

technique is delineated by the dotted lines.

OUTPUT

INPUT

LEVEL PRODUCED AFTER PRE-OPENING
OF EACH SEISMOGRAM
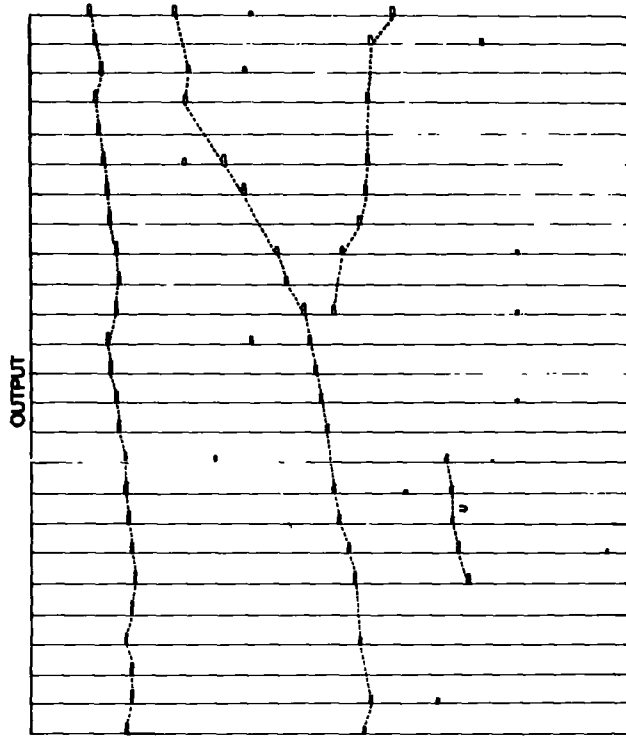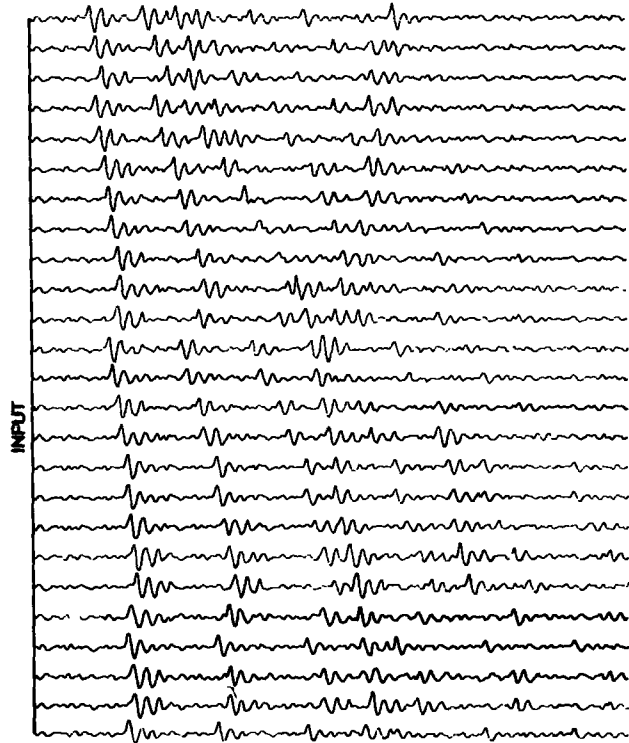
SYNTHETIC SECTION
TO BE ANALYZED

each peak that has been computed to be a primary arrival and not a multiple. This output model appears in excellent agreement with the input model.

b)   Pre-spiking

The use of a spiking filter to improve the resolution of the signal was found to help the program in choosing corresponding arrivals from one seismic record to the next. The seismic section that was analysed is shown on the left of Fig.3.14, whilst the output from the program is drawn on the right. The synthetic section in this instance contains noise, first arrivals and multiples from the seismic horizons. The major frequency of the signal is 20 c/s (at 6dB $\pm$ 5 c/s) and noise 28 c/s (at 6dB $\pm$ 5 c/s).

The model derived from the theory is again in good agreement with the known model, and although some multiples have not been removed all horizons have clearly been brought out by this technique. The success of the theory is shown by the fact that the horizon marked U can be readily picked from the output, whilst its onset in the input seismic section is not so clearly discernible.

3.7.3 Discussion of the 'INTERCEPT' technique

This technique has been shown to be a fairly efficient process for the removal of multiples from a seismic trace with the result that the primary arrivals and the subsequent structure are more clearly visible from the final output. Although this technique has certain limitations and assumptions it still has one major advantage over the 'CHNS'

technique in that it may remove the more complex inter-layer multiples. The great advantage that this 'INTERCEPT' method has over the optimized recursive filter is that it does not require prior knowledge of the reflection coefficients of the interfaces. However it must be noted that, in Chapter 4, it is shown that if these reflection coefficients are known accurately then the optimized recursive filter will have a greater efficiency of multiple removal than the 'INTERCEPT' and 'CHNS' techniques.

Major difficulties encountered with the 'INTERCEPT' theory include the following:

a)   If the horizons are horizontal then the value X(n,m) will occur at $\pm \infty$, thus the multiples cannot be removed. To overcome this problem for primary reverberations we can test the intercept value on the Y axis at X=0. Any integer values of one another will be primary multiples. It must be stated that this procedure is extremely dangerous since primary arrivals may also be removed. A safer method may be to observe which arrivals have been removed as being multiples on an adjacent dipping section and then follow these 'removed' arrivals through to the section where the layering is horizontal and thus gain a knowledge of which arrivals are multiples.

b)   More complex inter-layer multiples may be removed by this technique provided that the layer producing the multiples has a finite dip, otherwise X(n,m) values will again have points of intersection at $\pm \infty$

c)   The picking of corresponding arrivals on the sth and r^{th} seismic traces is of major importance and may cause some trouble if the signal

to noise ratio is low. If this is the case then it is found that the use of a pre-spiking filter helps in the picking of corresponding arrivals.

CHAPTER 4

4.1 Comparison of efficiencies of the multiple elimination techniques developed

This comparison is made on the seismic section shown in Fig.4.1.A in which three layers have been included along with water-layer reverberations. Throughout this section (Fig.4.1.A) the signal has its peak frequency at 35 c/s (at 6dB ± 10 c/s) and the noise at 38 c/s (at 6dB ± 5 c/s). For the formulation of the efficiency, inter-layer multiples were not included in the seismic section tested since they could not be removed effectively by the 'CHNS' technique. Thus it must be noted that the 'CHNS' technique would have its efficiency value decreased if these more complex multiple reflections were included. Another important point which is not shown by this example (Fig.4.1) is that the computation times for each technique will increase as the number of layers and/or number of points sampled increases, the optimized recursive filter having the largest increase in computation time of the three techniques developed.

Results from the application of the 'INTERCEPT' technique, optimized recursive filter and 'CHNS' technique to the input seismic section are displayed in Fig.4.1.B, C and D respectively.

These output sections from each technique show a number of important features:

1) the optimized recursive filter, although still allowing noise peaks through to the output section, has suppressed all the multiples, the other two techniques, whilst removing the majority of noise peaks, have
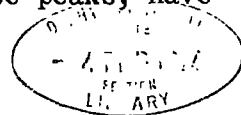
Fig. 4.1 Comparison of the three multiple elimination

techniques developed to the same seismic section

The three techniques tested are: B. the 'INTERCEPT' technique,

C. the optimized recursive filter, and D. the 'CHNS' technique. In

A. is shown the seismic section to be analysed by each.

A:- Input seismic section to be analysed

Two-way travel time (secs.)

B:- Output using the 'INTERCEPT' technique

Two-way travel time (secs.)

C:- Output using the optimized recursive filter

D:- Output using the 'CHNS' technique
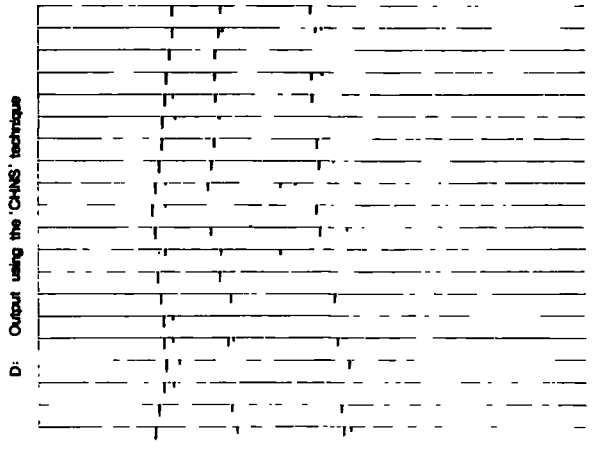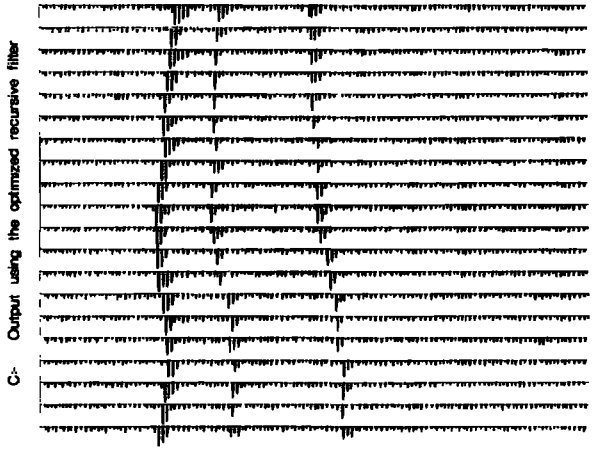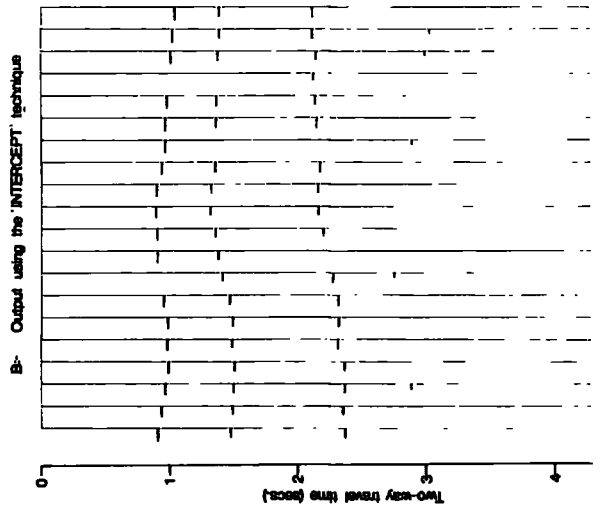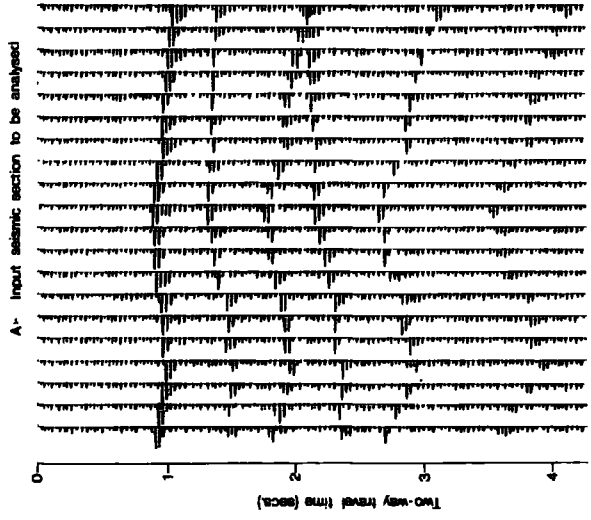
not completely removed all multiples, particularly in the case of the 'CHNS' technique.

2)   identification of the primary seismic signals from each reflecting horizon has been improved by each technique, (i.e. interpretation of the structural model has been made easier), the optimized recursive filter attaining the highest success at this identification process.

3)   although, in the case of the 'INTERCEPT' and 'CHNS' techniques, some of the primary multiples have been removed they have not been removed on a large scale over the seismic section, i.e. it is still possible to delineate the three seismic horizons from their output.

4.1.1 Derivation of the efficiency function

In Fig.4.2 the computation time required for processing the seismic section of Fig.4.1.A is plotted against the efficiency for each technique. The theory used to obtain an expression for efficiency is now given.

The efficiency for each process, applied to one individual seismic record, is defined on three known and measurable functions:

1.   the number of primary arrivals that are picked,

2.   the number of multiples removed,

and 3.   the time at which the primary arrivals are computed compared to the known times of arrival.

As a consequence the efficiency function E, for each seismic record, is defined as:

$$E = \left(\frac{N'}{N} \cdot 100 + \frac{M-M'}{M} \cdot 100 + \frac{1}{k} \cdot \sum_{j=1}^{k} \left(100 - \frac{|T_j - T_j'|}{T_j} \cdot 100 \right) \right) / 3$$

where:

$$N' \quad = \quad \text{number of primary arrivals chosen}$$

$$N \quad = \quad \text{actual number of primary arrivals known}$$

$$M' \quad = \quad \text{number of multiples not removed}$$

$$M \quad = \quad \text{known number of multiples}$$

$$T' \quad = \quad \text{time that primary arrival has been computed}$$

$$T \quad = \quad \text{known time of primary arrival}$$

$$K \quad = \quad \text{number of primary arrivals picked}$$

Thus the total efficiency (in percent) for the technique being considered over n seismograms is defined on:

$$E(n) = \frac{100}{3n} \cdot \sum^{n} \left(\frac{N'}{N} + \frac{M - M'}{M} + \frac{1}{k} \cdot \sum_{j=1}^{k} \left(1 - \frac{|T_j - T_j'|}{T_j} \right) \right) \qquad -(4.1.)$$

The individual efficiency values of 1., 2. and 3. above, for each filter, are shown in tabular form above the diagram in Fig.4.2. Again it must be emphasised that Fig.4.2 only shows the respective efficiencies for each technique when applied to seismic sections containing only water layer reverberations, thus resulting in the high efficiency values.

4.2 Summary and conclusions

A brief summary and the conclusions that may be drawn from this work are now given and will be considered under three sections: 1) computation time; 2) efficiency; and 3) application to various geological structures.

1) Computation time

With reference to Fig.4.2 the reason for the optimized recursive

Fig. 4.2 Efficiency of the three multiple elimination

techniques

This shows the plot of computation time against efficiency for the

20 seismic records shown in Fig. 4.1. The efficiency $E(n)$ is defined

by equation 4.1. Reasons for the high levels of efficiency are explained

in section 4.2.

TOTAL EFFICIENCY E(n) MADE UP OF THE FOLLOWING (values in %)

Technique	1st arrivals chosen	Multiples eliminated	Times to reflectors
'CHNS'	81·7	95·0	99·2
'INTERCEPT'	90·0	90·0	100·0
OPTIMIZED RECURSIVE FILTER	100·0	100·0	99·9
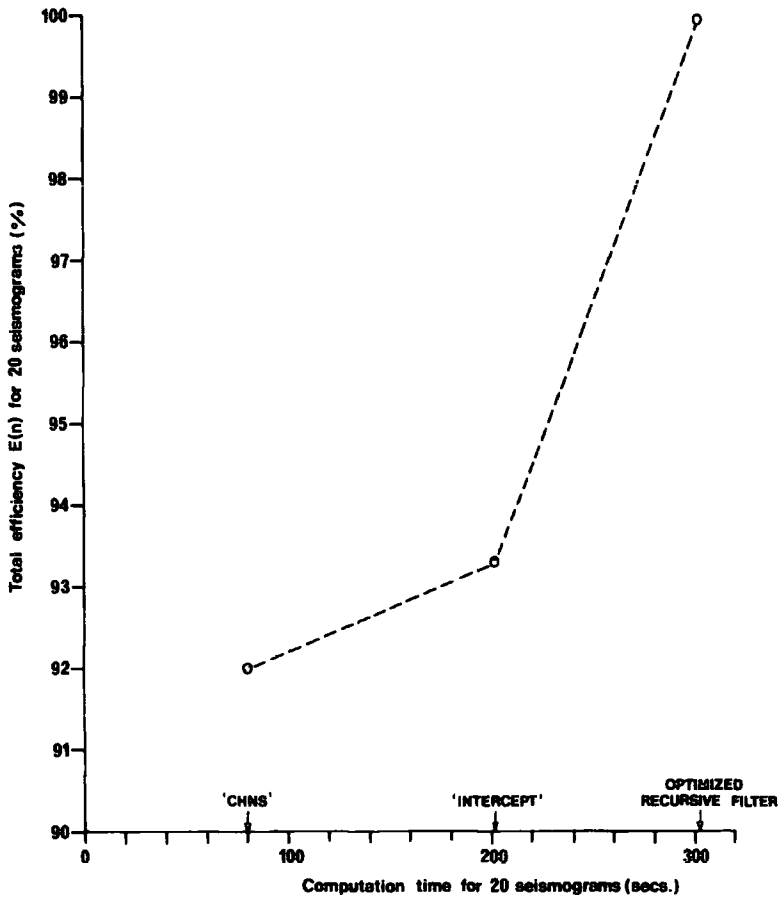
filter having a greater computation time than the other two techniques lies in the fact that it has a far greater number of correlations and convolutions, multiplication taking up the largest proportion of computation time. In Fig.4.2 the computation time for the 'CHNS' and 'INTERCEPT' techniques have pre-spiking included. Although the time for processing each seismic record will increase for each method as the number of samples is increased (i.e. considering a longer section of record) the overall shape of the plot in Fig.4.2 will remain the same. Since the speed of processing seismic data is normally of major concern, the optimized recursive filter would appear to be at a disadvantage to the 'CHNS' and 'INTERCEPT' methods. However, the efficiency of each process should also be considered in conjunction with the processing time and as a consequence the relative advantage that the 'CHNS' and 'INTERCEPT' methods have from time considerations will be reduced.

2)   Efficiency

The plot of equation 4.1 in Fig.4.2 clearly indicates a distinct advantage for the optimized recursive filter. This high efficiency level for the optimized recursive filter is due to the fact that all multiples may be defined and removed, and that the 'CHNS' and 'INTERCEPT' techniques rely a great deal on the accurate picking of corresponding seismic signals from one seismic record to another. This last fact may be improved by applying a spiking filter to the seismic records prior to processing. However an advantage that 'CHNS' and 'INTERCEPT' have over the optimized recursive filter is that the operator does not have to supply initial estimates of the reflection coefficient and travel time for each seismic horizon. In conclusion, from efficiency considerations only, the optimized recursive filter should have preference over the other two techniques

particularly when more complex inter-layer multiples exist on a record. However, if the parameters supplied to the optimized recursive filter, reflection coefficients and travel times, are unknown or unreliable, then in many cases preference should be given to the 'CHNS' and 'INTER-CEPT' techniques.

3) <u>Application to various geological structures</u>

In summary the choice of which technique to use to process a seismic section is extremely difficult since each will invariably have its limitations, and as a consequence the efficiency has to be considered along with computation time. A brief resumé of the problems involved with each technique, and which have to be considered when choosing a particular process for a particular geological structure, is now given:

1. optimized recursive filter:

> a) reflection coefficients should be reliable,
>
> b) travel time estimates should be reliable,
>
> and c) computation time is relatively slow.

2. 'CHNS':

> a) inter-layer multiples not removed,
>
> b) $\overset{.}{t^i_2} - \overset{.}{t^i_1}$ (definition in section 3.6.2) has to be greater than the sampling rate being used,
>
> and c) picking of corresponding arrivals has to be accurate.

3. 'INTERCEPT':

> a) horizontal layering results in multiples not being removed,
>
> and b) picking of corresponding arrivals has to be accurate.

Using these major limitations of the techniques developed, along with computation time, the tables drawn below may be used as an approximate guide to which process should be applied to a particular type of geological layering.

TYPE OF LAYERING	EFFICIENCY IMPORTANT, TIME UNIMPORTANT	
(may be simple or complex)	REFLECTION COEFFS) TRAVEL TIMES) RELIABLE	REFLECTION COEFFS) TRAVEL TIMES) UNRELIABLE
Horizontal layers (primary multiples)	O.R.F.	'CHNS'
Horizontal layers (primary & inter layer multiples)	O.R.F.	O.R.F.
Dipping layers (primary multiples)	O.R.F. or 'INTERCEPT'	'INTERCEPT' or 'CHNS'
Dipping layers (primary & complex multiples)	O.R.F.	'INTERCEPT'

TYPE OF LAYERING	EFFICIENCY & TIME IMPORTANT	
(may be simple or complex)	REFLECTION COEFFS) TRAVEL TIMES) RELIABLE	REFLECTION COEFFS) TRAVEL TIMES) UNRELIABLE
Horizontal layers (primary multiples)	'CHNS'	'CHNS'
Horizontal layers (primary & inter-layer multiples)	O.R.F.	'CHNS'
Dipping layers (primary multiples)	'CHNS' or 'INTERCEPT'	'CHNS' or 'INTERCEPT'
Dipping layers (primary & inter-layer multiples)	'INTERCEPT'	'INTERCEPT'

Where O.R.F. is the optimized recursive filter.

REFERENCES

Anstey, N. A. (1960) Attacking the problems of the synthetic seismogram. Geophys. Pros., 8, 242 - 259.

Anstey, N. A. (1964) Correlation techniques - A review. Geophys. Pros., 12, 355 - 382.

Anstey, N. A., and Newman, P. (1966) The sectional auto-correlogram and the sectional retro-correlogram. Geophys. Pros., 14, 389 - 426.

Allen, J. R. L. (1970) Physical processes of sedimentation an introduction. George Allen and Unwin Ltd.

Avery, O. E., Burton, G. D. and Heirtzler, J. R. (1968) An aeromagnetic survey of the Norwegian Sea. J. Geophys. Res., 73, 4583 - 4600.

Backus, M. M. (1959) Water reverberations - Their nature and elimination. Geophysics, 24, 233 - 261.

Båth, M. (1960) Crustal structure of Iceland. J. Geophys. Res., 65, 1793 - 1807.

Båth, M. (1962) Crustal structure in Iceland and surrounding ocean. ICSU Review, 4, 127 - 133.

Bernfeld, M. (1963) Pulse compression techniques. Proc. I.E.E.E., 51, 1261.

Blackman, R. B., and Tukey, J. W. (1958) The measurement of power spectra. Dover pub., Inc.

Bott, M. H. P. (1971) The interior of the Earth.
Edward Arnold.

Bott, M. H. P., Browitt, C. W. A., The deep structure of the Iceland –
and Stacey, A. P. (1971) Faeroe ridge.
Marine Geophys. Res., 1, 328 – 351.

Bott, M. H. P., and Stacey, A. P. Geophysical evidence on the origin
(1967) of the Faeroe Bank Channel – II A
gravity and magnetic profile.
Deep Sea Res., 14, 7 – 11.

Bott, M. H. P., and Watts, A. B. Deep sedimentary basins proved in
(1970) the Shetland – Hebridean continental
shelf and margin.
Nature, 225, 265 – 268.

Brekhovskikh, L. M. (1960) Waves in layered media.
In Vol.6 of Applied Mathematics and
Mechanics.
Academic Press.

Browitt, C. W. A. (1971) Seismic refraction experiments
between Iceland and Scotland.
Ph.D. Thesis, Durham University.

Bullard, E. C., Everett, J. E., The fit of continents around the
and Smith, A. G. (1965) Atlantic. In "A symposium on
continental drift".
Roy. Soc. London Philos. Trans.
series A., 258, 41 – 51.

Bullen, K. E. (1953) An introduction to the theory of
seismology.
(Second edition) Cambridge,
Cambridge University Press.

Carslaw, H. S. (1930) — Introduction to the theory of Fourier's series and integrals. (Third edition) Dover publications, Inc. Authors: James, F., and Roos, M.

CERN computer 6000 series program library (1969)

Clarke, G. K. C. (1968) — Time varying deconvolution filters. Geophysics, 33, 936 - 944.

Clay, C. S., and Liang, W. T., (1962) — Continuous seismic profiling with matched filter detector. Geophysics, 27, 786 - 795.

Crease, J. (1965) — The flow of Norwegian Sea water through the Faeroe Bank Channel. Deep Sea Res., 12, 143 - 150.

D'Hoeraene, J. and Wlodarczak, R. (1968) — A self adapting deconvolution and deringing program. Geophys. Pros., 17, 359 - 393.

Dobinson, A. (1970) — Magnetic survey of Faeroes Bank. Ph.D. Thesis, Durham University.

Dobrin, M. B. (1960) — Introduction to geophysical prospecting. (Second edition) McGraw Hill Book Co.

Dohr, G. (1971) — First experience and results with a new seismic interpretation method. Geophys. Pros., 19, 371 - 387.

Ellet, D. J. and Roberts, D. G. (1973) — The overflow of Norwegian Sea Deep Water across the Wyville-Thompson Ridge. Deep Sea Res., 20, 819 - 835.

Ewing, J. and Ewing, M. (1959)

Seismic refraction measurements in the Atlantic Ocean basins, in the Mediterranean Sea, on the Mid-Atlantic ridge, and in the Norwegian Sea. Bull. Geol. Soc. Am., 70, 291 - 318.

Ewing, M., Jardetzky, W. S., and Press, F. (1957)

Elastic waves in layered media. McGraw Hill Book Co.

Ewing, J., Worzel, J. L., Ewing, M., and Windisch, C. (1966)

Ages of horizon A and the oldest Atlantic sediments. Science, 154, 1125 - 1132.

Ewing, J., and Zaunere, R. (1964)

Seismic profiling with a pneumatic sound source. J. Geophys. Res., 69, 4913 - 4915.

Finetti, I., Nicolich, R., and Sancin, S. (1971)

Review of the basic theoretical assumptions in seismic digital filtering. Geophys. Pros., 14, 292 - 320.

Foster, M. R., Sengbush, R. L., and Watson, R. J. (1964)

Design of sub-optimum filter systems for multi-trace seismic data processing. Geophys. Pros., 12, 173 - 191.

Foster, M. R. Sengbush, R. L., and Watson, R. J. (1968)

Use of Monte Carlo techniques in optimum design of the deconvolution process. Geophysics, 33, 945 - 949.

Funnell, B. M., and Smith, A. G. (1968)

Opening of the Atlantic Ocean. Nature, 219, 1328 - 1333.

Galbraith, J. N. (1971)

Prediction error as a criterion for operator length. Geophysics, 36, 261 - 265.

Geotimes, Deep Sea Drilling
Project, leg 2. (1965), 11 - 12.

Grant, F. S., and West, G. F.   Interpretation theory in applied
(1965)   geophysics.
                                 McGraw Hill Book Co.

Gurbuz, B. M. (1972)   Signal enhancement of vibratory
                                 source data in the presence of
                                 attenuation.
                                 Geophys. Pros., 20, 421 - 438.

Harland, W. B. (1969)   Contribution of Spitsbergen to
                                 understanding of tectonic evolution
                                 of North Atlantic region.
                                 In "North Atlantic - geology and
                                 continental drift".
                                 The Am. Ass. of Pet. Geol.

Heiland, C. A. (1968)   Geophysical prospecting.
                                 Hafner Pub. Co. (second edition).

Herman, Y. (1972)   Origin of deep sea cherts in the
                                 North Atlantic.
                                 Nature, 238, 392 - 393.

Holmes, A. (1965)   Principles of physical geology.
                                 Nelson.

Hsu, H. P. (1967)   Outline of Fourier analysis.
                                 Unitech.

Jenkins, G. M., and Watts, D.G. Spectral analysis and its applications.
(1968)   Holden-Day.

Jones, E. J. W., Ewing, M.,   Influences of Norwegian Sea overflow
Ewing, J. I., and Eittreim, S. L. water on sedimentation in the northern
(1970)   North Atlantic and Labrador Sea.
                                 J. Geophys. Res., 75, 1655 - 1680.

Kay, M. (1968) North Atlantic continental drift. Am. Philos. Soc. Proc., 112, 321 - 324.

Kay, M. (1969) Continental drift in North Atlantic Ocean. In "North Atlantic - geology and continental drift". 965 - 973. The Am. Ass. of Pet. Geol.

Koefoed, O. (1960) Measurements of amplitudes of reflected seismic waves. Geophys. Pros., 8, 25 - 46.

Kukal, Z. (1971) Geology of recent sediments. Academic Press.

Kunetz, G. and Fourmann, J. M. (1968) Efficient deconvolution of marine seismic records. Geophysics, 33, 412 - 423.

Lange, F. H. (1967) Correlation techniques. Iliffe Books Ltd.

Lathi, B. P. (1968) An introduction to random signals and communication theory. International Textbook Co.

Le Pichon, X., Ewing, J., and Houtz, R. (1968) Deep sea sediment velocity determination made while reflection profiling. J. Geophys. Res., 73, 2597 - 2613.

Linsser, H. (1968) Identification of seismic impulses by digital template analysis. Intergeo - Rio (Leibniz Computing Centre).

Lisitzin, A. P. (1972)   Sedimentation in the world oceans. Soc. Economic Paleon. and mineral.

Marr, J. D., and Zagst, E. F. (1967)   Exploration horizons from new seismic concepts of CDP and digital processing.
Geophysics, 32, 207 - 224.

Mayne, W. H. (1962)   Common reflection point horizontal data stacking techniques.
Geophysics, 27, 927 - 938.

Mayne, W. H. (1967)   Practical considerations in the use of common reflection point techniques.
Geophysics, 32, 225 - 233.

Meyerhoff, H. J. (1966)   Horizontal stacking and multichannel filtering applied to common depth point seismic data.
Geophys. Pros., 14, 441 - 454.

Michon, D., Wlodarczak, R., and Merland, J. (1971)   A new method of cancelling multiple reflections, 'Souston'.
Geophys. Pros., 19, 615 - 625.

Middleton, D., and Whittlesey, J. R. B. (1968)   Seismic models and deterministic operators for marine reverberation.
Geophysics, 33, 557 - 583.

Moorbath, S., Sigurdsson, H., and Goodwin, R. (1968)   K-Ar ages of the oldest exposed rocks in Iceland.
Earth and Planet. Sci. Letters, 4, 197 - 205.

Nafe, J. E., and Drake, C. L. (1969)   Floor of the North Atlantic - Summary of geophysical data.
In "North Atlantic - geology and continental drift". 59 - 87.
The Am. Ass. of Pet. Geol.

Naimark, B. M. (1965)   Algorithm for automatic recognition of a seismic signal.
Rev. of Geophys., 3, 187 - 191.

Noe-Nygaard, A. (1962)   The geology of the Faeroes.
Quart. J. Geol. Soc. London, 118, 375 - 383.

O'Doherty, R. F., and
Anstey, N. A. (1971)   Reflections on amplitudes.
Geophys. Pros., 19, 430 - 458.

Pálmason, G. (1965)   Seismic refraction measurements of the basalt lavas of the Faeroe Islands.
Tectonophysics, 2, 475 - 482.

Pálmason, G. (1967)   Upper crustal structure in Iceland.
Soc. Sci. Islandica, 38, 67 - 68.

Pálmason, G. (1970)   Crustal structure of Iceland from explosion seismology.
Pub. of the Sci. Inst., Iceland University.

Peterson, M. N. A., and others. (1970)   Initial reports of the Deep Sea Drilling Project, vol II.
Washington, D.C. (U.S. Government Printing Office).

Pflueger, J. (1972)   Spectra of water reverberations for primary and multiple reflections.
Geophysics, 37, 788 - 796.

Raju, C. V. (1968)   A seismic study of the Iceland - Faeroes ridge.
Ph.D. Thesis, Durham University.

Ricker, N. (1940)   The form and nature of seismic waves and the structure of seismograms.
Geophysics, 5, 348 - 366.

Rice, R. B. (1962)   Inverse convolution filters.
                                     Geophysics, 27, 4 - 18.

Robinson, E. A. (1967a)   Statistical communication and
                                     detection with special reference to
                                     digital data processing of radar and
                                     seismic signals.
                                     Griffin.

Robinson, E. A. (1967b)   Multi-channel time series analysis
                                     with digital computer programs.
                                     Holden-Day.

Robinson, E. A. (1967c)   Predictive decomposition of time
                                     series with application to seismic
                                     exploration.
                                     Geophysics, 32, 418 - 484.

Rona, P. A. (1973)   Worldwide unconformities in marine
                                     sediments related to eustatic changes
                                     of sea level.
                                     Nature, 244, 25 - 26.

Rutten, K., Valeton, M., and   Measurement of the signal to noise
Van Grunsven, T. (1972)   ratio in seismic profiling.
                                     Marine Geophys. Res., 1, 445 - 450.

Saito, T., Burckle, L. H., and   Lithology and paleontology of the
Ewing, M. (1966)   reflective layer horizon A.
                                     Science, 154, 1173 - 1176.

Saxov, S., and Abrahamson, N.   A note on some gravity and density
(1964)   measurings in the Faeroe Islands.
                                     Bollettino Di Geofisca Teorica ed
                                     Applicata. 249 - 262.

Schneider, W. A. (1971) Developments in seismic data processing and analysis (1968 - 1970). Geophysics, 36, 1043 - 1073.

Stacey, A. P. (1968) Interpretation of gravity and magnetic anomalies of the north-east Atlantic. Ph.D. Thesis, Durham University.

Steele, J. H., Barrett, J. R., and Worthington, L. V. (1962) Deep currents south of Iceland. Deep Sea Res., 9, 465 - 474.

Stride, A. H., Belderson, R. H., Curray, J. R., and Moore, D. G. (1967) Geophysical evidence on the origin of the Faeroe Bank Channel - I Continuous reflection profiles. Deep Sea Res., 14, 1 - 6.

Talwani, M., and Eldholm, E. (1972) Continental margin off Norway: A geophysical study. Geol. Soc. Am., 83, 3575 - 3606.

Tarling, D. H., and Gale, N. H. (1968) Isotopic dating and palaeomagnetic polarity in the Faeroe Islands. Nature, 218, 1043 - 1044.

Treitel, S., and Robinson, E. A. (1966) Seismic wave propagation in layered media in terms of communication theory. Geophysics, 31, 17 - 32.

Treitel, S., and Robinson, E. A. (1969) Optimum digital filters for signal to noise ratio enhancement. Geophys. Pros., 18, 248 - 293.

Trorey, A. W. (1962) Theoretical seismograms with frequency and depth dependent absorption. Geophysics, 27, 766 - 785.

Tryggvason, E., and Båth, M. (1961)
Upper crustal structure of Iceland. J. Geophys. Res., 66, 1913 - 1925.

Turin, G. L. (1960)
An introduction to matched filters. I.R.E. Trans. on Information Theory, 1, 311 - 329.

Wainstein, L. A. and Zabakov, V. D. (1962)
Extraction of signals from noise. Prentice-Hall.

Watts, A. B. (1970)
Geophysical investigation in the Faeroes to Scotland region, north-east Atlantic. Ph.D. Thesis, Durham University.

White, J. E. (1965)
Seismic waves. Radiation, transmission, and attenuation. McGraw Hill.

Wuenschel, P. C. (1960)
Seismogram synthesis including multiples and transmission coefficients. Geophysics, 25, 106 - 129.

Ziolkowski, A. (1970)
A method for calculating the output pressure waveform from an air-gun. Geophys. J. Roy. Astron. Soc., 21, 137 - 161.

Ziolkowski, A. (1971)
Design of a marine seismic reflection profiling system using airguns as a sound source. Geophys. J. Roy. Astron. Soc., 23, 499 - 530.

LISTING OF COMPUTER PROGRAMS

All the major programs used by the author are listed in the following order:-

CORRN	–	Cross and autocorrelation of two functions
CONV	–	Convolution of two functions
HAN	–	Hanning window computed and applied to required function
AMPL	–	Amplitude spectrum
POW	–	Power spectrum
TEMPLATE	–	Computation of the optimized digital template
SIGREC	–	Signal recognition in noise
ORF	–	Optimized recursive filter (plus flow diagram)
CHNS	–	'CHNS' technique of multiple elimination (plus flow diagram)
INTERCEPT	–	'INTERCEPT' technique of multiple elimination (plus flow diagram)

```fortran
C     CONVOLUTION OF TWO FUNCTIONS X(LX) & Y(LY)
C     OUTPUT IN Z(LZ)
C
      SUBROUTINE CONV(X,LX,Y,LY,Z,LZ)
      DIMENSION X(LX),Y(LY),Z(LZ)
      DO 1 I=1,LZ
    1 Z(I)=0.0
      DO 2 I=1,LX
      DO 2 J=1,LY
      K=I+J-1
    2 Z(K)=Z(K)+X(I)*Y(J)
      RETURN
      END


C     CORRELATION OF TWO FUNCTIONS X(LX) & Y(LY)
C     FUNCTION Y(LY) IS MOVED W.R.T. X(LX)
C     COMPUTES THE POSITIVE HALF OF THE CROSS CORRELATION Z(LZ)
C
      SUBROUTINE CORRN(X,LX,Y,LY,Z,LZ)
      DIMENSION X(LX),Y(LY),Z(LZ)
      DO 1 J=1,LZ
      M=MINO(LY,LX-J+1)
      P=0.0
      DO 2 I=1,M
    2 P=P+X(I+J-1)*Y(I)
    1 Z(J)=P
      RETURN
      END
```

```
C      SUBROUTINE HAN COMPUTES THE HANNING WINDOW WHICH IS
C      THEN APPLIED TO THE INPUT FUNCTION E(LE)
C
C      THE FUNCTION E(LE)*C(LE) IS THEN OUTPUT. , WHERE
C      C(LE) IS THE HANNING WINDOW
C
       SUBROUTINE HAN(E,LE)
       DIMENSION E(LE),C(LE)
       C(LE)=0.0
       SUM=22.0/(7.0*FLOAT(LE))
       DO 1 I=1,LE
       TIME=FLOAT(I-1)*SUM
    1  C(I)=(1.0+COS(TIME))/2.0
       DO 2 I=1,LE
    2  E(I)=E(I)*C(I)
       RETURN
       END
```

```
C      SUBROUTINE AMPL COMPUTES THE AMPLITUDE SPECTRUM OF THE
C      INPUT FUNCTION E(LE).
C
C      C(LC) IS THE AMPLITUDE SPECTRUM OUTPUT
C
       SUBROUTINE AMPL(E,LE,C,LC)
       DIMENSION E(LE),C(101)
       LC=0
       DO 1 I=10000,41416,314
       LC=LC+1
       W=(FLOAT(I)-10000.)/10000.
       C1=0.
       S1=0.
       DO 2 J=1,LE
       RJ=FLOAT(J)*W
       C1=C1+E(J)*COS(RJ)
   2   S1=S1+E(J)*SIN(RJ)
   1   C(LC)=SQRT(C1**2+S1**2)
       RETURN
       END
```

```
C     SUBROUTINE POW COMPUTES THE POWER SPECTRUM OF THE
C     INPUT FUNCTION E(LE)
C
C     A(LA) IS THE AUTOCORRELATION FUNCTION OF E(LE)
C     H(LH) IS THE POWER SPECTRUM OUTPUT
C
      SUBROUTINE POW(E,LE,H,LH)
      DIMENSION E(LE),A(1500),H(101)
      LA=LE+LE-1
      CALL CORRN(E,LE,E,LE,A,LA)
      LH=0
      DO 5 I=10000,41416,314
      LH=LH+1
      W=(FLOAT(I)-10000.)/10000.
      S=0.0
      DO 6 J=2,LA
      TEMP=FLOAT(J-1)*W
    6 S=S+(1.0-(FLOAT(J-1)/FLOAT(LA)))*A(J)*COS(TEMP)
    5 H(LH)=A(1)+2.0*S
      RETURN
      END
```

```
C     THIS PROGRAM COMPUTES THE TEMPLATE OPTIMIZED TO AN INPUT
C     FUNCTION XOBS(I), THE THEORY IS THAT FOLLOWS IN SECTION 2.4.
C
C     EE=FREQUENCY OF THE SIGNAL (NO. OF CYCLES)
C     A=ECCENTRICITY +/-OR -
C     YS(I)=SINE WAVE FUNCTION
C     Y(I)=RAMP FUNCTION
C     KTOT=TOTAL NO. OF POINTS SAMPLED
C     D=SAMPLING RATE
C     DT(I)=TEMPLATE FUNCTION CALCULATED & OPTIMIZED
C     RESID(I)=RESIDUALS OF CALCULATED MINUS OBSERVED
C     RR=OBJECTIVE FUNCTION
C
      SUBROUTINE FCN(NPAR,GG,RF,XX,IFLAG)
      DIMENSION XX(20),GG(20),CC(20),RESID(500),XOBS(500),
     IYS(500),Y(500),DT(500),
      IF(IFLAG-1)16,11,16
   11 READ(5,2)EE,KTOT
    2 FORMAT(F10.0,I5)
      READ(5,151)(XOBS(I),I=1,KTOT)
  151 FORMAT(10F6.0)
      DO 22 I=1,KTOT
   22 XOBS(I)=100.*XOBS(I)
   13 CONTINUE
      A=XX(1)
      FR=0.
      NN=1
      LTC=KTOT-1
      C=(EE*360)/FLOAT(LTC)
      KE=IFIX(EE)*360
      KTC=(KE*KTOT)+LTC
      DO 20 N=LTC,KTC,KE
      RNN=(FLOAT(N)-FLOAT(LTC))/(FLOAT(LTC)*57.296)
      YS(NN)=SIN(RNN)
```

```fortran
   20 NN=NN+1
      R=(FLOAT(LTO)*(100.0+A))/200.0
      XMAX=R
      YMAX=1.0
      G=YMAX/XMAX
      GM=YMAX/(FLOAT(R)-R)
      I=IFIX(R)
      DO 3 N=1,I
   30 Y(N)=G*FLOAT(N-1)
      JRJ=KTOT-I
      N=I+1
      DO 40 K=1,JRJ
      Y(N)=YMAX-GM*FLOAT(K-1)
   40 N=N+1
      DO 60 N=1,KTOT
   60 DT(N)=Y(N)*YS(N)
      DO 62 N=1,KTOT
   62 DT(N)=100.0*DT(N)
      DO 70 K=1,KTOT
      RR=RR+((XOBS(K)-DT(K))*(XOBS(K)-DT(K)))
   70 RESID(K)=DT(K)-XOBS(K)
      RR=RR*1000.0
      IF(IFLAG-3)81,80,81
   80 DO 85 N=1,KTOT
      XOBS(N)=XOBS(N)/100.0
   85 DT(N)=DT(N)/100.0
      WRITE(6,82)
   82 FORMAT(' CALC. TEMPLATE OBS. TEMPLATE RESIDUALS')
      WRITE(6,83)(DT(K),XOBS(K),RESID(K),K=1,KTOT)
   83 FORMAT(10F14.2)
      WRITE(6,84)XX(1)
   84 FORMAT(F10.2)
   81 RETURN
      END
```

```fortran
C  SIGSPEC COMPUTES THE PRESENCE OF A SIGNAL IN A SEISMIC RECORD, THE
C  OUTPUT BEING IN THE FORM OF A HISTOGRAM. (THE THEORY IS GIVEN IN
C  DETAIL IN SECTION 2.5.
C
C  SUBROUTINE SPECTA COMPUTES THE POWER SPECTRUM
C  SUBROUTINE TURN COMPUTES THE FREQUENCY CONTENT
C  SUBROUTINE MAX COMPUTES THE AMPLITUDE CHARACTERISTICS
C  THE SUBROUTINES CCORN & MAX ARE NOT SPEC AS THEY HAVE
C  BEEN PREVIOUSLY LISTED
C
C         ***** INPUT CARDS *****
C
C  CARD 1 - (4I5 FORMAT) LA - LENGTH OF THE NOISE FUNCTION
C                        LX - LENGTH OF THE SEISMOGRAM
C                        LE - SAMPLING WINDOW LENGTH
C                        LB - LENGTH OF THE SIGNAL
C
C          ('LENGTH' IN THIS INSTANCE MEANS THE NUMBER OF SAMPLES)
C  CARD 2 - (10F6.0 FORMAT) B(I) - INPUT SIGNAL E.G. AIR GUN WAVELET
C  CARD 3 - (10F6.0 FORMAT) X(I) - SEISMOGRAM TO BE ANALYSED
C
      DIMENSION A(60),B(120),X(1200),HI(100),HM(100),DI(100),DN(100),
     1RA(120),PR(120),FR(120),RC(120)
      READ(5,1)LA,LX,LE,LB
      READ(5,2)(B(I),I=1,LB)
      LTCT=LX+LE-1
      CCUNT=2.0
      LCLT=2
C  LCUT IS A PRE-DETERMINED VALUE, IN THIS CASE THE VALUE MEANS
C  HALF THE POWER SPECTRUM (0 TO PI/2) IS COMPUTED
      CALL SPECTA(B,LB,LE,HA,LH,LTCT,CCUNT,LCUT)
      CALL TURN(HA,LH,DA,LDA,INCHN)
   67 READ(5,2,END=66)(X(II),I=1,LX)
    1 FORMAT(4I5)
    2 FORMAT(10F6.0)
```

```
      DO 777 I=1,LA
777   A(I)=X(I)
      CALL NMAX(A,LA,LE,PHI10,LTOT,COUNT)
      COUNT=1.
      DO 3 J=1,LTOT
      RA(J)=0.
      RB(J)=0.
      RC(J)=0.
      CALL NMAX(X,LX,LE,PHI1,J,COUNT)
      IF(ABS(PHI1)-ABS(PHI10))7,7,4
4     RA(J)=1.
7     CALL SPECTN(X,LX,LE,H,LH,J,CCUNT,LCUT)
      CALL TURN(H,LH,D,LD,INDH)
C     INDHN IS THE MAIN PEAK OF SIGNAL POWER SPECTRUM
C     INDH IS THE MAIN PEAK OF SEISMOGRAM POWER SPECTRUM
      ISHIFT=INDHN-INDH
      WRITE(6,740)INDH,ISHIFT
740   FORMAT(//,'INDH=',I5,5X,'ISHIFT=',I5)
      IF(IABS(ISHIFT)-2)103,104,104
103   LL=INDHN-5
      LLL=INDHN+5
      KK=LL+ISHIFT
      LTEMP=0
      DO 100 JK=LL,LLL
      S=H(JK)-HN(KK)
      W=HN(JK)/10.
      IF(ABS(S)-W)110,110,100
110   LTEMP=LTEMP+1
100   KK=KK+1
      LB=((LLL-LL)-(LLL-LL))/10
      IF(LTEMP-LB)104,111,111
111   RB(J)=1.
104   CONTINUE
3     IF(IABS(ISHIFT) .LT. 2)RC(J)=1.
```

```
      DO 35 J=1,LTOT
      B(J)=0.
   41 IF(RA(J)-1.0)25,41,25
   42 IF(RB(J)-1.0)25,42,25
   43 IF(RC(J)-1.0)25,43,25
      B(J)=1.
   25 CONTINUE
   35 CONTINUE
      M=0
      DO 14 I=5,LTOT,5
      M=M+1
      L=I-4
      X(M)=0.
      DO 15 J=L,I
   15 X(M)=X(M)+RA(J)+RB(J)+RC(J)+B(J)
   14 CONTINUE
      WRITE(6,16)
      WRITE(5,17)(X(J),J=1,M)
   16 FORMAT(//,'HISTOGRAM OF OUTPUT FROM SIGREC PROGRAM',//)
   17 FORMAT(10F11.1)
      WRITE(6,28)
      WRITE(6,27)
      WRITE(6,26)(RA(J),RC(J),RB(J),B(J),J=1,LTOT)
   28 FORMAT(//,15X,'COMPARISON OF THE 3 COMPUTED FUNCTIONS',//)
   27 FORMAT('AMPLITUDE',5X,'FREQUENCY',5X,'SPECTRA',5X,'SIGNAL? 1.0=YES
     1 ; 0.0=NO',//)
   26 FORMAT(3X,F3.1,12X,F3.1,11X,F3.1,10X,F3.1)
      GO TO 67
   66 STOP
      END
      SUBROUTINE SPECTN(Y,LY,LE,G,LH,LTOT,COUNT,LCUT)
      DIMENSION Y(LY),G(105),D(105),U(2000),DM(20)
      LH=0
      JKL=41416/LCUT
```

```
      IF(COUNT .EQ. 1.)GO TO 10
      CALL CORRN(Y,LY,Y,LY,U,LU)
C     APPLICATION OF A HANNING WINDOW IS OPTIONAL
      CALL HAN(U,LU)
      DO 3 KW=10000,JKL,314
      LH=LH+1
      W=(FLOAT(KW)-10000.)/10000.
      S=0.
      DO 2 J=2,LU
      TEMP=FLOAT(J-1)*W
    2 S=S+U(J)*COS(TEMP)
    3 G(LH)=U(1)+2.*S
      GO TO 15
   10 I=LTOT
      K=LTOT+LE-1
      N=0
      DO 14 J=I,K
      N=N+1
   14 D(N)=Y(J)
      CALL CORRN(D,N,D,N,U,LU)
C     APPLICATION OF A HANNING WINDOW IS OPTIONAL
      CALL HAN(U,LU)
      DO 11 KW=10000,JKL,314
      LH=LH+1
      W=(FLOAT(KW)-10000.)/10000.
      S=0.
      DO 12 J=2,LU
      TEMP=FLOAT(J-1)*W
   12 S=S+U(J)*COS(TEMP)
   11 G(LH)=U(1)+2.0*S
   15 RETURN
      END
      SUBROUTINE NMAX(Y,LY,LE,TEMP,LTOT,COUNT)
      DIMENSION Y(LY)
```

```
      IF(COUNT-1.0)3,7,3
7     I=LTOT
      K=LTOT+LE-1
      GO TO 4
3     I=1
      K=LY
4     IND=I
      DO 1 J=I,K
      IF(ABS(Y(IND)) .LT. ABS(Y(J)))IND=J
1     TEMP=ABS(Y(IND))
      RETURN
      END
      SUBROUTINE TURN(H,LH,D,LD,IND)
      DIMENSION H(LH),D(20)
      LD=0
      IND=2
      JND=2
      DO 1 I=2,LH
      IF(H(JND) .LT. H(I))JND=I
      IF(I .GT. (LH-1))GO TO 1
      IF(H(I)-H(I-1))1,2,2
2     IF(H(I)-H(I+1))1,3,3
3     LD=LD+1
      IF(H(IND) .LT. H(I))IND=I
      D(LD)=(FLOAT(I)/FLOAT(LH))/2.0
1     CONTINUE
      BIMBO=H(JND)
      DO 4 I=1,LH
4     H(I)=H(I)/BIMBO
      RETURN
      END
```

```
┌─────────────────────────┐                          ┌──────────────────────────┐
│ ESTIMATES OF REFLECTION │                          │  SEISMIC RECORD INPUT    │◄──────┐
│ COEFFICIENT & DEPTH TO  │                          └──────────────────────────┘       │
│ HORIZONS INPUT          │─────────┐                            │                       │
└─────────────────────────┘         │                ┌──────────────────────────┐       │
                                     │         ┌──────┤ DEPTH TO SEA BOTTOM COMPUTED │    │
                                     │         │      └──────────────────────────┘       │
                                     ▼         ▼                                          │
                        ┌─────────────────────────────────┐                              │
                        │ SEA BOTTOM MULTIPLES COMPUTED,   │                              │
                        │ OUTPUT IN SPIKED FORM, i.e. TIME,│                              │
                        │ AMPLITUDE & PHASE                │                              │
                        └─────────────────────────────────┘                              │
                                     │                                                    │
┌───────────────────────┐  ┌─────────────────────────────┐                               │
│ SOURCE WAVELET INPUT  │──┤ CONVOLUTION OF SPIKES & SOURCE │                             │
└───────────────────────┘  └─────────────────────────────┘                              │
                                     │                                                    │
                        ┌─────────────────────────────────┐                              │
                        │ REMOVAL OF SEA BOTTOM MULTIPLES  │                              │
                        └─────────────────────────────────┘                              │
                                     │                                                    │
            ┌──────────────►┌─────────────────────────────┐◄──────────┐                  │
            │               │ SEARCH MADE AROUND DEPTH TO │           │                  │
            │               │ NEXT HORIZON                │           │                  │
            │               └─────────────────────────────┘           │                  │
            │                        │                                 │                  │
            │               ┌─────────────────────────────┐           │                  │
            │               │ COMPUTATION OF ALL MULTIPLES │           │                  │
            │               │ ASSOCIATED WITH THIS LAYER   │           │                  │
            │               └─────────────────────────────┘           │                  │
            │                        │                                 │                  │
            │               ┌─────────────────────────────┐           │                  │
            │               │ CONVOLUTION OF SPIKES & SOURCE │         │                  │
            │               └─────────────────────────────┘    ┌──────────────────────┐  │
            │                        │                          │ OPTIMIZED DEPTHS ARE │  │
            │               ┌─────────────────────────────┐    │ USED AS THE INITIAL  │  │
            │               │ CORRELATE SYNTHETIC & RECORDED│   │ POINTS FOR THE SEARCH│──┘
            │               │ RECORDS - ∅sr               │    │ ROUTINE              │
            │               └─────────────────────────────┘    └──────────────────────┘
            │                        │                                 │
            │               ┌─────────────────────────────┐  NO        │
            │               │ HAS THE SEARCH RANGE BEEN   │────────────┘
            │               │ COMPLETED ?                 │
            │               └─────────────────────────────┘
            │                        │ YES
            │               ┌─────────────────────────────┐
            │               │ CALCULATE MAXIMUM OF ∅sr ,  │
            │               │ i.e. THE OPTIMIZED DEPTH    │
            │               └─────────────────────────────┘
            │                        │
            │               ┌─────────────────────────────┐
            │               │ REMOVAL OF MULTIPLES COMPUTED│
            │               │ AT THE OPTIMIZED DEPTH       │
            │               └─────────────────────────────┘
            │                        │
            │    YES       ┌─────────────────────────────┐   NO
            └──────────────┤ IS THERE ANOTHER HORIZON ?  │────────────
                           └─────────────────────────────┘
```

optimized   recursive   filter

```
C      OPTIMIZED RECURSIVE FILTER
C
C      THIS PROGRAM COMPUTES AND REMOVES MULTIPLES FOR THREE SEISMIC
C      HORIZONS
C
C      A PLOTTING ROUTINE IS INCLUDED IN THE LISTING AND REQUIRES THE
C      FOLLOWING CONTROL CARDS TO RUN :-
C      $RUN (SOURCE FILE)+*PLOTSYS 5=(DATA) 3=(DATA) 3=-P
C      $RUN *CURPLOT 1=-P 2=*PUNCH* 6=*DUMMY*
C      DEVICE 3 ONLY CONTAINS THE SOURCE FUNCTION, WHILST DEVICE 5
C      CONTAINS THE REMAINING INPUT DATA
C
C      THROUGHOUT THE COMPUTATION THE SEA/AIR INTERFACE HAS AN ASSUMED
C      REFLECTION COEFFICIENT OF -1
C
C                    ****** INPUT ******
C
C      CARD 1  -  (2I5 FORMAT)
C
C      -  IB  -  USER IDENTIFIER (ANY NO. BETWEEN 1 & 79)
C      -  LY  -  NO. OF SAMPLES REQUIRED FOR EACH SEISMIC RECORD
C
C      CARD 2  -  (2I5,9F6.0 FORMAT)
C
C      -  KT    -  NO. OF MULTIPLES REQUIRED
C      -  LZ    -  NO. OF SAMPLES OF THE SOURCE FUNCTION
C      -  RONE  -  REFLECTION COEFFICIENT OF THE SEA BOTTOM
C      -  RTWO  -  REFLECTION COEFFICIENT OF THE FIRST LAYER
C      -  RTHREE -  REFLECTION COEFFICIENT OF THE SECOND LAYER
C      -  XLAX  -  THIS HAS THREE POSSIBLE OPTIONS AS FOLLOWS :-
C                  = 1.0  ------  JUST SEA BOTTOM MULTIPLES
C                  = 2.0  ------  TWO LAYER MULTIPLES
C                  = 3.0  ------  THREE LAYER MULTIPLES
C      -  TONE  -  SHOT/RECEIVER DEPTH (2-WAY TIME IN M.SECS.)
```

```
C          - RN - ESTIMATE OF 2-WAY TIME IN SECS. FROM SHOT TO FIRST LAYER
C          - BBN - SEARCH RANGE ABOUT RN
C          - SN - ESTIMATE OF 2-WAY TIME IN SECS. FROM SHOT TO SECOND LAYER
C          - AAN - SEARCH RANGE ABOUT SN
C
C      CARD 3  -  (1CF6.0 FORMAT)
C
C          - ZZ(I) - ARRAY CONTAINING SOURCE FUNCTION
C
C      CARD 4  -  (10F6.0 FORMAT)
C
C          - BAB(I) - ARRAY CONTAINING THE SEISMIC RECORD
C
C                     ****** OUTPUT ******
C
C      ALL PRINTED OUTPUT IS SELF EXPLANATORY, WHILST THE GRAPHED OUTPUT
C      CONSISTS OF THE SEISMOGRAM LESS MULTIPLES ABOVE THE ORIGINAL INPUT
C      SEISMOGRAM
C
      COMMON Z(1CO),Y(1500),SEIS(1500),E(1500),RONE,RTWO,RTHREE,TONE,
     1TTWO,TTHREE,TFOUR,TX,TY,KT,SSR,LA,LZ
      DIMENSION BAB(1500),TA(50),TB(50),H(50),G(1500),A(1CO),T(100),
     1ZZ(100)
      READ(5,1010)IB,LY
 1010 FORMAT(2I5)
      READ(5,1)KT,LZ,RONE,RTWO,RTHREE,XLAX,TONE,RN,BBN,SN,AAN
    1 FORMAT(2I5,9F6.0)
      READ(3,2)(ZZ(I),I=1,LZ)
    2 FORMAT(10F6.0)
      DO 1700 I=1,LY
 1700 G(I)=FLOAT(I)
      IND=1
      DO 3 I=2,LZ
```

```
  3 IF(ZZ(IND) .LT. ZZ(I)) IND=I
    ZSCALE=ZZ(IND)
    NOB=0
    CALL PLTXMX(60.0)
    CALL PSYMB(0.8,4.0,0.0.6,'DGP03',90.0,5)
    CALL PSYMB(0.8,7.0,0.0.6,IB,90.0,-1)
    NTIT=0
    RXXO=1.0
    RYXO=1.0
    XXO=0.0
    YXO=0.0
    SSR=4.0
    LA=LY
  7 READ(5,2,END=16)(BAB(I),I=1,LA)
    IND=1
    DO 4 I=1,LA
    IF(BAB(I) .GT. 0.5)GO TO 5
  4 CONTINUE
  5 ILZ=I+LZ
    IND=1
  6 DO 6 J=I,ILZ
  6 IF(BAB(IND) .LT. BAB(J))IND=J
    BSCALE=BAB(IND)
    SCALE=BSCALE/(ZSCALE*RONE)
C   SCALE IS A FUNCTION TO SCALE THE SOURCE FUNCTION TO THE INPUT RECORD
    DO 12 I=1,LZ
 12 Z(I)=ZZ(I)*SCALE
    IND=1
    DO 474 I=2,100
474 IF(BAB(IND) .LT. BAB(I))IND=I
    RNOISE=BAB(IND)+BAB(IND)/10.
C   PLOTTING ROUTINE FOR THE INPUT SEISMOGRAM
    NTIT=NTIT+1
    IF(NTIT-4)1730,1730,1731
```

```
1731    NTIT=1
        RXXO=16.5
        RYXO=16.5
        GO TO 1721
1730    IF(NTIT-1)1720,1721,1720
1721    XXO=XXO+RXXO
        XYO=1.0
        YXO=YXO+RYXO
        YYO=0.5
        GO TO 1722
1720    XYO=XYO+1.5
        YYO=YYO+1.5
1722    CALL PAXIS(XXO,XYO,'  ',1,16.0,0.0,0.0,75.0,1.0)
        CALL PAXIS(YXO,YYO,'  ',1,1.3,90.0,-1.0,2.0,0.5)
        CALL PLTOFS(0.0,75.0,0.0,1.0,XXO,XYO)
        CALL PLINE(G,BAB,1200,1,0.0,1.0)
        IF(NOB-1)903,903,903
903     TTHREE=RUB
        TFOUR=SUB
C       CALCULATION OF THE 2-WAY TIME FROM SHOT TO SEA BOTTOM
902     KH=0
        DO 230 I=1,LA
        IF(KH-1)901,899,899
899     KH=KH+1
        GO TO 230
901     IF(ABS(BAB(I))-RNOISE)230,230,900
900     KH=KH+1
        NNN=I
230     CONTINUE
        TTWO=(FLOAT(NNN)-2.0)*SSR
        WRITE(5,237)TTWO
237     FORMAT(//,'TTWO=',F11.5,//)
C       REMOVES SEA BOTTOM MULTIPLES FROM RECORD
        WX=0.
```

```fortran
      WY=0.
      WZ=0.
      TX=0.
      TY=0.
      CALL SYNS(WX,WY,WZ,LY)
      DO 240 I=1,LA
240   SEIS(I)=BAB(I)-Y(I)
      WRITE(6,335)
      WRITE(6,396)(SEIS(I),I=1,LA)
335   FORMAT(//,'RECORD MINUS WATER MULTIPLES',//)
396   FORMAT(10F11.5)
      IF(XLAX-1.0)8,777,8
C     CALCULATION OF THE OPTIMUM DEPTH TO THE SECOND LAYER
8     IF(NOB .GT. 1)RN=ET
      K=IFIX((RBN+BBN)*SSF)
      RBBN=FLOAT(K)*2.0
      DO 95 I=1,K
95    TA(I)=(RN-RBBN)+FLOAT(I-1)*SSR
      WX=0.
      WY=2.
      WZ=0.
      LH=0
      DO 94 I=1,K
      TX=TA(I)
      CALL SYNS(WX,WY,WZ,LY)
      LH=LH+1
94    CALL DENIS(LH,H)
      IND=1
      DO 1005 I=2,LH
1005  IF(H(IND) .LT. H(I))IND=1
      SCALE=H(IND)
      DO 1006 I=1,LH
1006  H(I)=H(I)/SCALE
      WRITE(6,53)
```

```
      WRITE(6,396)(H(I),I=1,LH)
   53 FORMAT(//,'A/C FOR VARIOUS POSITIONS',//)
      CALL NMAX(LH,H,XMAX,IND)
      TX=TA(IND)
      WX=2.
      WY=2.
      WZ=0.
      CALL SYNS(WX,WY,WZ,LY)
      DO 855 I=1,LY
  855 SEIS(I)=SEIS(I)-Y(I)
      WRITE(6,520)TX,IND
      WRITE(6,521)
      WRITE(6,396)(SEIS(I),I=1,LA)
  520 FORMAT(//,'TX=',F11.5,'IND=',I5,//)
  521 FORMAT(//,'REMOVAL OF SEA & FIRST LAYER MULTIPLES',//)
      IF(XLAX .EQ. 2.0)GO TO 777
C     CALCULATION OF THE OPTIMUM DEPTH TO THE THIRD LAYER
      IF(NOB .GT. 1)SN=FT
      WX=0.
      WY=0.
      WZ=2.
      LH=0
      K=IFIX((AAN+AAN)*SSR)
      RAAN=FLOAT(K)*2.0
      DO 950 I=1,K
  950 TB(I)=(SN-RAAN)+FLOAT(I-1)*SSR
      DO 849 I=1,K
      TY=TB(I)
      CALL SYNS(WX,WY,WZ,LY)
      LH=LH+1
  849 CALL DENIS(LH,H)
      IND=1
      DO 2005 I=2,LH
 2005 IF(H(IND) .LT. H(I))IND=I
```

```
        SCALE=H(IND)
        DO 2006 I=1,LH
2006    H(I)=H(I)/SCALE
        CALL NMAX(LH,H,XMAX,IND)
        WRITE(6,53)
        WRITE(6,396)(H(I),I=1,LH)
        TY=TB(IND)
        WX=2.
        WY=0.
        WZ=2.
        CALL SYNS(WX,WY,WZ,LY)
        RUB=TTHREE
        SUB=TFOUR
        ET=TX
        FT=TY
        DO 857 I=1,LA
857     SEIS(I)=SEIS(I)-Y(I)
        WRITE(5,523)TY,IND
        WRITE(6,524)
        WRITE(6,396)(SEIS(I),I=1,LA)
523     FORMAT(//,'TY=',F11.5,'IND=',I5,//)
524     FORMAT(//,'FINAL RESULT MINUS ALL REQUIRED MULTIPLES',//)
        NOB=2
C       PLOTTING ROUTINE FOR THE OUTPUT RECORD (LESS MULTIPLES)
777     NTIT=NTIT+1
        IF(NTIT-4)1630,1630,1631
1631    NTIT=1
        RXXO=16.5
        RYXO=16.5
        GO TO 1621
1630    IF(NTIT-1)1620,1621,1620
1621    XXO=XXO+RXXO
        XYO=1.0
        YXO=YXO+RYXO
```

```
      YYO=0.5
      GO TO 1622
1620  XYO=XYO+1.5
      YYO=YYO+1.5
1622  CALL PAXIS(XXO,XYO,' ',1,16.0,0.0,0.0,75.0,0,1.0)
      CALL PAXIS(YXO,YYO,' ',1,1.0,90.0,-1.0,2.0,0,1.0)
      CALL PLTOFS(0.0,75.0,0.0,1.0,XXC,XYO)
      CALL PLINE(G,SEIS,1200,1,0,0,1.0)
      GO TO 7
15    CALL PLTEND
      STOP
      END
      SUBROUTINE SYNS(WX,WY,WZ,LY)
C     SUBROUTINE SYNS COMPUTES ALL MULTIPLES ASSOCIATED WITH A
C     PARTICULAR LAYER
      COMMON Z(100),Y(1500),SEIS(1500),E(1500),RONE,RTWO,RTHREE,TONE,
     1TTWO,TTHREE,TFOUR,TX,TY,KT,SSR,LA,LZ
      DIMENSION A(100),T(100)
      TFOUR=TY-TX
      TTHREE=TX-TTWO
      T12=TONE+TTWO
      T123=T12+TTHREE
      T23=TTWO+TTHREE
      T1234=T123+TFOUR
      T234=T23+TFOUR
      T34=TTHREE+TFOUR
      R12=1.-(RONE**2)
      R22=1.-(RTWO**2)
      LK=KT+2
      DO 243 I=1,LK
      A(I)=0.0
243   T(I)=0.0
      M=0
      DO 100 N=1,KT
```

```
      NN=N+1
      IF(WZ .GT. 1.)GO TO 49
      IF(WY .GT. 1.)GO TO 34
      M=M+1
      A(M)=((-1.)**NN)*(RONE**N)
      T(M)=T12*FLOAT(N)-TONE
      IF(N .GT. -1)GO TO 1438
      M=M+1
      A(M)=-A(M-1)
      T(M)=T(M-1)+TONE
 1438 CONTINUE
      A(1)=0.
      GO TO 100
   34 M=M+1
      A(M)=((-1.)**NN)*(RTWO**N)*(R12**N)
      T(M)=T123*FLOAT(N)-TONE
      M=M+1
      A(M)=-A(M-1)
      T(M)=T(M-1)+TONE
      M=M+1
      A(M)=((-1.)**N)*(RONE**N)*(RTWO**NN)*(R12)
      T(M)=T23+TTHREE*FLOAT(N)
      M=M+1
      A(M)=-A(M-1)
      T(M)=T(M-1)+TONE
      IF(WX .GT. 1.)GO TO 99
      GO TO 100
   99 A(1)=0.
      GO TO 100
   49 M=M+1
      A(M)=((-1.)**NN)*(R12**N)*(R22**N)*(RTHREE**N)
      T(M)=T1234*FLOAT(N)-TONE
      M=M+1
      A(M)=-A(M-1)
```

```
      T(M)=T(M-1)+TONE
      M=M+1
      A(M)=((-1.)**N)*R12*R22*(FTWO**N)*(RTHREE**NN)
      T(M)=T234+TFOUR*FLOAT(N)
      M=M+1
      A(M)=-A(M-1)
      T(M)=T(M-1)+TONE
      M=M+1
      A(M)=((-1.)**N)*(RONE**N)*(RTWO**N)*(RTHREE**N)*R12*R22
      T(M)=T234+TTHREE*FLOAT(N)
      M=M+1
      A(M)=-A(M-1)
      T(M)=T(M-1)+TONE
      M=M+1
      A(M)=((-1.0)**N)*(RONE**N)*(RTHREE**NN)*R12*R22
      T(M)=T234+T34*FLOAT(N)
      M=M+1
      A(M)=-A(M-1)
      T(M)=T(M-1)+TONE
      IF(WX .GT. 1.)A(1)=0.
 122  CONTINUE
      L=M+1
      DO 122 I=1,M
      K=I+1
      DO 12 J=K,L
      IF(T(I) .LE. T(J)) GO TO 12
      TEMP=T(I)
      T(I)=T(J)
      T(J)=TEMP
      TEMP=A(I)
      A(I)=A(J)
      A(J)=TEMP
  12  CONTINUE
 122  CONTINUE
```

```
      M=M+1
      DO 30 I=1,M
      DO 31 J=1,M
      IF(J-I)32,31,32
32    IF(ABS(T(J)-T(I))-2.0)33,33,31
33    A(I)=A(I)+A(J)
      A(J)=0.0
      T(J)=0.0
      GO TO 30
31    CONTINUE
30    CONTINUE
      JR=1200
      DO 133 J=1,JR
      RNF=FLOAT(J-1)*SSR
      E(J)=0.0
      DO 134 I=1,N
      IF(T(I)-RNF)134,36,134
36    E(J)=A(I)
      GO TO 133
134   CONTINUE
133   CONTINUE
      LY=JR+LZ-1
      CALL CONV(JR,LY)
      IF(WX .LT. 2.)RETURN
      RETURN
      END
      SUBROUTINE DENIS(LH,H)
C     SUBROUTINE DENIS IS A CORRELATION ROUTINE
      COMMON Z(100),Y(1500),SEIS(1500),E(1500),RONE,RTWO,RTHREE,TONE,
     1TTWO,TTHREE,TFOUR,TX,TY,KT,SSR,LA,LZ
      DIMENSION H(LH)
      H(LH)=0.
      DO 2 I=1,LA
2     H(LH)=H(LH)+SEIS(I)*Y(I)
```

```
      RETURN
      END
      SUBROUTINE CONV(JR,LY)
C     SUBROUTINE CONV IS THE CONVOLUTION OF TWO FUNCTIONS
      COMMON Z(100),Y(1500),SEIS(1530),E(1500),RONE,RTWO,RTHREE,TONE,
     1TTWO,TTHREE,TFOUR,TX,TY,KT,SSR,LA,LZ
      DO 2 I=1,LY
    2 Y(I)=0.
      DO 1 I=1,JR
      DO 1 J=1,LZ
      K=I+J-1
    1 Y(K)=Y(K)+E(I)*Z(J)
      RETURN
      END
      SUBROUTINE NMAX(LX,X,XMAX,IND)
C     SUBROUTINE NMAX COMPUTES THE MAXIMUM OF A FUNCTION
      DIMENSION X(LX)
      IND=1
      DO 1 I=1,LX
    1 IF(X(IND) .LT. X(I))IND=I
      XMAX=X(IND)
      RETURN
      END
```

```
SEISMIC INPUT 1                           SEISMIC INPUT 2

PEAKS ABOVE NOISE LEVEL                   PEAKS ABOVE NOISE LEVEL
ONTO CHN1                                 ONTO CHN 2

SEARCH CHN 1 FOR ARRIVAL.        OBTAIN t₁'
STORE PHASE & AMPLITUDE

SEARCH DOWN CHN2 FOR      YES    OBTAIN t₂'
ARRIVAL WITH SIMILAR PHASE
& MAGNITUDE AS CHN1

         NO

REMOVE ARRIVAL FROM CHN1         EQUATE BETWEEN t₁' AND t₂' TO
                                 FIND V₁ AND Z₁

                         NO      IF ı>1 CHECK IF V₁>V₁₋₁ AND
                                 Z₁ > Z₁₋₁

                                         YES

REPEAT THE SEARCH ON             CACULATE ARRIVAL TIME FOR
CHN2 L TIMES IF >L THEN          CHN 3 . ie t₃'
REMOVE ARRIVAL FROM CHN1

SEISMIC INPUT 3   PEAKS ABOVE NOISE LEVEL   NO   SEARCH AROUND t₃' ON CHN 3
                  ONTO CHN 3                     FOR A SIMILAR ARRIVAL AS
                                                 ON CHN 1

                                         YES

                                 CALCULATE t₄' FOR CHN 4

SEISMIC INPUT 4   PEAKS ABOVE NOISE LEVEL        SEARCH AROUND t₄' ON CHN 4
                  ONTO CHN 4                     FOR A SIMILAR ARRIVAL AS
                                                 ON CHN 1

                                  YES                            NO

                          STORE ARRIVAL ON         REMOVE ARRIVAL ON
                          CHN1                      CHN1

                                  DISPLAY CHN1
```

CHN 1,2,3 & 4 are the four seismic channels containing data from
the four active sections of the array

'chns' technique

```
C     THIS PROGRAM (CHNS) ELIMINATES MULTIPLES FROM A SEISMOGRAM BY
C     USING 4 ACTIVE SECTIONS OF AN ARRAY. THE THEORY USED IS THAT
C     DESCRIBED IN SECTION 3.6.
C     FOR PLOTTING PURPOSES THE DURHAM IBM1130 FACILITIES ARE USED, THEY
C     HAVE NOT BEEN INCLUDED IN THIS LISTING
C
C                  ****** INPUT CARDS ******
C
C     THE DATA CARD (THIRD LINE OF THE PROGRAM) CONTAINS THE DISTANCES
C     IN KMS. OF THE ACTIVE SECTIONS FROM THE SHOT (X1,X2,X3,X4) AND
C     THE NUMBER OF SAMPLES OF EACH SEISMIC CHANNEL USED
C
C     CARD 1 - IB IS THE USER IDENTIFIER (NOS. 1-75) FOR THE PLOTTING
C              ROUTINE WHICH IS OPTIONAL (I5 FORMAT)
C            - NREC IS THE NUMBER OF SHOTS TO BE PROCESSED (I5 FORMAT)
C     CARD 2 - CONTAINS THE DIGITIZED DATA OF THE FIRST CHANNEL
C     CARD 3 - SECOND CHANNEL DATA
C     CARD 4 - THIRD CHANNEL DATA
C     CARD 5 - FOURTH CHANNEL DATA
C     ALL THE CARDS 2-5 ARE IN 10F6.0 FORMAT
C
C                  ****** OUTPUT ******
C
C     THE FINAL OUTPUT IS THE FIRST SEISMIC CHANNEL LESS MULTIPLES (10F11.5)
C
      DIMENSION CHN1(1500),CHN2(1500),CHN3(1500),CHN4(1500),
     1Z(800),VK(800)
      DATA X1,X2,X3,X4,LCHN/0.130,0.340,0.500,0.660,1200/
      READ(4,1010)IB,NREC
 1010 FORMAT(2I5)
      DO 1100 INR=1,NREC
      READ(5,1)(CHN1(I),I=1,LCHN)
      READ(5,1)(CHN2(I),I=1,LCHN)
      READ(5,1)(CHN3(I),I=1,LCHN)
```

```fortran
      READ(5,1)(CHN4(I),I=1,LCHN)
    1 FORMAT(10F6.0)

C     ALL 4 CHNS. HAVE THEIR NOISE AMPLITUDE CALCULATED SINCE THE NOISE
C     VALUE MAY VARY FROM EACH
C     THE FIRST 50 VALUES CONSIDERED FOR THE MEAN VALUE
C
      L1=1
      L2=1
      L3=1
      L4=1
      DO 74 I=2,50
      IF(ABS(CHN1(L1))  .LT.  ABS(CHN1(I)))L1=I
      IF(ABS(CHN2(L2))  .LT.  ABS(CHN2(I)))L2=I
      IF(ABS(CHN3(L3))  .LT.  ABS(CHN3(I)))L3=I
   74 IF(ABS(CHN4(L4))  .LT.  ABS(CHN4(I)))L4=I
      AMP1=ABS(CHN1(L1))
      AMP2=ABS(CHN2(L2))
      AMP3=ABS(CHN3(L3))
      AMP4=ABS(CHN4(L4))
      WRITE(6,44)AMP1,AMP2,AMP3,AMP4
   44 FORMAT(//,'AMP1=',F8.5,2X,'AMP2=',F8.5,2X,'AMP3=',F8.5,2X,'AMP4=',
     1F8.5,//)
      CALL TURN(CHN1,LCHN,AMP1,LC)
      CALL TURN(CHN2,LCHN,AMP2,JAN)
      CALL TURN(CHN3,LCHN,AMP3,JAN)
      CALL TURN(CHN4,LCHN,AMP4,JAN)
      WRITE(6,45)
   45 FORMAT(//,'CHN(I) ARRAY',//)
      WRITE(6,46)(CHN1(I),I=1,LCHN)
   46 FORMAT(10F11.5)
      LP=0
      N1=0
      N2=0
```

```
      DO 39 II=1,LC
      COUNT=0.0
      DO 3 I=1,LCHN
      IF(COUNT-1.0)16,3,16
   16 IF(I-N1)3,3,6
    6 IF(ABS(CHN1(I))-ABS(AMP1))3,3,4
    4 COUNT=1.0
      N1=I
      T1=(FLOAT(I)*4.0)/1000.-0.004
      AMP=CHN1(I)
      IF(CHN1(I))14,75,75
   14 SIGN1=-1.0
      GO TO 3
   75 SIGN1=1.0
    3 CONTINUE
      SCALE=AMP1+AMP1/10.
      WRITE(6,105)N1,T1,AMP,SIGN1
  105 FORMAT('N1=',I5,2X,'T1=',F11.5,2X,'AMP=',F11.5,2X,'SIGN1=',F11.5)
      R=0
   19 IND=0
      R=R+1
      N2=0
      MM=N1-10
      NN=N1+10
      DO 71 I=MM,NN
      IF(ABS(CHN2(I)) .LT. AMP2)GO TO 7
      IF(I .LE. N2)GO TO 7
      IF(IND-1)8,7,8
    8 COUNT=CHN2(I)-AMP
      IF(ABS(COUNT)-SCALE)421,421,7
  421 IF(CHN2(I))9,10,10
   10 SIGN2=1
      GO TO 908
    9 SIGN2=-1
```

```
908 IF(SIGN1-SIGN2)7,909,7
909 IND=1
    N2=I
    T2=(FLOAT(I)*4.0)/1000.-0.004
  7 CONTINUE
 71 CONTINUE
    IF(IND .GT. 0)GO TO 914
    WRITE(6,915)
915 FORMAT(//,'NO ARRIVAL AT CORRESPONDING TIME ON CHN2(I)',//)
    IF(N2-1)40,90,90
C   IFN2=0 THEN NO ARRIVALS FOUND THROUGHOUT COMPLETE SEARCH RANGE
C   THUS REMOVE THE ARRIVAL. COULD HAVE WIDENED THE SEARCH AREA THOUGH
C   BY GOING BACK & ALTERING MM & NN
914 WRITE(6,106)N2,T2
106 FORMAT(''N2=',I5,2X,'T2=',F11.5)
    T=ABS(T2-T1)
    IF(T-.001)201,200,200
201 T3CAL=T2
C   WHEN LP=0 WE HAVE NOT FOUND A LAYER THUS THE VELOCITY SET EQUAL
C   TO 1.48
C   WHEN LP=1 WE HAVE ONLY FOUND ONE LAYER AND THUS SET VELOCITY
C   EQUAL TO A MEAN OF TWO LAYERS OF 1.80
    IF(LP .EQ. 0)VKC=1.48
    IF(LP .EQ. 1)VKC=1.80
    IF(LP .GT. 1)VKC=VK(LP)-VK(LP-1)+VK(LP)
    ZC=VKC*T3CAL
    WRITE(6,278)VKC,ZC,T3CAL
278 FORMAT('ADJUSTED VELOCITY=',F8.5,2X,'ADJUSTED DEPTH=',F8.5,2X,'T3C
   1AL=',F8.5)
    GO TO 202
200 ZC=SQRT(((T1**2)*(X2**2)-(X1**2)*(T2**2))/(4.*T*(T2+T1)))
    VKC=2.*(SQRT((X1**2)/4.+(ZC**2)))/T1
    WRITE(6,666)ZC,VKC
666 FORMAT('ZC=',F11.5,2X,'VKC=',F11.5)
```

```
        IF(LP-1)88,89,89
     89 IF(ZC-Z(LP))90,90,188
    188 IF(VKC-VK(LP))90,90,88
     90 IF(R-3.0)19,19,40
     88 T3CAL=2.0*SQRT((X3**2)/4.+(ZC.**2))/VKC
        WRITE(6,107)ZC,VKC,T3CAL
    107 FORMAT('ZC=',F11.5,2X,'VKC=',F11.5,2X,'T3CAL=',F11.5)
    202 T3CAL=T3CAL*1000./4.
        IT3CAL=IFIX(T3CAL)
C       THE VALUE 10 IS ARBITARY & MUST BE ASSUMED BEFOREHAND
        J=IT3CAL-10
        K=IT3CAL+10
        IND=0
        DO 111 I=J,K
        IF(IND-1)17,11,17
     17 COUNT=CHN3(I)-AMP
        IF(ABS(COUNT)-SCALE)25,25,11
     25 IF(CHN3(I))22,23,23
     22 SIGN3=-1.0
        GO TO 24
     23 SIGN3=1.0
     24 IF(SIGN1-SIGN3)11,15,11
     15 IND=1
        IF(ABS(T)-0.001)203,204,204
    203 T4CAL=T3CAL*4.0/1000.
        WRITE(6,205)T4CAL
    205 FORMAT(//,'SINCE T1=T2 T4CAL SET EQUAL TO T3CAL=',F11.5,//)
        GO TO 207
    204 T4CAL=2.*SQRT((X4**2)/4.+(ZC**2))/VKC
        WRITE(6,108)T4CAL
    108 FORMAT('T4CAL=',F11.5)
    207 T4CAL=(T4CAL*1000.)/4.0
        IT4CAL=IFIX(T4CAL)
     11 CONTINUE
```

```fortran
111   CONTINUE
      IF(R-3.0)21,20,20
21    IF(IND)30,19,30
20    IF(IND)30,40,30
30    J=IT4CAL-10
      K=IT4CAL+10
      IND=0
      DO 311 I=J,K
      IF(IND-1)32,31,32
32    COUNT=CHN4(I)-AMP
      IF(ABS(COUNT)-SCALE)33,33,31
33    IF(CHN4(I))35,36,36
35    SIGN4=-1.0
      GO TO 37
36    SIGN4=1.0
37    IF(SIGN1-SIGN4)31,38,31
38    IND=1
31    CONTINUE
311   CONTINUE
      IF(IND-1)40,399,40
399   LP=LP+1
      VK(LP)=VKC
      Z(LP)=ZC
      GO TO 39
40    KK=IFIX((T1+0.004)*250.)+1
      CHN1(KK)=0.0
      WRITE(6,777)KK
777   FORMAT('KK=',I5)
39    CONTINUE
      WRITE(6,41)(CHN1(I),I=1,LCHN)
41    FORMAT(10F11.5)
1100  CONTINUE
      STOP
      END
```

```fortran
      SUBROUTINE TURN(CHN,LCHN,AMP,LC)
C
C     SUBROUTINE TURN COMPUTES THE PEAKS ABOVE THE NOISE LEVEL FOR
C     EACH SEISMIC CHANNEL IN TURN

      DIMENSION CHN(LCHN),A(1500)
      K=LCHN-1
      A(1)=0.
      A(LCHN)=0.
      LC=0
      DO 1 I=2,K
      A(I)=0.
      IF(ABS(CHN(I))-AMP)1,1,3
    3 IF(CHN(I) .GE. CHN(I-1))GO TO 2
      IF(CHN(I) .LT. CHN(I+1))GO TO 4
      GO TO 1
    2 IF(CHN(I) .LT. CHN(I+1))GO TO 1
    4 A(I)=CHN(I)
      LC=LC+1
    1 CONTINUE
      DO 5 I=1,LCHN
    5 CHN(I)=A(I)
      RETURN
      END
```

```
┌─────────────────────────┐        ┌─────────────────────────┐
│ FIRST SEISMOGRAM INPUT A│        │ NEXT SEISMOGRAM INPUT B │◄───┐
└────────────┬────────────┘        └────────────┬────────────┘    │
             ▼                                   ▼                 │
┌─────────────────────────┐        ┌─────────────────────────┐    │
│ CONVOLVED WITH SPIKING  │        │ CONVOLVED WITH SPIKING  │    │
│      COEFFICIENTS        │        │      COEFFICIENTS        │    │
└────────────┬────────────┘        └────────────┬────────────┘    │
             ▼                                   ▼                 │
┌─────────────────────────┐        ┌─────────────────────────┐    │
│  PEAKS ABOVE NOISE LEVEL │        │  PEAKS ABOVE NOISE LEVEL │    │
└────────────┬────────────┘        └────────────┬────────────┘    │
             │      ┌─────────────────────────────────┐           │
             └─────►│   SEARCH ROUTINE TO FIND         │◄──────────┘
                    │   CORRESPONDING ARRIVALS         │◄──┐
                    └────────────┬────────────────────┘    │
                                 ▼                     NO   │
                    ┌─────────────────────────────────┐    │
                    │ HAVE THESE CORRESPONDING         ├────┘
                    │ ARRIVALS BEEN FOUND?             │
                    └────────────┬────────────────────┘
                                 │ YES
                                 ▼
                    ┌─────────────────────────────────┐    ┌──────────────┐
                    │ CALCULATE CO-ORDS OF             │    │  SET ARRAY   │
                    │ THESE PEAKS                      │    │    A = B     │
                    └────────────┬────────────────────┘    └──────▲───────┘
                                 ▼                                 │
                    ┌─────────────────────────────────┐           │
                    │ INTERSECTION POINTS OF THE       │           │
                    │ LINES DRAWN THROUGH THE          │           │
                    │ PEAKS    X(k,n), Y(k,n)          │           │
                    └────────────┬────────────────────┘           │
                                 ▼                                 │
                    ┌─────────────────────────────────┐           │
                    │ TEST FOR SIMILAR POINTS          │           │
                    │ OF INTERSECTION                  │           │
                    └──────┬────────────────────┬─────┘           │
                      YES  │                     │ NO             │
                           ▼                     ▼                │
              ┌──────────────────┐      ┌──────────────────┐      │
              │ REMOVE ARRIVAL   │      │ KEEP ARRIVAL     │      │
              │ FROM RECORD B    │      │ ON RECORD B      │      │
              └────────┬─────────┘      └────────┬─────────┘      │
                       │      ┌──────────────┐   │                │
                       └─────►│   OUTPUT     │◄──┘                │
                              └──────┬───────┘                    │
                                     └───────────────────────────┘
```

'Intercept' technique

INTERCEPT METHOD OF MULTIPLE ELIMINATION

THE THEORY BEHIND THIS TECHNIQUE IS THAT DESCRIBED IN SECTION **3.7.**

***** INPUT *****

CARD 1 (2F6.0,4I5 FORMAT)

- XVAL - LIMITS FOR ALLOWING THE CO-ORDS OF X(K,N) & X(K,N+1)
  TO BE STATED AS BEING AS THE SAME POINT
- YVAL - SIMILAR TO ABOVE EXCEPT FOR Y(K,N) & Y(K,N+1)
  (IDEALLY BOTH THESE VALUES SHOULD EQUAL 0.0)
- KVAL - SEARCH RANGE (IN NO. OF SAMPLES) TO FIND THE SAME
  EVENT FROM ONE SEISMIC TRACE TO THE NEXT
- LA - NO. OF SAMPLES OF THE SEISMIC TRACE REQUIRED
- NSPIKE - POSITION AT WHICH THE SOURCE WAVELET IS SPIKED
  WHEN CONVOLVING WITH THE SPIKING COEFFICIENTS
  (THIS VALUE SHOULD BE OBTAINED WHEN DETERMINING
  THE SPIKING COEFFICIENTS)
- LE - LENGTH OF THE SPIKING FILTER IN NO. OF SAMPLES

CARD 2 (10F6.0 FORMAT)

- E(I) - ARRAY CONTAINING THE SPIKING FILTER COEFFICIENTS

CARD 3 (10F6.0 FORMAT)

- A(I) - INPUT OF FIRST RECORD (ONLY PERFORMED AT THE START
  OF THE PROGRAM). AT THE END OF EACH RUN OF THE
  PROGRAM A(I) IS SET EQUAL TO E(I))

CARD 4 (10F6.0 FORMAT)

- E(I) - INPUT OF SEISMIC DATA FOR THE NEXT SHOT

```
C
C
C      ALL THE OUTPUT IS SELF EXPLANATORY. THE LAST ITEM THAT IS OUTPUT
C      IS THE RECORD IN THE FORM OF A SERIES OF SPIKES. THESE SPIKES
C      REPRESENT THE PHASE AND AMPLITUDE OF THE PEAKS THAT HAVE BEEN CHOSEN
C      AS FIRST ARRIVALS, MULTIPLES HAVING BEEN REMOVED
C
       DIMENSION A(1500),B(1500),C(1500),D(1500),YONE(100),YTWO(100),
      1PINT(50),X(100,100),Y(100,100),F(100),F(1500),F(1500)
       READ(5,1)XVAL,YVAL,KVAL,LA,NSPIKE,LE
       READ(5,2)(E(I),I=1,LE)
       READ(5,2)(A(I),I=1,LA)
     1 FORMAT(2F6.0,4I5)
     2 FORMAT(10F6.0)
       CALL CONV(A,LA,E,LE,RNOISE)
C      CONTINUOUS READ IN OF EACH SEISMOGRAM
   770 READ(5,2,END=116)(B(I),I=1,LA)
       CALL CONV(B,LA,E,LE,RNOISE)
C      CALCULATION OF THE TURNING POINTS ABOVE THE NOISE LEVEL
C      THESE POINTS ARE PUT ONTO ARRAYS C(I) & D(I)
       K=LA-1
       C(1)=0.0
       C(LA)=0.0
       A(1)=0.0
       DO 751 I=2,K
       C(I)=0.0
       IF(ABS(A(I))-RNOISE)751,751,753
   753 IF(A(I) .GE. A(I-1))GO TO 752
       IF(A(I) .LT. A(I+1))GO TO 754
       GO TO 751
   752 IF(A(I) .LT. A(I+1))GO TO 751
   754 C(I)=A(I)
   751 CONTINUE
```

```fortran
      D(1)=0.0
      D(LA)=0.0
      B(1)=0.0
      DO 761 I=2,K
      D(I)=0.0
      IF(ABS(B(I))-RNOISE)761,761,763
  763 IF(B(I) .GE. B(I-1))GO TO 762
      IF(B(I) .LT. B(I+1))GO TO 762
      GO TO 761
  762 IF(B(I) .LT. B(I+1))GO TO 761
  754 D(I)=B(I)
  761 CONTINUE
      WRITE(6,200)
      WRITE(6,201)(C(I),I=1,LA)
      WRITE(6,202)
      WRITE(5,201)(C(I),I=1,LA)
  202 FORMAT(//)
  201 FORMAT(10F11.5)
  200 FORMAT('PULSES ABOVE NOISE LEVEL FOR 2 RECORDS')
C
C     ARRAY F IS MADE EQUAL TO ARRAY D WHICH CONTAINS THE SPIKES SINCE
C     D VALUES ARE SET EQUAL TO 0.0 DURING THE SEARCH ROUTINE BETWEEN
C     C & D ARRAYS
      DO 777 I=1,LA
  777 F(I)=D(I)
C     SEARCH ROUTINE BETWEEN 2 ARRAYS TO FIND COMMON PEAKS
      AMP=RNOISE
      L=0
      DO 251 I=1,LA
      IF(C(I) .EQ. 0.)GO TO 251
      AMP=ABS(C(I))/10.
      SEX=0.
      DONE=1.
      DO 620 J=1,KVAL
      IF(SEX .GT. 0.)GO TO 25
```

```
      N=I+J-1
      IND=1
      GO TO 182
  181 IF(SEX .GT. 0.)GO TO 25
      M=I-J+1
      IND=2
C     TEST IF OUTSIDE RANGE OF D ARRAY
  182 IF(M .LT. 1)GO TO 257
      IF(M .GT. LA)GO TO 257
C     TEST IF ANY PEAKS ON ARRAY D
      IF(ABS(D(N)) .EQ. 0.)GO TO 257
C     TEST IF AMPLITUDE IS COMPATIBLE
      IF(ABS(C(I)-D(N)) .GT. AMP)GO TO 257
C     TEST IF SIGN IS COMPATIBLE
      IF(C(I))28,29,29
   28 IF(D(N))30,257,257
   29 IF(D(N))257,257,30
C     IF SIGN & AMPLITUDE ARE COMPATIBLE THEN:
   30 SEX=1.
      L=L+1
      YONE(L)=FLOAT(I)
      YTWO(L)=FLOAT(N)
      C(I)=0.
      D(N)=0.
      DONE=2.
C     DONE IS USED TO FIND OUT IF A VALUE ON D(I) HAS BEEN FOUND
  257 IF(IND .EQ. 2)GO TO 25
      IF(DONE .EQ. 2)GO TO 25
      GO TO 181
   25 CONTINUE
  629 CONTINUE
  251 CONTINUE
C****** FOR USE ONLY WHEN PRE-SPIKING ******
      DO 1003 I=1,L
```

```fortran
      YONE(I)=YONE(I)-FLOAT(NSPIKE)
1003  YTWO(I)=YTWO(I)-FLOAT(NSPIKE)
C     *********************************
      WRITE(6,203)
      WRITE(6,204)(YONE(I),YTWO(I),I=1,L)
203   FORMAT(1H0,//,'    YONE(I)      YTWO(I)',//)
204   FORMAT(1H0,2F11.5)
C
C     CALCULATION OF INTERSECTION VALUES OF THE LINES
C     A(K,N) : K=LINE CONSIDERING
C              : N=LINE INTERSECTING
C     SUCH THAT WE OBTAIN TRIANGULAR MATRICES FOR X(K,N)  &  Y(K,N)
C
      DO 300 K=1,L
300   RINT(K)=YONE(K)+YONE(K)-YTWO(K)
      WRITE(6,205)
      WRITE(5,201)(RINT(K),K=1,L)
205   FORMAT(1H0,//,'INTERCEPT VALUES',//)
      DO 302 K=1,L
      DO 301 N=1,K
      IF(N .EQ. K)GO TO 304
      TEMP=YTWO(K)-YONE(K)-YTWO(N)+YONE(N)
      IF(TEMP-0.)307,308,307
309   X(K,N)=0.
      GO TO 309
307   X(K,N)=(RINT(N)-RINT(K))*100./TEMP
309   Y(K,N)=(YTWO(K)-YONE(K))*X(K,N)/100.+RINT(K)
      GO TO 301
304   X(K,N)=0.
      Y(K,N)=0.
301   CONTINUE
302   CONTINUE
      WRITE(6,441)
441   FORMAT(//,' X(K,N) MATRIX',//)
```

```
      WRITE(5,440)((X(K,N),N=1,L),K=1,L)
  440 FORMAT(10FIL.2)
      WRITE(6,442)
  442 FORMAT(//,'Y(K,N) MATRIX',//)
      WRITE(6,440)((Y(K,N),N=1,L),K=1,L)
C     REMOVAL OF MULTIPLES
      DO 912 K=1,L
      DO 112 N=1,K
      IF(N .EQ. K)GO TO 112
      COUNT=0.0
      DO 111 I=1,L
      DO 110 M=1,I
      IF(I .EQ. M)GO TO 110
      IF(K .EQ. I .AND. N .EQ. M)GO TO 110
      IF(ABS(X(K,N)-X(I,M)) .GT. XVAL)GO TO 110
      IF(ABS(Y(K,N)-Y(I,M)) .GT. VVAL)GO TO 110
C     THIS IS ONLY FOR SPIKING, REMOVE NSPIKE OTHERWISE
      KK=IFIX(YTWO(I))+NSPIKE
C     ****************************************
      F(KK)=0.0
      COUNT=2.0
  110 CONTINUE
  111 CONTINUE
      IF(COUNT .LT. 1.0)GO TO 112
C     THIS IS ONLY FOR SPIKING, REMOVE NSPIKE OTHERWISE
      KK=IFIX(YTWO(K))+NSPIKE
C     ****************************************
      F(KK)=0.0
  112 CONTINUE
  912 CONTINUE
C     THE FOLLOWING 3 LOOPS TEST FOR INTERCEPT VALUES THAT ARE INTEGRAL
C     VALUES OF OTHER INTERCEPTS. THESE ARE DUE TO HORIZONTAL
C     LAYERING, AND WHICH WOULD NOT HAVE BEEN REMOVED BY THE ABOVE
C     ROUTINE
```

```
C     THIS ROUTINE SHOULD BE REMOVED IF IT IS FELT THAT THE LAYERING
C     IS NOT HORIZONTAL SINCE THIS ROUTINE IS SOMETIMES DANGEROUS TO
C     APPLY BECAUSE FIRST ARRIVALS MAY BE REMOVED
      DO 223 N=1,L
      DO 229 J=1,L
      IF(J .EQ. N)GO TO 229
      DO 225 K=2,5
      BIC=(YTWO(N)-1.0)*FLOAT(K)+1.0
      IF(BIC-YTWO(J))226,840,226
  840 YTWO(J)=0.0
C     THIS IS ONLY FOR SPIKING, REMOVE NSPIKE OTHERWISE
      I=IFIX(YTWO(J))+NSPIKE
C     ***********************************************
      F(I)=0.
  225 CONTINUE
  229 CONTINUE
  228 CONTINUE
      DO 428 I=1,LA
      IF(F(I) .LT. 0.0)F(I)=0.0
  428 CONTINUE
      WRITE(6,841)
      WRITE(6,201)(F(I),I=1,LA)
  841 FORMAT(1H0,//,'MULTIPLE REMOVAL + MULTIPLES OF HORIZ LAYERS',//)
C     PUT VALUES OF B ONTO A AND THEN GO BACK TO STATEMENT 70 TO
C     INPUT NEW RECORD ONTO B
      DO 90 I=1,LA
   90 A(I)=B(I)
      GO TO 770
  116 STOP
      END
      SUBROUTINE CONV(X,LX,Y,LY,RNOISE)
C     SUBROUTINE CONV CONVOLVES THE SEISMIC RECORD WITH THE SPIKING
C     FILTER COEFFICIENTS
      DIMENSION X(LX),Y(LY),Z(1500)
```

```
      LZ=LX+LY-1
      DO 1 I=1,LZ
    1 Z(I)=0.0
      DO 2 I=1,LX
      DO 2 J=1,LY
      K=I+J-1
    2 Z(K)=Z(K)+X(I)*Y(J)
      IND=1
      DO 3 I=2,50
    3 IF(ABS(Z(IND)) .LT. ABS(Z(I))) IND=I
C     RNOISE IS THE MAX. NOISE LEVEL OF THE FIRST 50 SAMPLES
      RNOISF=ABS(Z(IND))+ABS(Z(IIND))/10.0
      DO 4 I=1,LX
    4 X(I)=Z(I)
      RETURN
      END
```